POLITECNICO DI TORINO

Corso di Laurea Magistrale
in Ingegneria Civile

Tesi di Laurea Magistrale

NONLINEAR FE ANALYSIS OF STATICALLY-INDETERMINATE SFRC COLUMNS WITH A CONCRETE DAMAGED PLASTICITY MODEL

Relatore

Prof. Rosario Ceravolo

Candidato

Fabio Calabrò

A.A. 2017/2018

Abstract

The investigation presented in this thesis is closely related to the modelling of the structural behaviour of steel fibre-reinforced concrete (SFRC) beams using a non-linear finite-element (FE) analysis with a Concrete Damaged Plasticity Model.
In particular, the aim of this investigation is to verify if this kind of Model can be used to analyse a SFRC element and to discuss the results.
Afterwards, to carry out this analysis, different aspects of the phenomenon were examined. First of all, in the validation part, the load-deflection curve is compared with experimental and Brittle Cracking Method outcomes; then damage parameters, kinetic energy, strength and ductility were evaluated as well.
In the validation part, the plasticity parameters, namely the dilatation angle
φ, eccentricity ε, ratio of second stress invariants K and the ratio between biaxial compressive yield strength and uniaxial compressive yield strength f_{b0}/f_{c0}, are chosen to obtain results as close as possible to the experimental one.
Successively the same beam was analysed modifying two key parameters, namely reducing transverse reinforcement while increasing the amount of fibres. The reduction in conventional reinforcement (obtained by increasing stirrups spacing) is very important in practice as it helps mitigate reinforcement congestion, the latter is a typical issue in the seismic detailing of critical regions such as beam-column joints.
Afterwards the same procedure was carried out taking into account a cyclic load that simulates a seismic load condition.
For the SFRC constitutive model, that one proposed by Lok and Xiao (1999) has been chosen in tension because of its validity in a wide range of fibre volume fraction and to be consistent with Abbas, A., Mohsin, S. and Cotsovos, D. (2014), in compression instead a new constitutive model is chosen from the author because it is more suitable for the Concrete Damaged Plasticity Model, in fact it presents a formula to evaluate the damage parameters.
The results show that steel fibres increase the load-carrying capacity and stiffness, which are important parameters to take into account for design consideration. Fibres were found also to improve ductility (as well as altering the mode of failure from a brittle to a ductile one) and using the Concrete Damaged Plasticity Model this phenomenon is clearly displayed.

To my father,

the reason for every good thing I do

Acknowledgements

For the realization of this research dissertation I have to thank first of all Professor Ali Abbas, without his help I would never have arrived at University of East London, he welcomed me from the first day and he imparted to me his passion in studying and analysing Steel Fibres Reinforced Concrete element. I am very proud to have worked with him and to have learnt so much notions and concepts from him during the course of this research.

Afterwards I would express my gratitude to all the PhD students with whom I shared my period here, Jide, Ahmed and Hasanain helped me during all these months and conversing with them and learning from their experience was fundamental for my growing and for the developing of this work, they made my time at UEL better without any doubt.

Acknowledgements is due to my housemates Diane, Neil and Nayma, they know how hard I worked on this thesis and they supported me all the time.

I cannot forget to thank the Politecnico di Torino and Professor Rosario Ceravolo in particularly, that gave me this opportunity to carry out my research dissertation abroad.

I am deeply thankful to my mother, she, in spite of everything, allowed me to realize my dream of spending time in London for my studies, no one deserves my acknowledgements more than she.

My gratitude to my brother Nino and my sister Elisa, I know that they will be ready to help me in every moment.

In the end, I want to manifest all my gratitude and love to my girlfriend Enrica that supported my every day, she was by my side in the good moments but even more in the strenuous moments during my research, and I know that I have always a support even if she is far from me.

Table of Contents

List of Tables

List of Figures

1. Introduction

1.1 Overview

Since the dawn of civilization, civil engineers have understood how combining different materials is often the most effective solution to structural problems. One such successful combination is reinforced concrete, which is an example of how two materials, plain concrete and steel bars, with such different characteristics can be joined together to create a new, high-performance material.
Recently, there has been growing interest in adding steel fibres to the concrete mix to improve the ductile behaviour of concrete and reduce the concentration of steel bars.
Fibres are added in the concrete mix in order to enhance the properties of the brittle and crack-prone cement-based matrix. In this way, the material can achieve higher tensile and flexural strength and also develops a crack control mechanism. The latter quality is composed of two steps: firstly, steel fibres, being randomly distributed in the concrete, intercept micro-cracks as they inhibit the tendency for them to form into larger cracks. Then, after cracking, the fibres spanning the crack will provide a degree of residual load-carrying capacity. This capacity can be considerable, depending on the dosage and the type of fibre used, and can be employed in a plastic design approach. The Steel Fibre Reinforced Concrete (SFRC) elements have the makings of becoming the principal building material, especially in seismic zones. For this reason, it is important to determine its real behaviour under different actions and also the optimum material design.

1.2 Aim and background

This dissertation is an extension of the work done by Abbas et al (2014), in which an investigation was carried out to evaluate the contribution of steel fibres in a reinforced concrete beam. In both pieces of research, after a validation stage based on experimental data, the element's constitutive model was modified in ABAQUS software to verify the structural improvements due to the fibres percentage increment. Therefore, thanks to the large amount of data available, a further investigation could be undertaken, taking into account the results obtained from Abbas et al. (2014) using the Brittle Cracking Model and those obtained from the author using the Concrete Damaged Plasticity Model. The aim of this research is to verify whether using a Concrete Damaged Plasticity Model (CDPM) can lead to acceptable outcomes for the analysis of a SFRC element. The drawback of this model is that there are many parameters involved, all of which, theoretically, have to be set by calibration against experimental results. The Concrete Damaged Plasticity Model can represent the ductility of concrete behaviour, so it is beneficial to analyse Steel Fibre Reinforced Concrete, which is certainly more ductile than plain concrete.
Unfortunately, the sheer number of parameters in the damage plasticity model makes the solution sensitive to any change in these numerous factors.

1.3 Results and conclusions

The analysis carried out with the Concrete Damaged Plasticity Model begins from the validation against the experimental and the Brittle Cracking Model outcomes in terms of load-deflection curves. The main issue with the Concrete Damaged Plasticity Model is linked to the parameters configuration. In this case the plasticity parameters are obtained from the literature, when available, otherwise a calibration work is necessary. Theoretically, for every kind of structural element, loading pattern, support conditions, the plasticity parameters could change, so it could be very difficult to calibrate all the parameters. In this investigation, to obtain the best agreement with experimental results the author calibrated the model with respect to the dilatation angle ψ. In this case in fact, this is the parameter that affects more the overall behaviour in terms of load carrying capacity and failure point. After the validation, the plasticity parameters are defined, so it is possible to highlight the outcomes obtained with the Concrete Damaged Plasticity Model: more than the load deflection curves, the main results are the damaged parameter values when the failure occurs. The damaged parameters allow the understanding of the failure mechanisms correlating them with well-defined quantities. For this reason, it is usefully to use a constitutive model that links clearly the damage parameter with not only the strain, but also with other quantities, like the fracture energy or the mesh size, that can deeply represent the element configuration and its loading condition. Therefore, in Chapter 3 the damage parameters are described and afterwards in Chapter 4 all the outcomes are showed and explained

2. Literature Review

2.1 Introduction

The aim of this research is to evaluate the extent to which the Concrete Damaged Plasticity Model provides a satisfying method to analyse a SFRC structure. Thus, the literature review starts with the experimental work of Kotsovos et al. (2006), it contains all the experimental data on which this dissertation is based, such as the element configuration, the loading pattern and the experimental outcomes obtained in laboratory. In section 3.3 there is an overview of all the experimental details. Afterwards, it is necessary to describe steel fibres, from the production to the verification, also highlighting the environmental impact that this new building material could have. Nowadays, it is widely accepted that steel fibres can be successfully used inside reinforced concrete, but its contribution to reducing environmental pollution is less well known.
Furthermore, the work done by Kotsovos et al. (2006) was taken as a starting point by Abbas et al. (2014), who used a Brittle Cracking Model to analyse the element and assessed the contribution of steel fibres to reducing the concentration of standard reinforcement. This is an opportunity to compare the Concrete Damaged Plasticity Model against an alternative model, indeed the comparison of different outcomes is clear since the two analyses start from the same premises. Another important aspect of this dissertation is the choice of the SFRC constitutive model. Different models have been developed in recent years, using various preconditions, hypotheses and, most importantly, range of validity. Since the percentage of fibres inside concrete mix can change a great deal, it is important to choose the constitutive model that best complies with the percentage used in the analysis. Thus, in section 2.3 different models are presented and other considerations are made on the chosen model. Finally, the Concrete Damaged Plasticity Model is presented starting from the work of Lubliner et al. (1989), afterwards strengths and weaknesses of this model are analysed.

2.2 Steel Fibres

Among all the different typology of fibre used as structural element (carbon, steel, plastic), this research focuses on steel fibres.
In the beginning of the fibres application in concrete, as Zollo (1997) reported, the fibres were rough, because they derived from automobile tires and textile industries. Consequently, it was very difficult to vary the fibres' shape or characteristics and, furthermore, using coarse fibres implicated difficulties in casting. For these reasons, initially the opinions on fibre reinforced concrete were negative, there was too much space between fibres and so they couldn't increase the concrete strength. After this, new kinds of fibres were created and produced, it was possible to add a bigger amount of fibres in the concrete mix improving the fibre bond efficiency. As reported in the *Guidance for the design of steel-fibre-reinforced concrete* (2007) nowadays steel fibres are designed and made in different shapes, as it is shown in Figure 2.1. The main difference is they can be either straight or deformed, the diameter can range between 0.4 and 1.3mm and their lengths are between 25 and 60mm. More than standard reinforcement, fibres need to develop bond with concrete, so they have a big surface area and a tensile strength between 2 and 3 times greater than traditional steel bar.

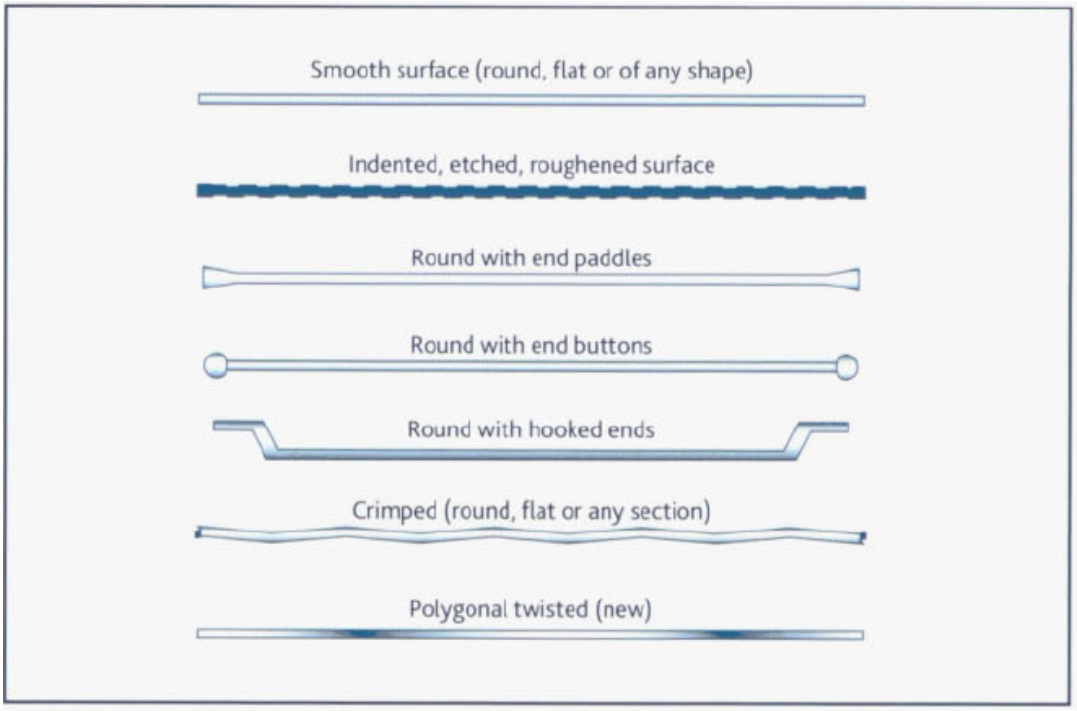

Figure 2.1 *Different shapes of steel fibre*

The most important physical characteristics of steel fibres are related whether to the interaction with concrete (bond mechanisms) or to their own characteristics (tensile strength, elastic modulus) or to the conditions of use (dosage, number of fibres per kg of fibre).
Due to the broad range of fibres types today a lot of different fibres classification exists, in Europe the BS EN 14889-1 classifies steel fibres into five Groups, according to the method of manufacture, as follows:
Group I Cold-drawn wire
Group II Cut sheet
Group III Melt extract
Group IV
Group V Milled from blocks
The SFRC element behaviour is not easy to analyse, for this reason, BS EN 14889-1 requires the effect of fibres on the strength of concrete to be determined in accordance with BS EN 14845, using the standard notched beam test in BS EN 14651.The supplier is required to declare the amount of fibres in kg/m^3 to achieve a residual (post-cracking) flexural strength of 1.5Mpa at a 0.5mm opening of the crack and a residual strength of 1Mpa at a 3.5mm opening.
Other aspects, always more important in the building world, are recycling as well as environmental pollution. Fibres can help environmental conservations making demolition materials more recyclable, but they can also be produced through a recycling process. In fact, it is possible, as explained in Pilakoutas et al. (2004), to extract Recycled Steel Fibres from used tyres, thanks to tyre shredding and cryogenic process. Single and double pull-out tests were carried out to evaluate the optimal fibre length in order to develop sufficient bond with concrete. The strength of SRSF was best utilised when the fibre length was about 20mm, dimension similar to industrial fibres one.

Wang et al. (2000) demonstrated that “steel fibres recycled from used tyres (RSF) can be effectively used to reinforce concrete. In addition, it was indicated that the mechanical behaviour of concrete reinforced with tyre-recycled steel fibres (RSFRC) is comparable to that of conventional steel fibre reinforced concrete (SFRC)”.
Furthermore, using recycled fibres can be convenient also from the economic point of view, as Achilleos et al. (2011) said the use of steel fibres produced by post-consumer tyres is cheaper than the industrial process and could expand the use of fibre reinforced concrete.
The steel fibre can be mixed with other kind of fibres, giving different characteristics at the concrete mix, as stated in Chen, B. and Liu, J. (2005), the effect of polypropylene and steel fibres can improve the uniformity of the mix, the carbon-steel fibres can low the brittleness and the shrinkage of concrete instead. Chiefly the use of different kind of fibres in the concrete mix is convenient because it can avoid the disruptive effect, namely the presence of voids and aggregate particle segregation, of “highmodulus” and course fibres inside concrete.
Moreover, in order to reduce the amount of steel bars in favour of steel fibres, it is important to bear in mind corrosion. It is well known how damaging corrosion could be for reinforced concrete structure, according to Granju, J. and Ullah Balouch, S. (2005) steel fibres are less vulnerable to corrosion than steel bars. In fact, after they carried out experiment with cut specimens, they found out that after one year exposure to marine saline fog the strength of the element was increased. This unexpected effect is due to two contributions: first of all, the corrosion is too light to depress the fibre’s load-bearing capacity and then the corrosion makes the fibres’ surface rougher, so the slipping of the fibres in concrete is more difficult.

2.3 Different constitutive models for SFRC

From the first application of fibres in reinforced concrete, different constitutive models have been used to describe in the best way the behaviour of Steel Fibre Reinforced Concrete. Different authors developed different models depending on different experimental data they had or the particular aim they pursued. Thus, there are differences not only in the constitutive models but also in the field of application. In fact, it is widely accepted that the compression behaviour of SFRC is similar to the plain concrete's one, because fibres do not have remarkable effect on this aspect, on the other hand the behaviour in tension is very various and it depends on the fibres percentage.

The first model proposed herein is based on the stress-strain relation exposed in RILEM TC 162-TDF (2003), in this model, valid for concrete with compressive strength up to C50/60, the fundamental parameters are the crack mouth opening displacement ($CMOD_i$) and the residual flexural tensile strength, $f_{R,I}$. In Figure 2.2 the stress-strain diagram is showed with the size factor k_h. As said before the behaviour in compression is the same of plain concrete, instead for tension the values of characteristic stress and strain are function of the residual flexural tensile strength $f_{R,1}$ and $f_{R,4}$, defined at specifics crack mouth opening displacement. The values for $f_{R,1}$ and $f_{R,4}$ are determined from the following expression:

$$f_{R,i} = \frac{3F_{R,i}L}{2bh_{sp}^2} \qquad (N/mm^2)$$

with b is the width of the specimen (mm), h_{sp} is the distance between tip of the notch and top of cross section (mm) and L is the span length of the specimen (mm). The values for $F_{R,i}$ are determined from the experimental load-deflection curve, based on its respective $CMOD_i$ or $\delta_{R,i}$.

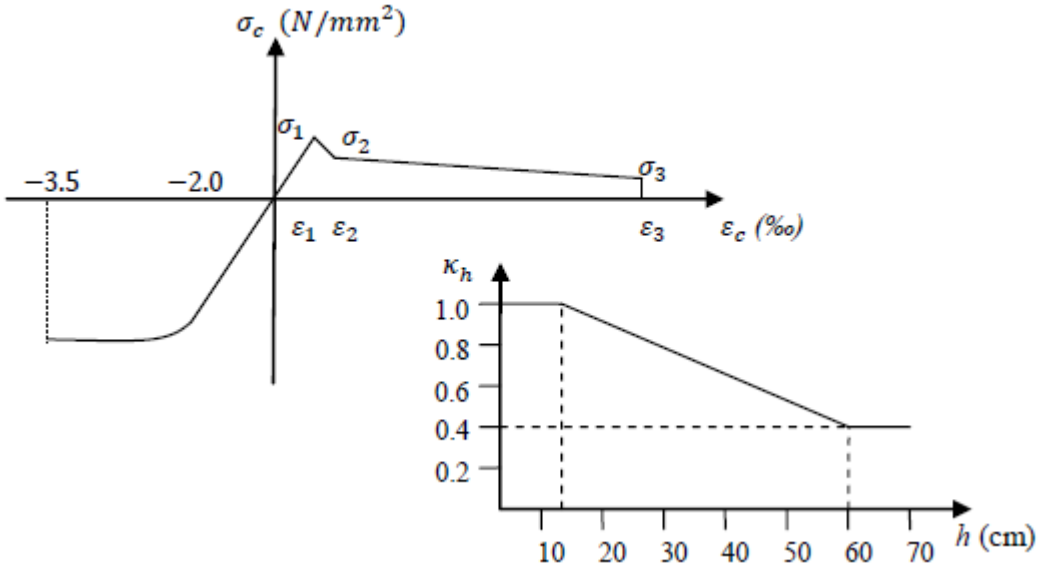

Figure 2.2 *Stress-strain and size factor, κ_h, graphs (RILEM TC 162-TDF 2003)*

The model proposed by Lim et al. (1987) uses parameters referred to fibres characteristics, namely the fibre volume fractions V_f, the ratio between cross sectional area and the perimeter of the fibres and the fibre orientation factor η_0'. The diagram in

Figure 2.3 represents the tensional behaviour of Steel Fibre Reinforced Concrete. The behaviour of concrete after cracking is described by a constant stress σ_{tu} function of the average ultimate pull-out bond strength τ_u of the fibres. This model is suitable for a fibre volume fraction between 0.5% and 1.5%.

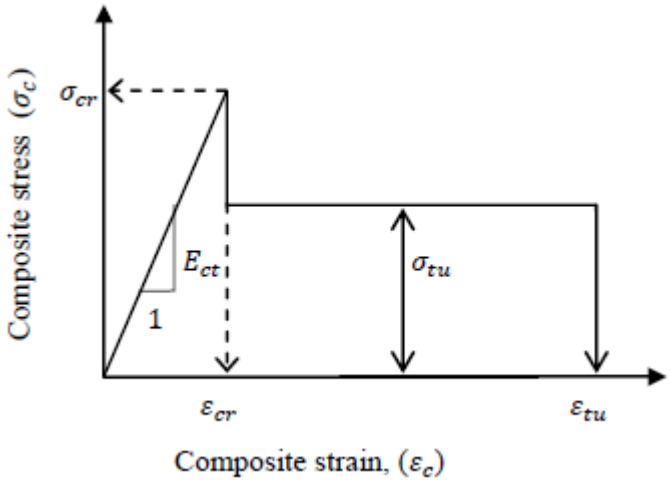

Figure 2.3 *Composite stress-strain relations in tension (Lim et al., 1987)*

As stated before, the concrete properties are functions of fibres characteristics, in fact the tensile elastic modulus is:

$$E_{ct} = E_{mt}V_m + \eta_l\eta_0 E_f V_f$$

where V_m and V_f are the total volume fraction of the concrete matrix and fibres, respectively; E_{mt} and E_f are the tensile elastic modulus for the matrix and the Young's modulus of steel fibres; η_l is the ratio of the average fibre stress to the maximum fibre stress, η_0 orientation factor in the elastic range.
On the other hand, the ultimate strength is given by:

$$\sigma_{tu} = \eta_l\eta_0' V_f l_f \frac{\tau_u}{2r}$$

with η_0' orientation factor due to fibres realigning across the crack, where l_f is the fibre length, τ_u is the ultimate bond stress, r is the ratio of fibre cross-sectional area to its perimeter.
In the end, the last value that characterises the model is the post cracking strain

$$\varepsilon_{tu} = \omega_u / l^*$$

where $\omega_u = l_f/16$ and l^* is a reference length taken as the average crack spacing.
After the previous models, valid only for limited fibre volume fraction, now a generic constitutive model is presented. This model derived from the flexural behaviour of a Steel Fibres Reinforced Concrete investigated by Lok and Pei (1998). This model considers that the structural behaviour could present whether strain softening or hardening behaviour as the fibres properties change. The compressive behaviour is the same of plain concrete, so now the tensile behaviour is described. As shown in Figure 2.4, the tensile side of the stress-strain relationship is composed of two stages: the pre-cracking stage and the post-cracking one.

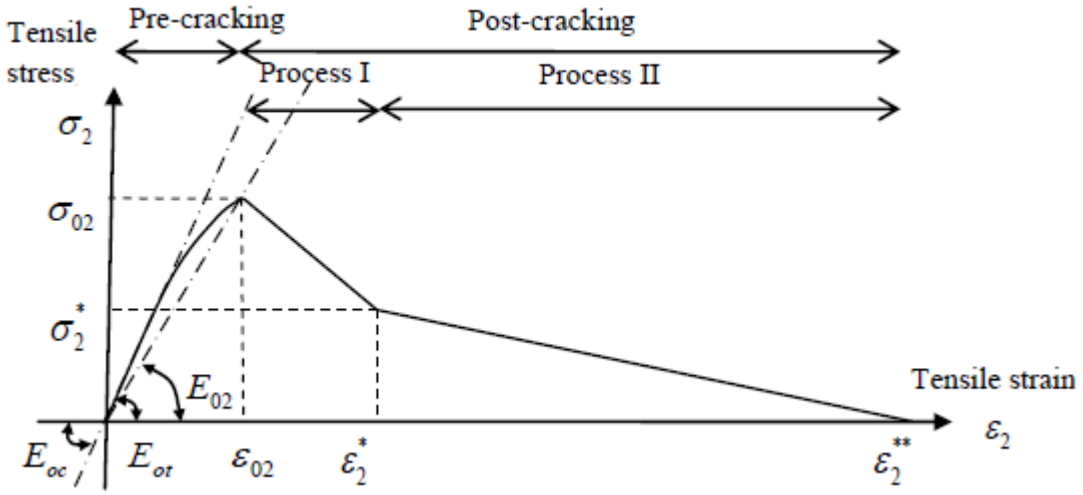

Figure 2.4 *Tensile stress-strain relationship for SFRC (Lok and Pei, 1998)*

The fibres become active in the second stage because in the first one, when the concrete is intact, their effect is negligible. Moreover, this model hires that the steel fibres bond perfectly to the concrete matrix and that no slippage occurs at the fibre-matrix interface. So, in the second stage the bond stress increases up to reach the maximum value at the end of Process I, in correspondence of a strain equal to:

$$\varepsilon_2^* = \tau_d \frac{L}{d} \frac{1}{E_{fp}}$$

In the previous equation E_{fp} is elastic modulus of steel fibres, τ_d is dynamic bond stress and L/d is the fibre aspect ratio. The maximum tensile strain after failure ε_2^{**} can range from 2 x 10^{-4} to 10 x 10^{-4}. In this investigation, the constitutive model chosen is that one designed by Lok and Xiao (1998) described in more detail in section 3.1. This choice was made to remain consistent with the work made by Abbas et al (2014) and so to corroborate the comparison between the different model used in ABAQUS.

2.4 Investigation on Damaged Plasticity Concrete Model

It was widely accepted that to mimic the behaviour of concrete elements under flexural actions two different approaches, a fracture mechanism in tension and a plasticity theory in compression, should be used. On the other hand, as explained by Lubliner et al. (1989) this approach has some drawback that limit its usefulness, such as the difficulties to model the combined effects of cracking and plasticity, or the problem of defining the cracks behaviour under cyclic loading. So Lubliner et al. (1989) suggest the use of a single constitutive model that can represent the non-linear behaviour of concrete both in tension and in compression. The essential parameters in this kind of models are the yield criterion, the flow rule and the hardening rule. The plastic-damage model uses a variable k as the hardening variable, when its maximum value is reached in one point of an element it represents the total damage, namely the formation of a macroscopic crack.
It is important to understand, like Krätzig, W. and Pölling, R. (2004) claim, that micro-fracturing and damage theories are equal, in fact damage by tension and micro-cracking in compression follow the same elasto-plastic damage theory.
Damage or stiffness degradation is related to the entire cracking process, from micro cracks growth to their interconnection, to simulate this phenomenon Luccioni et al. (1996) introduced a continuum damage mechanics
On the other hand, as claimed by Nguyen, G. and Korsunsky, A. (2008), the choice of model parameters sometimes appears to be rather arbitrary, without a clear connection with the experimental methods used to determine the mechanical properties of the material.
An analysis on the combination of a damage approach with a plasticity one is made by Grassl (2009), the researcher considers the disadvantages and the qualities of both approaches.
The main drawbacks of the stress-based plasticity models are the implicit stress evaluation procedure and the inability to describe the stiffness degradation. On the other hand, strain-based damage mechanics models are based on the concept of a gradual reduction of the elastic stiffness driven by a total strain measure, but it cannot describe irreversible deformations. Combinations of plasticity and damage are usually based on isotropic plasticity combined with either isotropic or anisotropic damage. Anyway, combinations of isotropic damage and plasticity are widely used, indeed one popular class of models relies on a combination of stress-based plasticity formulated in the effective stress space combined with a strain-based damage model.
In the end, the constitutive parameters that govern the damage plasticity model are well described in Jankowiak, T. and Łodygowski, T. (2005), they are four different value that identify not only the shape of the flow potential surface but also the characteristics of the yield surface. In this case, for the flow potential G, it is used the Drucker-Prager hyperbolic function as shown in the equation below:

$$G = \sqrt{(f_c - m \cdot f_t \cdot \tan\beta)^2 + \bar{q}^2} - \bar{p} \cdot \tan\beta - \sigma$$

with f_t is the uniaxial tensile strength of concrete and f_c is the compressive one; the dilatation angle in the p-q plane at high confining pressure is indicated with the letter β; in the end m is the eccentricity of the plastic potential surface. The flow potential surface is defined in the p-q plane, where $\bar{p} = -\frac{1}{3}\bar{\sigma} \cdot I$ is the effective hydrostatic stress and $\bar{q} = \sqrt{\frac{3}{2}\bar{S}^2}$ is the Mises equivalent effective stress, where S is the deviatoric part of

the effective stress tensor $\bar{\sigma}$. Starting from the loading function proposed by Lubliner, the following equation is used to represent the yield condition that the plastic-damage model uses:

$$F = \frac{1}{1-\alpha}(\bar{q} - 3\alpha \cdot \bar{p} + \theta(\tilde{\varepsilon}^{pl})\langle\bar{\sigma}_{max}\rangle - \gamma\langle-\bar{\sigma}_{max}\rangle) - \bar{\sigma}_c(\tilde{\varepsilon}^{pl})$$

In this equation, the parameter γ delineates the shape of loading surface in the deviatoric plane while the parameter α is obtained from the Kupfer's curve. $\bar{\sigma}_{max}$ represents the algebraically maximum eigenvalue of the tensor $\bar{\sigma}$. In the previous equation, the Macauley bracket $\langle\cdot\rangle$ is present, it is defined by $\langle x\rangle = \frac{1}{2}(|x| + x)$. In the end, the function $\theta(\tilde{\varepsilon}^{pl})$ is obtained using the following equation:

$$\theta(\tilde{\varepsilon}^{pl}) = \frac{\bar{\sigma}_c(\tilde{\varepsilon}^{pl})}{\bar{\sigma}_t(\tilde{\varepsilon}^{pl})}(1-\alpha) + (1+\alpha)$$

where $\bar{\sigma}_t$ and $\bar{\sigma}_c$ are the effective tensile and compressive cohesion stresses, respectively, and the parameter α:

$$\alpha = \frac{(f_{b0}/f_c) - 1}{2(f_{b0}/f_c) - 1}$$

To evaluate the parameter α a biaxial laboratory test is needed, in fact it depends on the ratio of the biaxial compressive strength f_{b0} and uniaxial compressive strength.
Furthermore, a triaxial compression test is necessary to evaluate the parameter γ, in fact it is obtained from the following formula:

$$\gamma = \frac{3(1-\rho)}{2\rho + 2}$$

in which there is the quantity ρ, defined at a given state $\bar{p}$ as:

$$\rho = \frac{\left(\sqrt{J_2}\right)_{TM}}{\left(\sqrt{J_2}\right)_{CM}}$$

where J_2 is the second invariant of stress deviator for the Tensile Meridian ($\sigma_1 > \sigma_2 = \sigma_3$) and the Compressive Meridian ($\sigma_1 = \sigma_2 > \sigma_3$) in the yield surface.
In Figures 2.5 and 2.6 the dependences between stress-cracking strain ($\tilde{\varepsilon}_t^{ck}$) in tension and stress – crushing strain ($\tilde{\varepsilon}_c^{in}$) in compression are shown.

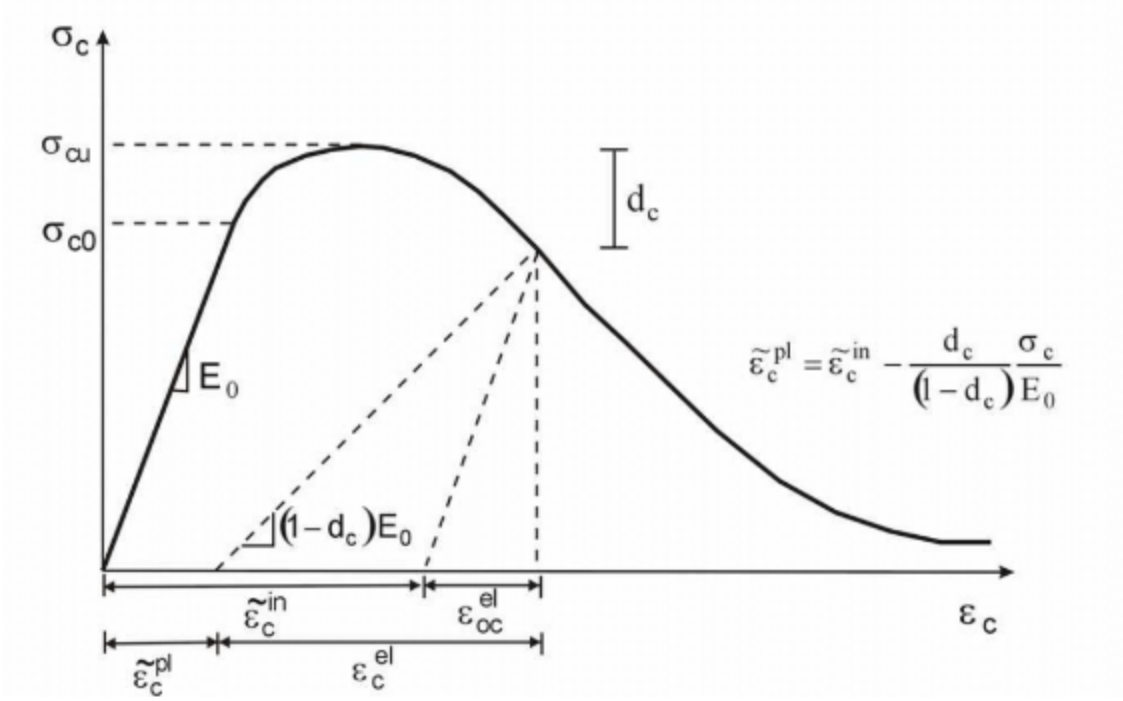

Figure 2.5 *Dependence $\sigma - \varepsilon$ in compression for CDP model*

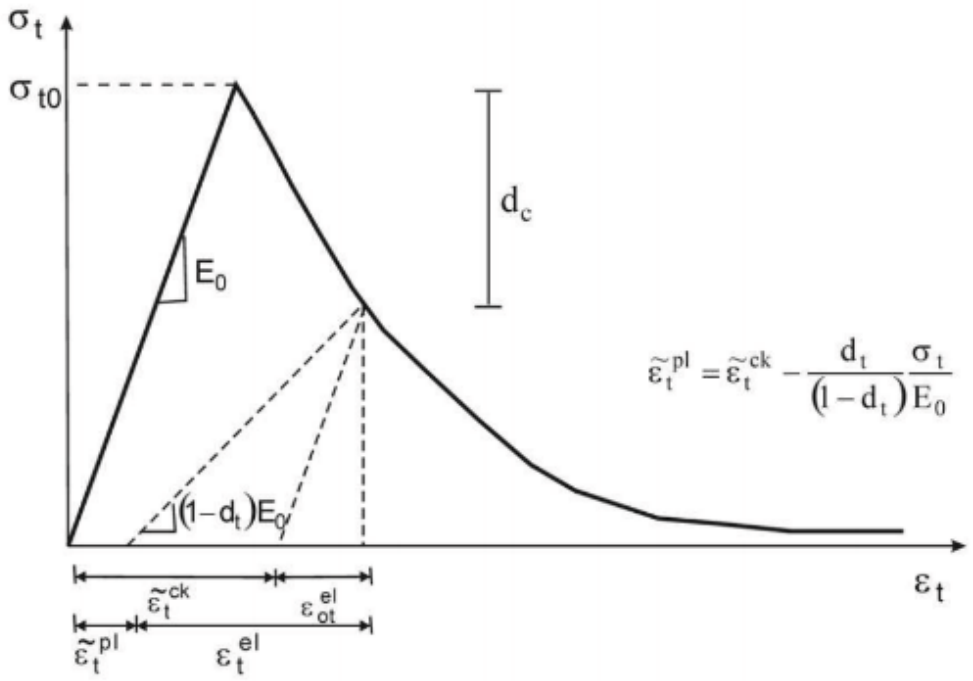

Figure 2.6 *Dependence $\sigma - \varepsilon$ in tension for CDP model*

It is important to determine the reliance between d_t and cracking strain and d_c and crushing strain. To characterise the aspect of flow potential and the loading surfaces four parameters are used, namely $\beta, m, f,$ and γ. The latter modifies the shape of the loading surface in the deviatoric plane, it is widely agreed a value equal to 0.66667 for this parameter.

The parameter f is obtained from the Kupfer's curve, the parameter α is a function of f, as it is shown in a precedent equation.
Finally, m and β are evaluated fulfilling the best fitting of the curve, in the meridian plane, to the experimental results. Usually m ranges between 1 and 1.5 and β ranges between 0.6 and 0.75.

3. Methodology

3.1 Constitutive SFRC Model

The constitutive SFRC model designed by Lok and Xiao (1998) is particularly suitable for this dissertation work, not only because it was used in the Abbas et al (2014) paper, that is the basis of this work, but also because of its wide range of validity, in fact this model can be used, with good results, for a range of fibre volume fraction between 0.5% and 2.5%, namely the range considered by Kotsovos et al. (2006) in the experiments. In Figure 3.1 is represented the stress-strain relationship both in tension and in compression.

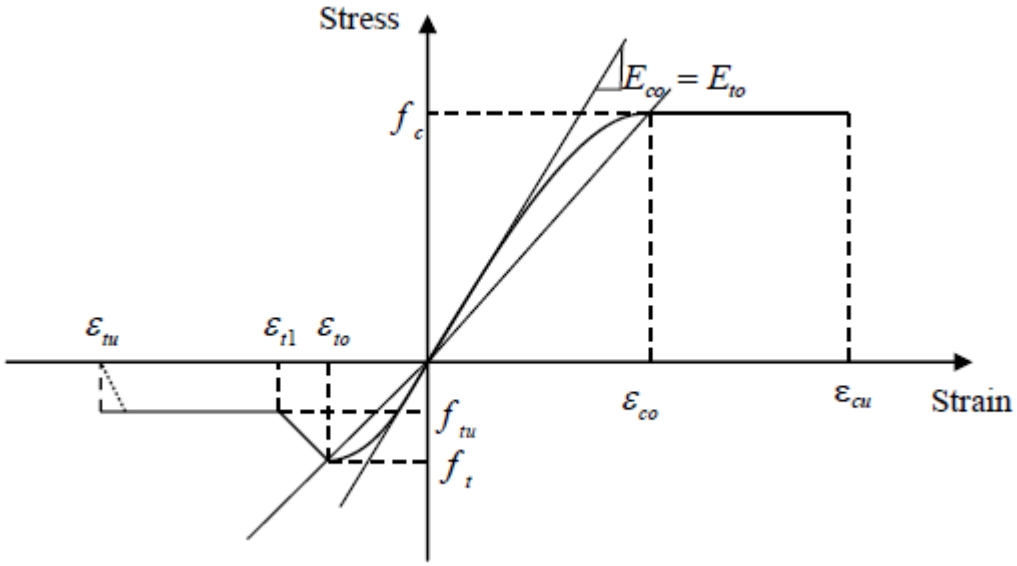

Figure 3.1 *Constitutive stress-strain relationship (Lok and Xiao, 1998)*

The compressive part of the constitutive model designed by Lok and Xiao (1999) is the classic parabola-rectangle trend used in the Eurocode 2 as well, they stated that the effect of fibres in compression is negligible. The model is characterized by two parts: the first one is obtained from the following expression:

$\sigma = f_c[2(\varepsilon/\varepsilon_{co}) - (\varepsilon/\varepsilon_{co})^2] \qquad (\varepsilon \leq \varepsilon_{co})$

where f_c is compressive strength of concrete, the second part is constant with $\sigma = f_c$ up to the ultimate strain ε_{cu}.

Lok and Xiao (1999) stated that the ultimate compressive strain, ε_{cu} for SFRC at 0.003 may be conservative. For fibre volume fraction between 0.5 and 2%, Lok and Xiao (1999) suggested the value of 0.0038.

However, in this work the author preferred to use a different constitutive model in compression taking into account the Concrete Damaged Plasticity Model that needs the definition of a damage parameter in compression. Thus, the chosen model in compression is described in section 3.2.

Regarding the tensile relationship this model is similar to the Lok and Pei (1998) one. It is possible to divide the trend in three intervals in terms of strain, thus the following expressions describe the stress-strain relations:

$$\sigma = f_t \left[2\left(\frac{\varepsilon}{\varepsilon_{t1}}\right) - \left(\frac{\varepsilon}{\varepsilon_{to}}\right)^2\right] \qquad 0 \leq \varepsilon \leq \varepsilon_{to}$$

$$\sigma = f_t \left[1 - \left(\frac{1}{f_{tu}}\right)\left(\frac{\varepsilon - \varepsilon_{to}}{\varepsilon_{t1} - \varepsilon_{to}}\right)^2\right] \qquad \varepsilon_{to} \leq \varepsilon \leq \varepsilon_{t1}$$

$$\sigma = f_{tu} \qquad \varepsilon_{t1} \leq \varepsilon \leq \varepsilon_{tu}$$

The first part represents the elastic behaviour that ends when the ultimate tensile strength f_t is reached, afterwards, as in Lok and Pei (1998), cracking starts and fibres act to improve the concrete behaviour. When the strain ε_{t1} is reached and so the residual strength f_{tu}, the second part is over.
These values are defined by Lok and Pei (1998) as:

$$f_{tu} = \eta \nu_f \tau_d \frac{L}{d}$$

$$\varepsilon_{t1} = \tau_d \frac{L}{d} \frac{1}{E_s}$$

where η is fibre orientation factor in a 3-dimensional (3D) case, Lok and Xiao (1999) used the value of η as 0.405 for beams. As seen before τ_d is the bond stress interaction between concrete and steel fibres, L/d is aspect ratio of the steel fibre and E_s is the elastic modulus of steel fibre and ν_f is defined as the fibre volume fraction.
The third part symbolize fibres bridging the crack until they pull out.
This model can be correlate with the moment-curvature curve showing an important aspect of SFRC, namely the relation between fibre volume fraction and softening or hardening behaviour. As shown in Figure 3.2, the contribution of fibres is relevant after cracks arising, in fact in the range between the strains ε_{to} and ε_{t1} concrete and fibres both bear the load, so depending on the fibres pull-out, fibre volume fraction and bridging behaviour, the flexural moment-curvature response could be classified as softening (Case 1), idealised elasto-plastic (Case 2), or hardening (Case 3).

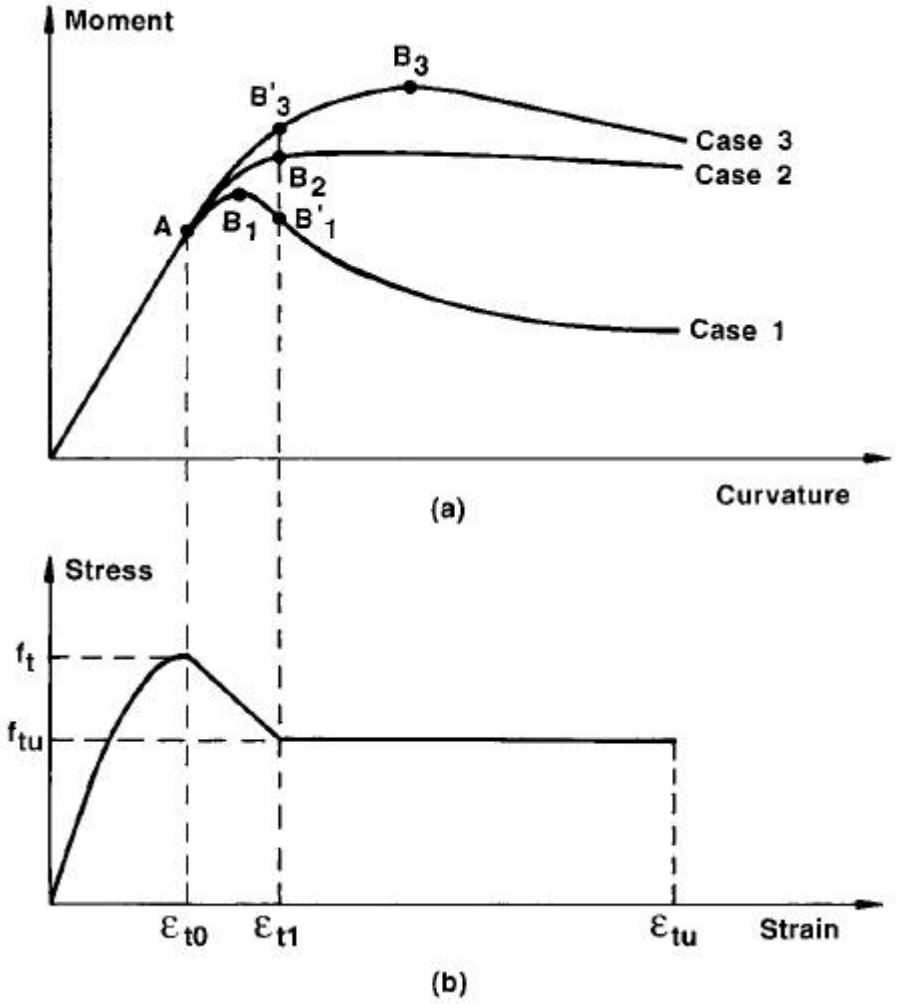

Figure 3.2 *Relationship between (a) Moment-curvature response and (b) Tensile stress-strain behaviour (adapted from Lok and Xiao, 1999)*

3.2 Concrete Damaged Plasticity Model

The Concrete Damaged Plasticity Model, implemented in ABAQUS software, is born from the Drucker–Prager strength hypothesis and it was modified with respect the failure surface, in fact, as shown in Figure 3.3, the deviatoric cross section must be not a circle. As stated from Kmiecik, P. and Kaminski, M. (2011), the failure surface is governed by K_c, parameter that represents the ratio of the distances between the hydrostatic axis and respectively the compression meridian and the tension meridian in the deviatoric cross section. This parameter ranges from 0.5 to 1, value for which the deviatoric cross section of the failure surface is a circle, like in the Drucker-Prager theory. The Concrete Damaged Plasticity model suggests to adopt K_c=2/3.

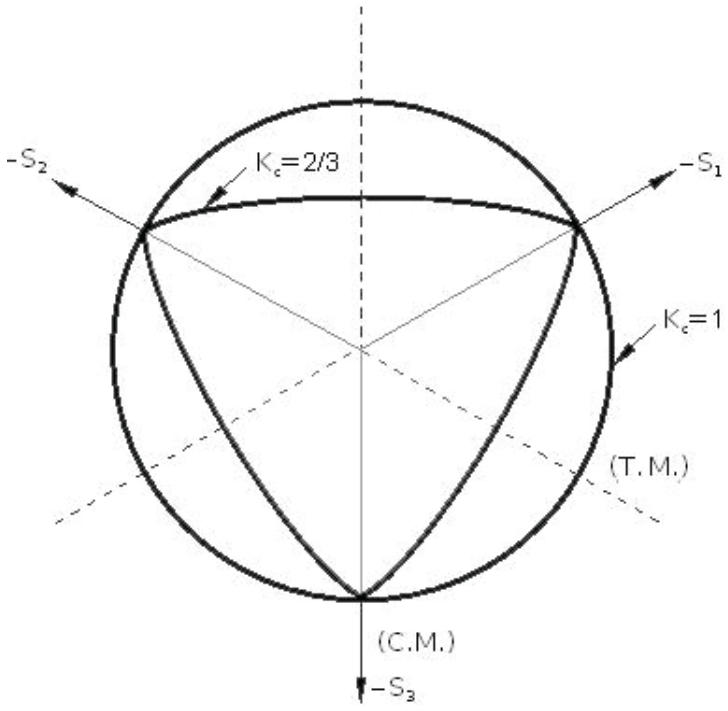

Figure 3.3 *Deviatoric cross section of failure surface in CDP model*

Furthermore, also in the meridian plane in the stress space something changes, in fact experimental results show that meridians are curves and that the plastic potential surface is a hyperbola as shown in Figure 3.4.

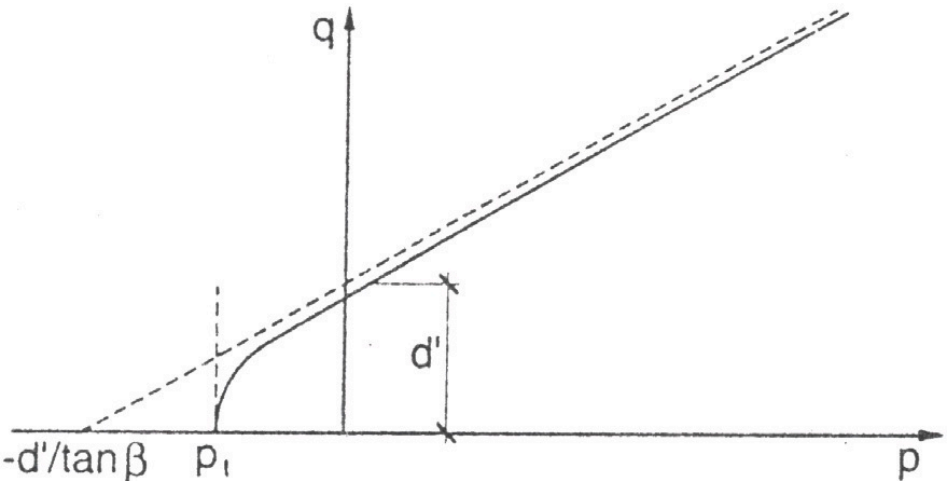

Figure 3.4 *Hyperbolic surface of plastic potential in meridional plane*

The hyperbola's shape can be modified by *eccentricity,* namely a small positive value that indicates the rate of approach of the hyperbola to its asymptote, in other words, this parameter expresses the distance between the vertex of hyperbola and its centre. It is determined as the ratio of tensile strength to compressive strength and the suggested value is ε = 0.1.

In the end, the last parameter that is necessary to well described the concrete behaviour is the dilatation angle ψ, it is defined as the angle of inclination of the failure surface measured in the meridional plane, physically it represent the internal friction angle of concrete.

The uncontested merit of this Model is that the parameters, which manage the overall behaviour, represent clearly physical characteristics.

It is well known that concrete is a brittle material, characterized by cracking, but as stated by Alfarah et al. (2017), when the stress is cyclic reversal the cracks can be closed again and so the broken parts can be repaired. But in reinforced concrete there is reinforcement as well, very ductile material that cannot be reassembled, so the overall behaviour can be described using a model that combine the damage, used to analyse concrete, and plasticity, suitable for steel bars. In Figure 3.5 three different models are graphically displayed in terms of uniaxial stress-strain. Observing the three models, it is clear that damage causes a stiffness degradation, in fact the elastic modulus E_0, which represent the undamaged material in the loading branches, is reduced by the terms $(1-d)$ in the unloading branches. Thus, it is possible to express the trend of the elastic stiffness in terms of a scalar degradation variable d:

$$E = (1-d)E_0$$

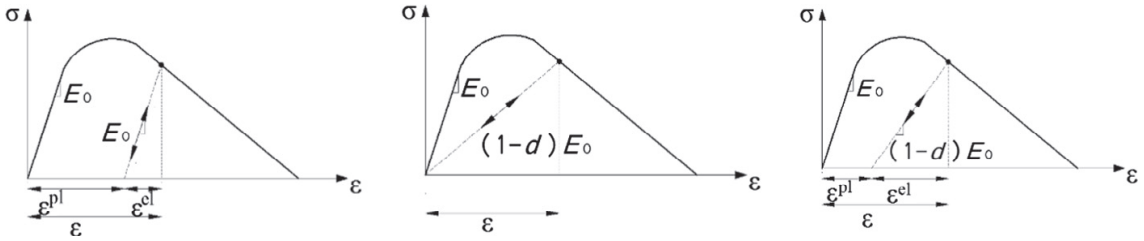

(a) Plasticity Model (b) Damage Model (c) Plastic Damage Model

Figure 3.5 *Representation of CPDM*

The damage parameter d range between 0, intact material, and 1 complete failure. Therefore, the stress-strain relation in the damage plasticity model are:

$$\sigma_c = (1 - d_c)E_0\left(\varepsilon_c - \varepsilon_c^{pl}\right)$$

$$\sigma_t = (1 - d_t)E_0\left(\varepsilon_t - \varepsilon_t^{pl}\right)$$

In the previous expressions, the degradation variable is decomposed in the compressive and tensile factor, the relation between them all is:

$$1 - d = (1 - s_t d_c)(1 - s_c d_t)$$

where s_c and s_t are dimensionless coefficients accounting for stress state and stiffness recovery effects, being given by:

$$s_c = 1 - h_c\left(1 - r^*(\sigma_{11})\right)$$

$$s_t = 1 - h_t r^*(\sigma_{11})$$

In the previous equations σ_{11} is the first principal uniaxial stress (positive for tension), r^* is a stress state parameter being $r^*(\sigma_{11}) = 1$ for tension and $r^*(\sigma_{11}) = 0$ for compression, and h_c and h_t are weighting factors ranging between 0 and 1.
Factor h_c accounts for re-closing of cracks after tension-compression reversal; h_t represents recovery of crushed concrete after compression-tension reversal.

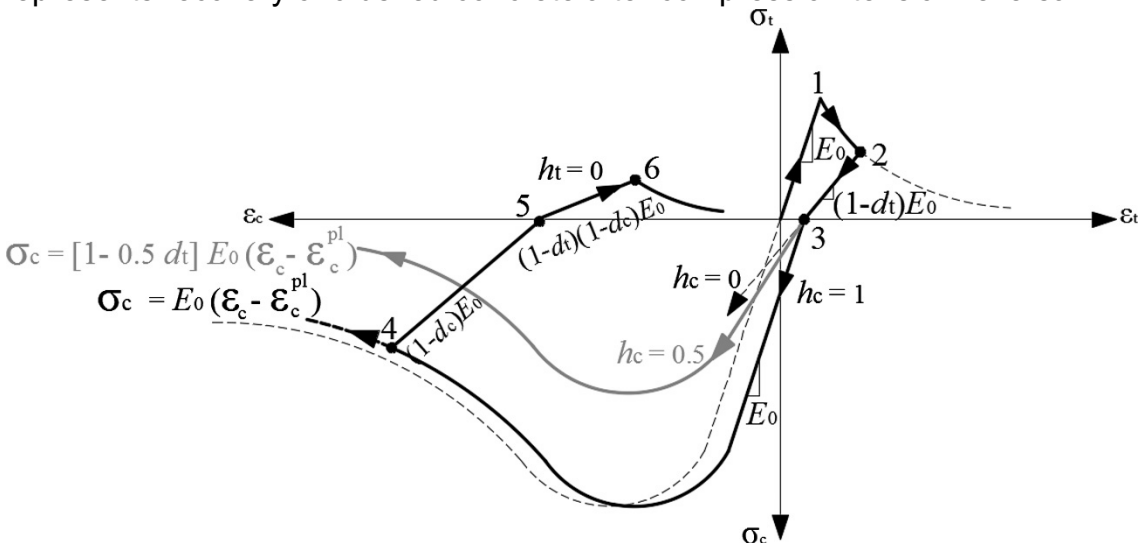

Figure 3.6 *Uniaxial loading-unloading law*

In Figure 3.6 a graph drawn from ABAQUS manual is displayed to better understand how h_c and h_t influence the overall behaviour during a cyclic loading. So, cracking start after the peak point 1 and proceed until point 2, which correspond to the onset of the unloading branch, in this point $d_c = 0$, $r^* = 1$, and $s_c = 1$. Moreover, in this case $d = d_t$ and afterwards the unloading branch has a slope equal to $(1 - d_t)E_0$. From point 2 to point 3 cracks decrease until complete closure. After point 3 the load is reversed and the parameter h_c assume an important role, in fact from previous equations the following value are obtained $r^* = 0$, $s_c = 1 - h_c$, $s_t = 1$, $d_c = 0$, and $d = (1 - h_c)d_t$. It is evident how the trend depends on h_c, so three different values of h_c are plotted in Figure 3.6:

- $h_c = 0$ (no crack is closed) with slope $(1 - d_t)E_0$;
- $h_c = 0.5$ (half of the cracks are closed) with slope $(1 - 0.5d_t)E_0$;
- $h_c = 1$ (all cracks are closed) with slope E_0.

In the third case the compressive strength remains constant.
The compressive part of the diagram ends in point 4, correspondent of point 2 in tension, so from now on an unloading branch begins with $r^* = 0$, $s_c = 1 - h_c$, $s_t = 1$, and
$1 - d = (1 - d_c)[1 - (1 - h_c)d_t] = 1 - d_c$
Point 5 represents stress reversal, considering $h_t = 0$, the subsequent branch has a slope $(1 - d_c)(1 - d_t)E_0$. In the end, point 6 is the tensile peak from which the cycle starts again.
After the cycle is defined, it is clear that the damage parameters in compression and in tension have a critical role. So, defining these parameters is very important to understand the entire behaviour. Compressive and tensile parameters are defined as the part of normalized energy dissipated by damage:

$$d_c = \frac{1}{g_c}\int_0^{\varepsilon_c^{ch}} \sigma_c d\varepsilon_c^{ch} \qquad d_t = \frac{1}{g_t}\int_0^{\varepsilon_t^{ck}} \sigma_t d\varepsilon_t^{ck}$$

where ε_c^{ch} and ε_t^{ck} are the crushing and cracking strains respectively. Normalization coefficients g_c and g_t, displayed in Figure 3.7, represent the energies per unit volume dissipated by damage during the entire deterioration process:

$$g_c = \int_0^{\infty} \sigma_c d\varepsilon_c^{ch} \qquad g_t = \int_0^{\infty} \sigma_t d\varepsilon_t^{ck}$$

Previous equations demonstrate that d_c and d_t range between 0 (no damage) and 1 (destruction).

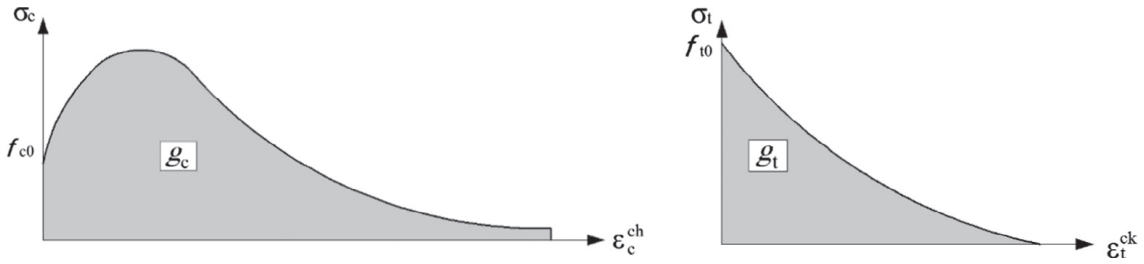

Compression (g_c), Tension (g_t)

Figure 3.7. *Parts of energy dissipated by damage*

Using the Lok and Xiao constitutive model also for compression lead outcomes not consistent with the experimental, so in compression the model designed by Alfarah et al. (2017) is used. In this section, the stress-strain law is presented together with the equation to evaluate the damage parameter in compression. In Figure 3.8 the constitutive model in compression is shown, thus the main quantities are described in detail.

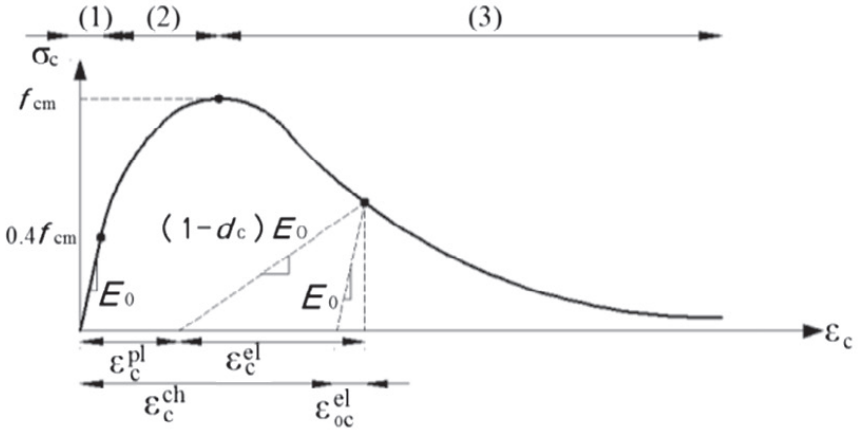

Figure 3.8 *Assumed uniaxial model of concrete behaviour in compression*

First of all, the characteristics of the concrete are depicted: f_{cm} represents the compressive stress strength and the corresponding strain is ε_{cm}, that is assumed $\varepsilon_{cm} = 0.0022$; this stress and the deformation modulus are expressed in Mpa. Then the strains that characterise the constitutive behaviour are delineated: ε_c^{ch} and ε_{0c}^{el} are the crushing and elastic undamaged components of strain; instead ε_c^{pl} and ε_c^{el} are the plastic and elastic damaged components.
The first branch in Figure. 3.8 is linear, $\sigma_{c(1)} = E_0 \varepsilon_c$, until the stress reaches the value $0.4 f_{cm}$, E_0 is the secant modulus that corresponds to 0.4 f_{cm} stress and it is in function of E_{ci}, described later.
The second segment, that works from 0.4 f_{cm} and f_{cm} is quadratic:

$$\sigma_{c(2)} = \frac{E_{ci}\frac{\varepsilon_c}{f_{cm}}\left(\frac{\varepsilon_c}{\varepsilon_{cm}}\right)^2}{1 + \left(E_{ci}\frac{\varepsilon_{cm}}{f_{cm}} - 2\right)\frac{\varepsilon_c}{\varepsilon_{cm}}} f_{cm}$$

In the previous equation, E_{ci} is the modulus of deformation of concrete for zero stress, obtained by $E_{ci} = 10000 {f_{cm}}^{1/3}$ and $E_0 = (0.8 + 0.2 f_{cm}/88) E_{ci}$, both are in Mpa.
The third branch is the descending one, in this segment the model designed by Alfarah et al. (2017) diverges considerably from the classic behaviour used also by Lok and Xiao (1999).
The following equation is used to model the descending branch:

$$\sigma_{c(3)} = \left(\frac{2 + \gamma_c f_{cm} \varepsilon_{cm}}{2 f_{cm}} - \gamma_c \varepsilon_c + \frac{\varepsilon_c^2 \gamma_c}{2\varepsilon_{cm}}\right)^{-1}$$

$$\gamma_c = \frac{\pi^2 f_{cm} \varepsilon_{cm}}{2\left[\frac{G_{ch}}{l_{eq}} - 0.5 f_{cm}\left(\varepsilon_{cm}(1-b) + b\frac{f_{cm}}{E_0}\right)\right]^2} \qquad b = \frac{\varepsilon_c^{pl}}{\varepsilon_c^{ch}}$$

These equations are in function of G_{ch} is the crushing energy per unit area, and l_{eq} is the characteristic length, which depends on the mesh size, the type of finite element and the crack direction. In this case, regular hexahedron elements are utilized so the characteristic length is equal to 30mm, because it is taken as the volume divided by the largest face area. Using these parameters, the model becomes more sophisticate

because it takes into account not just an energy parameter but also a parameter that derived from the finite element model representation.
To evaluate the value of the parameter b, an iterative procedure is necessary, the initial value assumed is b=0,9. The final value of b affects the softening branch of the compressive stress strain relation.
As stated previously the descending branch is very different from the standard constitutive model for concrete in compression, in fact it approaches asymptotically to zero. In this case the maximum strain value in compression, that normally is taken as 0,0035, has to be estimated by imposing the equivalence between the crushing energy G_{ch} and the area under the corresponding compressive stress-strain law multiplied by the characteristic length.
The author found that for an ultimate strain equal to 0,035, and a l_{eq} equal to 30mm the equivalence is fulfilled.
In all the literature regarding the Concrete Damaged Plasticity Model, equations explaining clearly the contribution of the compressive damage parameter are limited. Alfarah et al. (2017) instead found a clear relationship between the damage parameter in compression and not only the concrete strength but also the crushing and fracture energies and the mesh size:

$$d_c = 1 - \frac{1}{2 + a_c}[2(1 + a_c)exp(-b_c\varepsilon_c^{ch}) - a_c exp(-2b_c\varepsilon_c^{ch})]$$

Assuming $f_{c0} = 0.4f_{cm}$ and $f_{tm} = f_{t0} = 0.3016{f_{ck}}^{2/3}$ the coefficients, participating in the d_c equation, are obtained:

$$a_c = 7.873 \quad a_t = 1 \quad b_c = \frac{1.97(f_{ck} + 8)}{G_{ch}} l_{eq} \quad b_t = \frac{0.453{f_{ck}}^{2/3}}{G_F} l_{eq}$$

In Figure 3.9 the damage parameter used in this work is depicted.

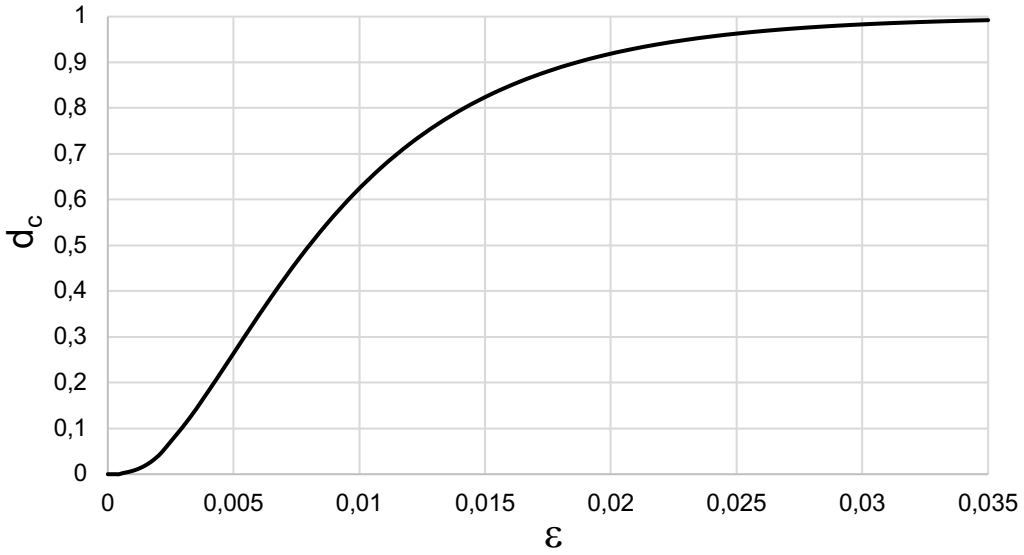

Figure 3.9 *Damage parameter in compression*

On the other hand, for the damage parameter in tension, a linear function was used by the author. As shown in Figure 3.10 it starts from 0 in correspondence of the tensile stress strength, evaluated in section 3.1 and it reaches the value of 0,99 in correspondence of the ultimate tensile strain equal to 0,02.

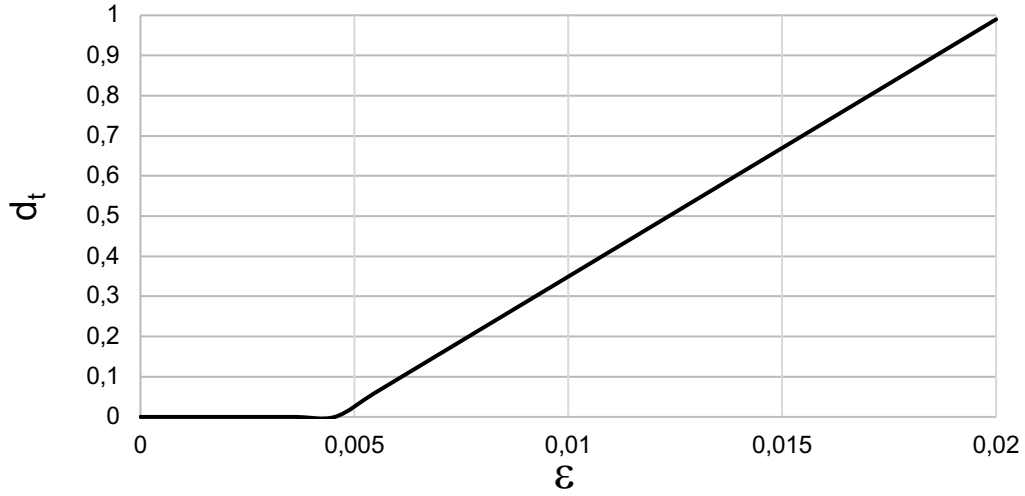

Figure 3.10 *Damage parameter in tension*

Finally, Alfarah et al. (2017) present an algorithm to draw the stress-strain curve in compression, the algorithm is composed by the following ten steps:

1. The input data are the concrete compressive strength f_{ck}, the parameters of Concrete Damaged Plasticity Model, namely the dilatation angle φ, eccentricity ε, ratio of second stress invariants K, the viscosity parameter *v* and the ratio between biaxial compressive yield strength and uniaxial compressive yield strength f_{b0}/f_{c0}, the mesh sizel_{eq}, and the ratio b. Initial assumption is b = 0.9.
2. Calculate the compressive and the tensile stress strength
   $f_{cm} = f_{ck} + 8 \quad f_{tm} = 0.3016{f_{ck}}^{2/3}$
3. State the strain at compressive stress strength as $\varepsilon_{cm} = 0.0022$.
4. Calculate the initial tangent modulus of deformation of concrete
   $E_{ci} = 10000{f_{cm}}^{1/3}$and the undamaged modulus of deformation
   $E_0 = (0.8 + 0.2f_{cm}/88)E_{ci}$.
5. Calculate the fracture/crushing energy (N/mm)
   $G_F = 0.073f_{cm}^{0.18} \quad G_{ch} = \left(\frac{f_{cm}}{f_{tm}}\right)^2 G_F$
6. Build the three segments of the concrete uniaxial compressive law. As stated before, the compressive strain is bounded; the selected upper bound should fulfil the condition that the crushing energy G_{ch} is reached.
7. Calculate the damage parameters according:
   $$a_c = 7.873 \quad a_t = 1 \quad b_c = \frac{1.97(f_{ck} + 8)}{G_{ch}} l_{eq} \quad b_t = \frac{0.453{f_{ck}}^{2/3}}{G_F} l_{eq}$$
8. Calculate the compressive damage variables (damage evolution)
9. Calculate the compressive plastic strain:
   $$\varepsilon_c^{pl} = \varepsilon_c^{ch} - \frac{\sigma_c d_c}{(1 - d_c)E_0}$$
10. Calculate the average value of ratio b and compare with the assumption in step 1. Repeat until reaching convergence.

3.3 Case study

The experimental element designed and used by Kotsovos et al. (2006) is shown in Figure 3.11. As explained in the Kotzovos paper, in this section the experimental features are presented. The element is supported by roller and hinge positioned under the bottom flange of the frame beam, this is necessary to allow reactions to act both upwards and downwards during cyclic loading.

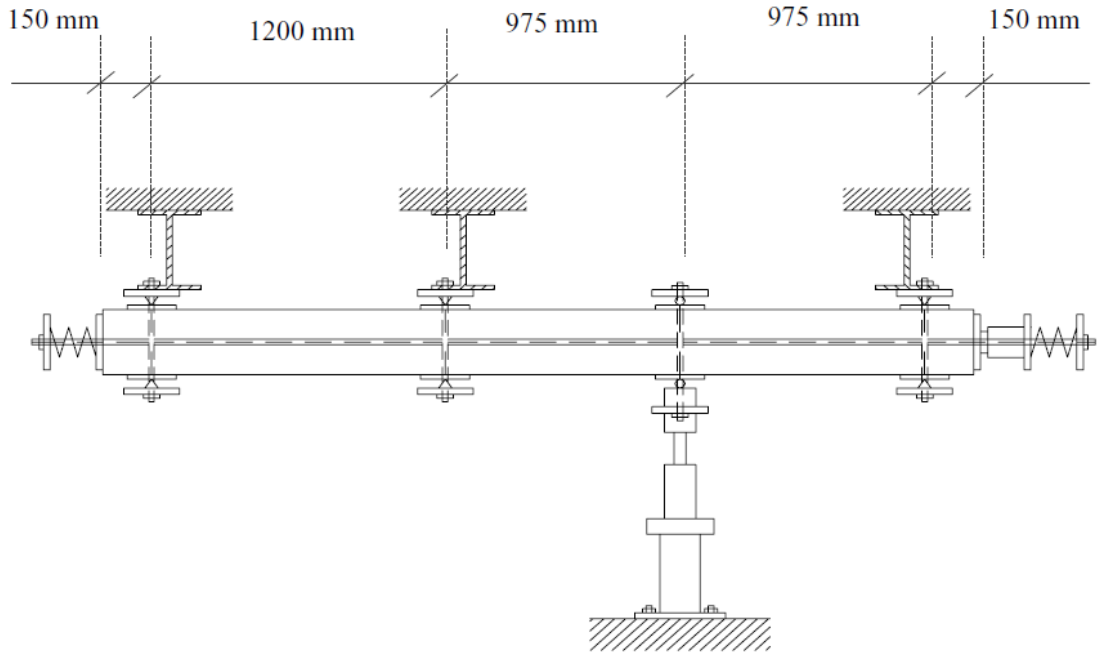

Figure 3.11 *Experimental setup*

Specimens analysed by Kotsovos et al. (2006) are made of whether plain concrete or fibre reinforced concrete, in this dissertation only two beams are examined, namely D16-FC-30-C and D16-FC-30-M. The fibres used in the experiments were DRAMIX RC-80/60-BN, with a length of 60mm and a diameter equal to 0.75mm. The specimens have a three-part name, with the constituent parts arranged in sequence as follows: *part 1*, the diameter of the longitudinal steel reinforcement; *part2*, the concrete mix used; *part 3*, the loading history adopted (monotonic or cyclic). In Figure 3.12 the reinforcement arrangement is shown, the longitudinal bars have a diameter of 16mm and an average yield-stress (f_y) and ultimate strength (f_u), as obtained from tension tests, equal to 556Mpa and 743Mpa respectively. On the other hand, stirrups have an 8mm diameter, an average yield-stress equal to 471Mpa and ultimate strength equal to 684Mpa. The modulus of elasticity for steel (*Es*) is 200 Gpa.
The mix design was provided by Unibeton, using local aggregate furnished by their subsidiary in Greece, Halyps S.A. The specimen (including six test cylinders) is cured under wet hessian for one month, after which it is stored under laboratory ambient conditions at a temperature of approximately 20°C and a relative humidity of approximately 50%. The concrete compressive strength is determined by crushing the six cylinders at the time of testing, approximately two months after casting. The corresponding compressive strengths is equal to 37Mpa.

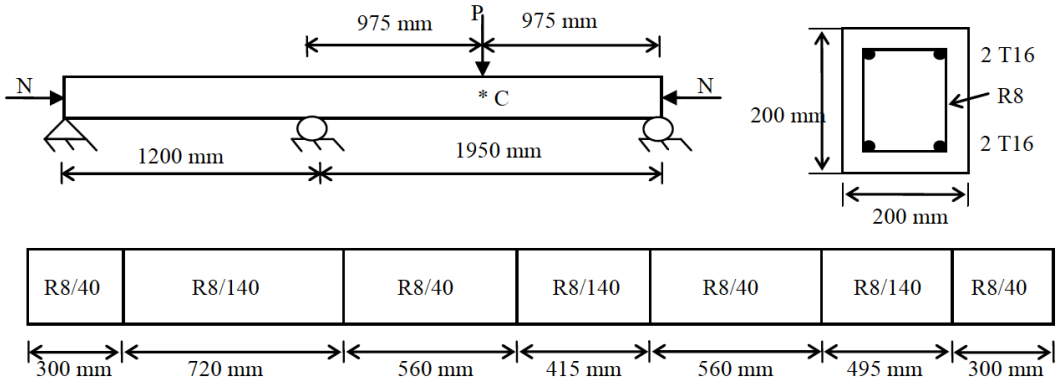

Figure 3.12 *Dimensions, loading arrangement and reinforcement detailing of the column (adapted from Kotsovos et al, 2007)*

Regarding the load pattern, the element is loaded by whether axial or transverse force to better mimic a column load pattern.
At the beginning, axial load *N* is applied and increases to a value equal to $N \approx 0.2N_u = 0.2f_c bh$, where N_u is the maximum value of *N* that can be sustained by the specimen in pure compression and f_c the uniaxial cylinder compressive strength. The transverse load is displacement controlled and its trend is capable of marking cracks, the axial-compressive force is applied concentrically using an external pre-stressing force induced by high yield steel rods instead. The loading history used in the FE analyses is represented in Figures 3.13 and 3.14 both for monotonic and cyclic forces.

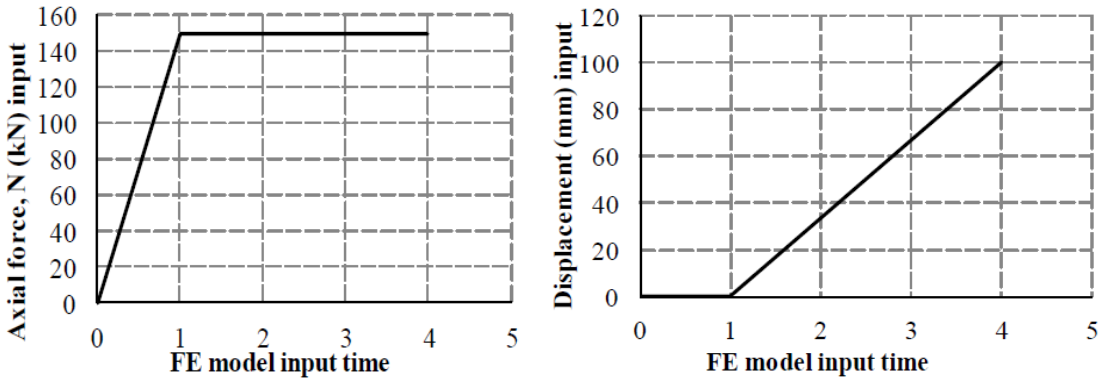

Figure 3.13 *Monotonic loading history*

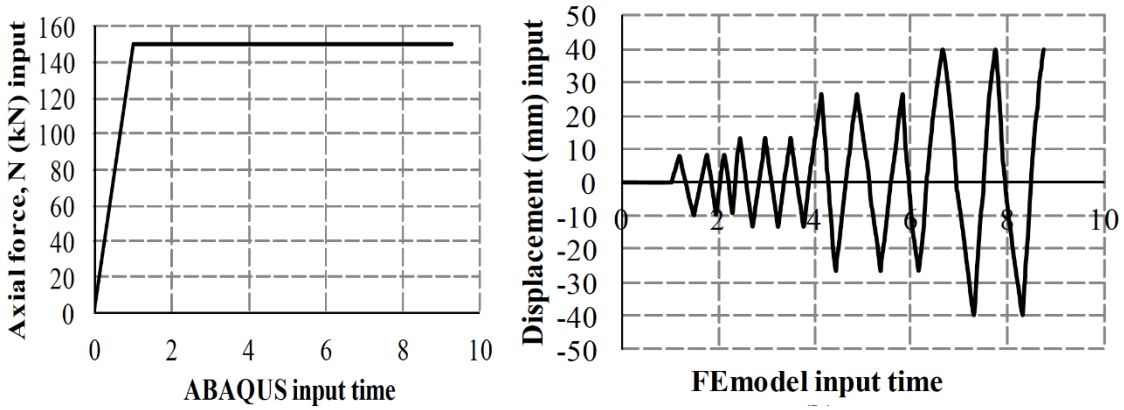

Figure 3.14 *Cyclic loading history*

4. Results and Discussion

4.1 Monotonic Load

In this section, the beam under monotonic load is analysed. First of all, a validation test is carried out to verify the model used, afterwards different beam arrangements are investigated to take into account the increasing in the fibres volume percentage V_f and the increasing in the stirrups spacing SI as well. The constitutive models used in tension and in compression are those previously analysed in sections 2 and 3, on the other hand, regarding the plasticity parameters, in the following section they are investigated in more detail. In all the analyses carried out in this section the ABAQUS dynamic solver is used, so to mimic a quasi-static FE analysis is important to avoid dynamic effect, to take into account this problem the energy ratio, namely the ratio between the kinetic energy and the strain energy, has to be smaller than 0.5%

4.1.1 Experimental validation

The validation of the Concrete Damaged Plasticity Model, against the experimental outcome and the result obtained using the Brittle Cracking Model as Abbas et al. (2014) did, is carried out. The beam used for the validation has a fibres volume percentage equal to 0,4% and the stirrup spacing is 0%, so the reinforcement arrangement used in this case is considered as the standard one. In Figure 4.1 the stress-strain relation is displayed.

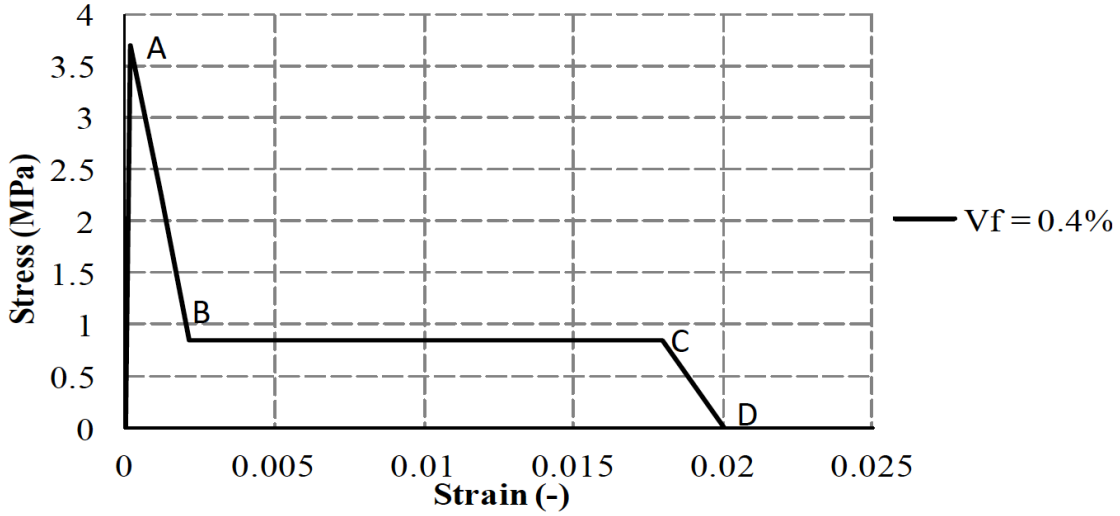

Figure 4.1 *Tensile stress-strain diagram adopted for calibration work of Kotsovos et al. (2007) SFRC columns*

The relation main points are listed in Table 4.1, this are obtained using the Lok and Xiao (1998) theory stated in section 2. The compressive behaviour is not conditioned by fibres, so it is always the same described in section 3.

Point	Stress (MPa)	Strain (‰)
0	0	0
Peak tensile stress (A)	3.70	0.215
Beginning of plateau (B)	0.85	2.120
End of plateau (C)	0.85	18
Ultimate cracking strain (D)	0	20

Table 4.1 *Tensile stress-strain for a SFRC mixture with V_f = 0,4%*

The mesh size used is the same of the Brittle Cracking Model analysis so it is equal to 30mm. In Figure 4.2 the load deflection curves are displayed for the cases investigated, the curves show a trend similar, especially until a displacement equal to 30 mm, then both the FE curves exhibit a higher trend, but the CDPM reaches a point of failure closer to the experimental one.

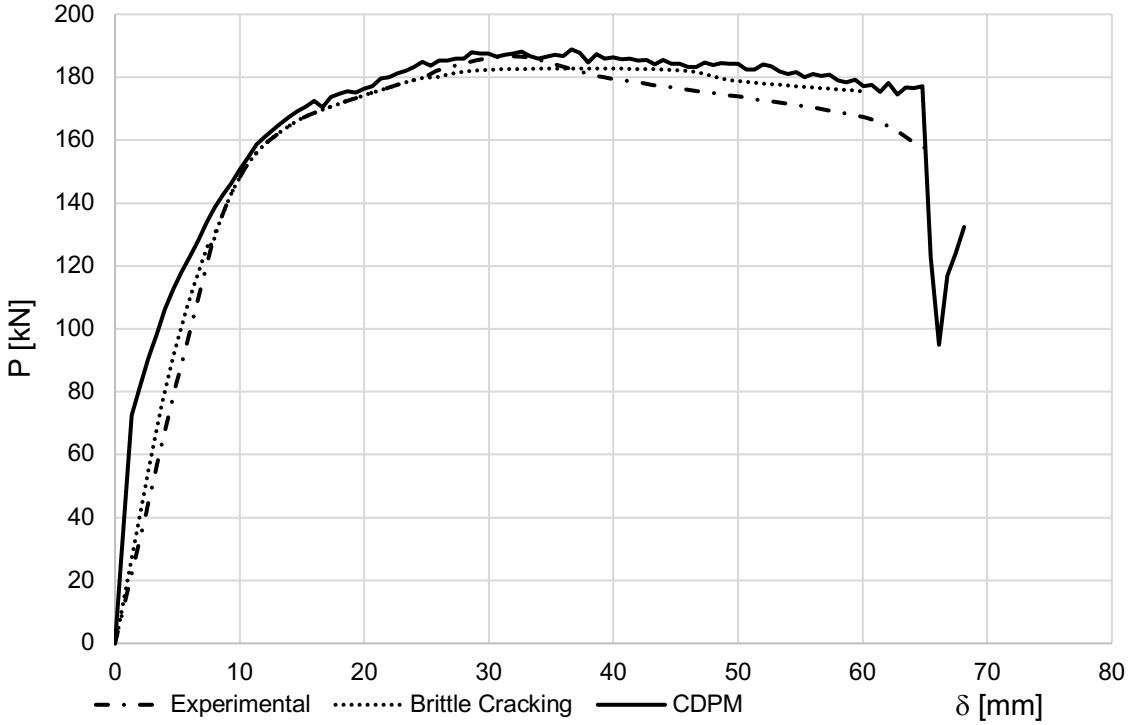

Figure 4.2 *Validation of CDPM load deflection curve with experimental and Brittle Cracking Model ones*

From the load deflection curves, it is possible to extrapolate the characteristic values listed in Table 4.2, namely the load at yield point P_y, the maximum load P_{max} and ultimate load of the column at failure P_u, and their respective deflections δ_y, δ_{Pmax} and δ_u, moreover the ductility μ, evaluated as the ratio between the deflection at failure and the deflection at yield point, and the ratio between the maximum load and the yield one is evaluated as well.

	P_y [kN]	δ_y [mm]	P_u [kN]	δ_u [mm]	P_{max} [kN]	δ_{Pmax} [mm]	$\mu=\delta_u/\delta_y$	P_{max}/P_y
Experimental	155	11	158	65,5	187	31,1	6,0	1,21
Brittle	144,3	9,7	174,1	60,3	182,9	44,7	6,2	1,267
CDPM	150,70	10	177,0	64,8	188,85	36,60	6,5	1,253

Table 4.2 *Characteristic values of load deflection curves*

Using the Concrete Damaged Plasticity Model the author had to choose the right value for the Plasticity parameters, namely the dilatation angle φ, eccentricity ε, ratio of second stress invariants K, the viscosity parameter *v* and the ratio between biaxial compressive yield strength and uniaxial compressive yield strength f_{b0}/f_{c0}. The value of the parameters, except the dilatation angle φ, are shown in Table 4.3.

K	e	f_{b0}/f_{c0}	*v*
0,66667	0,1	1,16	0,003

Table 4.3 *Plasticity parameters*

For the dilatation angle a more accurate analysis was carried out because this parameter influences more than the others the load deflection curves.
As shown in Figure 4.3 three different angles were chosen, namely ψ = 15°, ψ = 30° and ψ = 42°, this parameter represents the inclination of the failure surface and so when it is increased the correspondent load deflection curve mimics the behaviour of a stronger concrete.

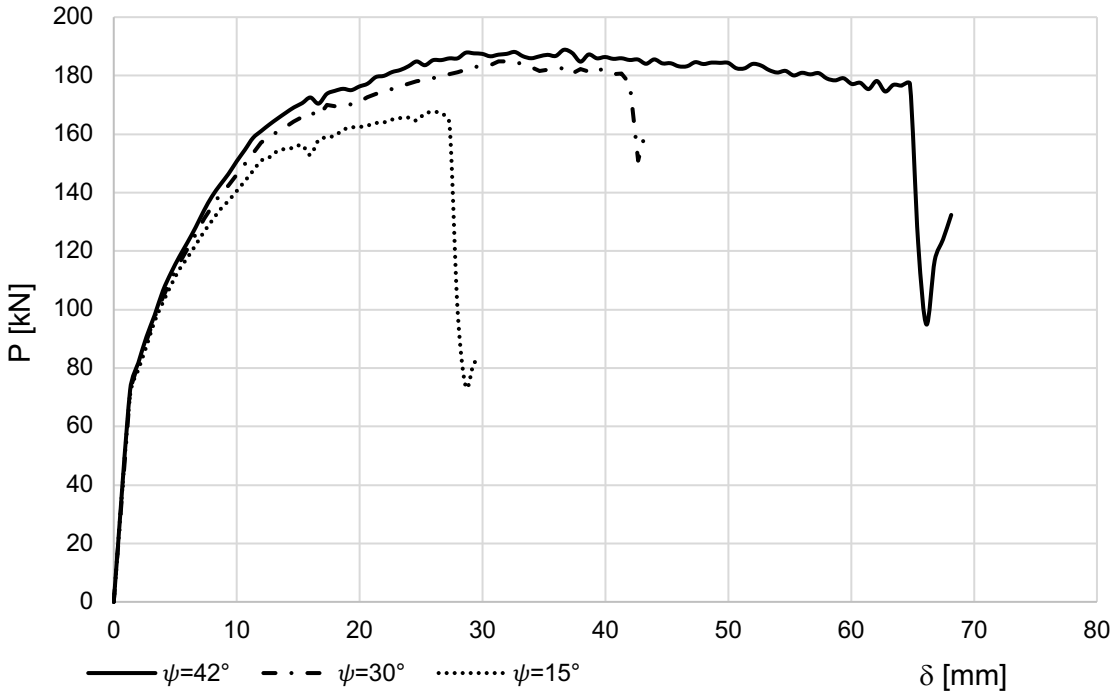

Figure 4.3 *Comparative analysis of* dilatation *angle*

In order to obtain the failure point of the column, the kinetic energy is plotted versus the deflection for all the different value as depicted in Figures 4.4, 4.5 and 4.6 for ψ = 42°, ψ = 30° and ψ = 15° respectively. The failure point corresponds to a sudden jump in the kinetic energy, it happens for a deflection equal to 64,8mm for ψ = 42°, 41,3mm for ψ = 30° and 26,7mm for ψ = 15°.

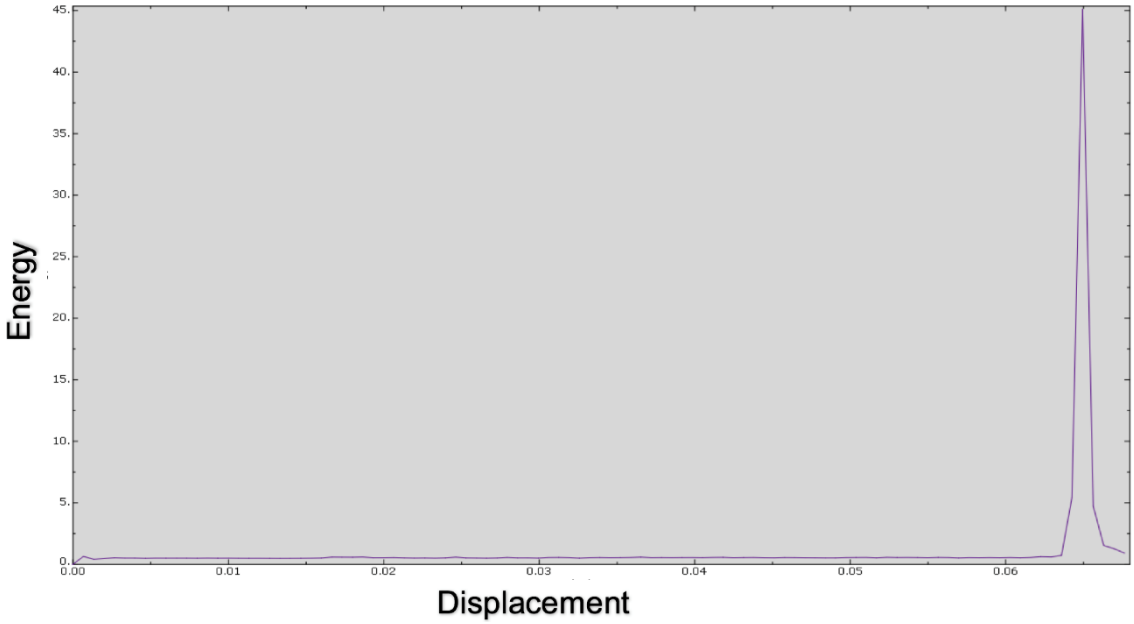

Figure 4.4 *Kinetic energy for ψ = 42°*

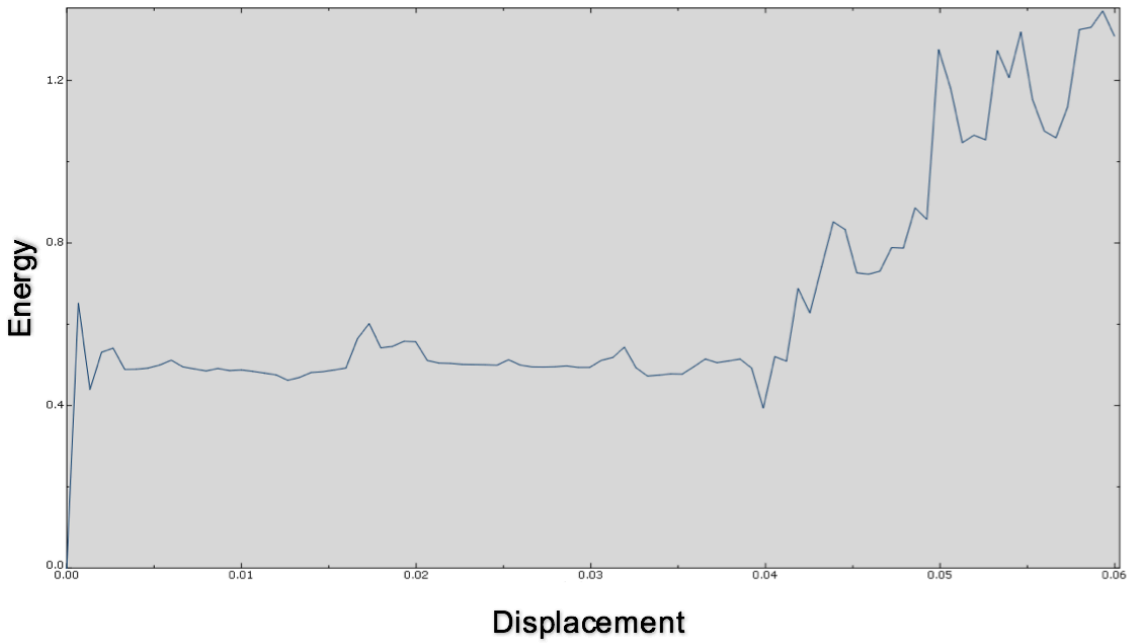

Figure 4.5 *Kinetic energy for ψ = 30°*

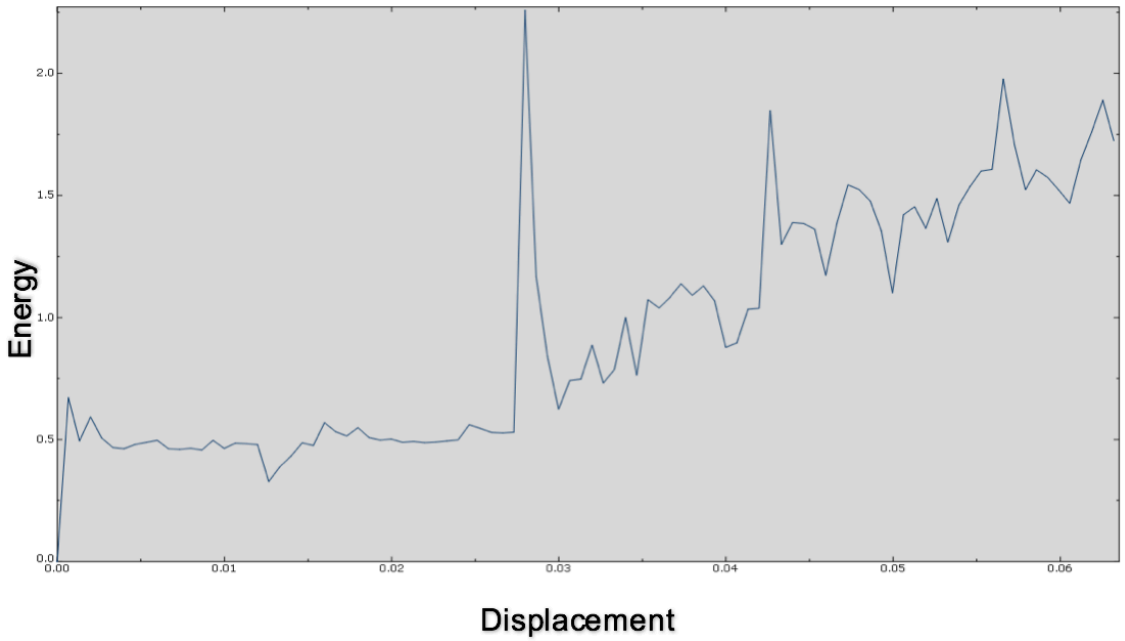

Figure 4.6 *Kinetic energy for ψ = 15°*

Using the Damaged Plasticity Parameter, it is possible to highlight the cracks at the failure point using the damage parameter in tension d_t, Figure 4.7, and the parts damaged by crushing in compression using the damage parameter in compression d_c, shown in Figure 4.8. The damaged parameter in tension represent the crack opening, in fact in Figure 4.7 it can be seen how the highest value of d_t is in correspondence of the load point in the bottom part of the beam and in correspondence of the support in the top part, these clearly represent the cracks.

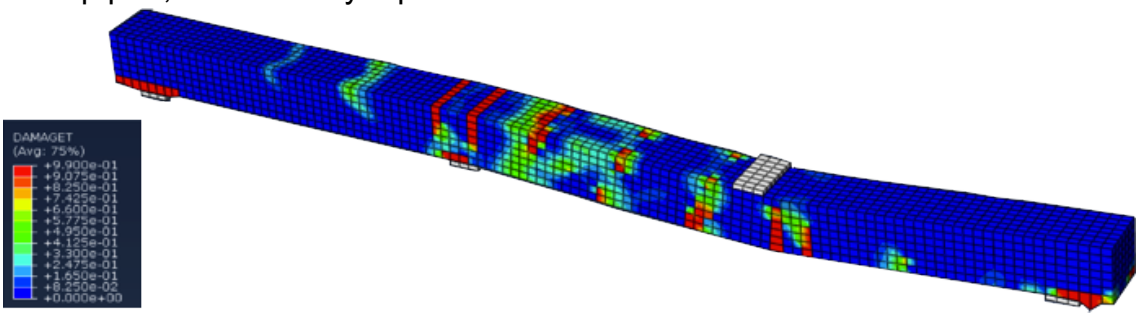

Figure 4.7 *Tension Damage Parameter*

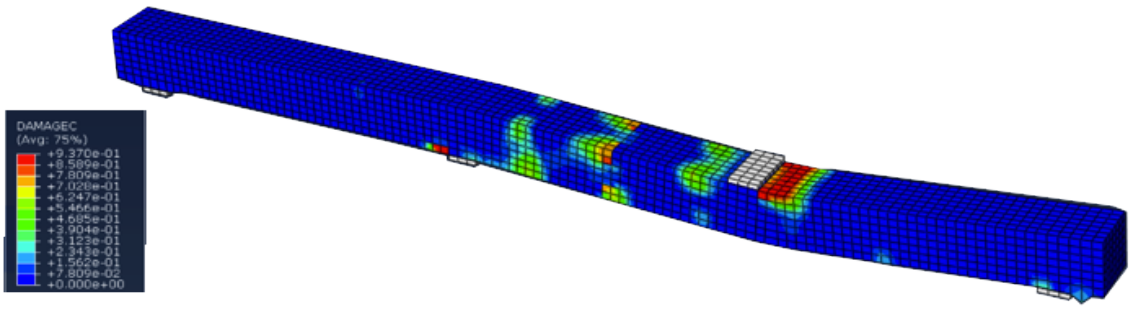

Figure 4.8 *Compression Damage Parameter*

4.1.2 Parametric study

Once the validation work gives good results compared with experimental ones, the model is used to evaluate the effects of fibres to replace conventional reinforcement. So first of all, the fibres volume percentage is increased considering five different percentages: 0%, 1%,1,5%, 2% and 2,5%. Afterwards the spacing between stirrups is increased as well, three different spacing percentage are used, namely SI = 0%, 50% and 100%, in this way it is possible to highlight if the fibres can replace the traditional reinforcement. To evaluate the effect of fibres the strength and the ductility are evaluated for each case.
According to Lok and Xiao (1999) theory, increasing the volume of fibres modifies the tensional behaviour of concrete, the different stress-strain relations in tension are depicted in Figure 4.9.

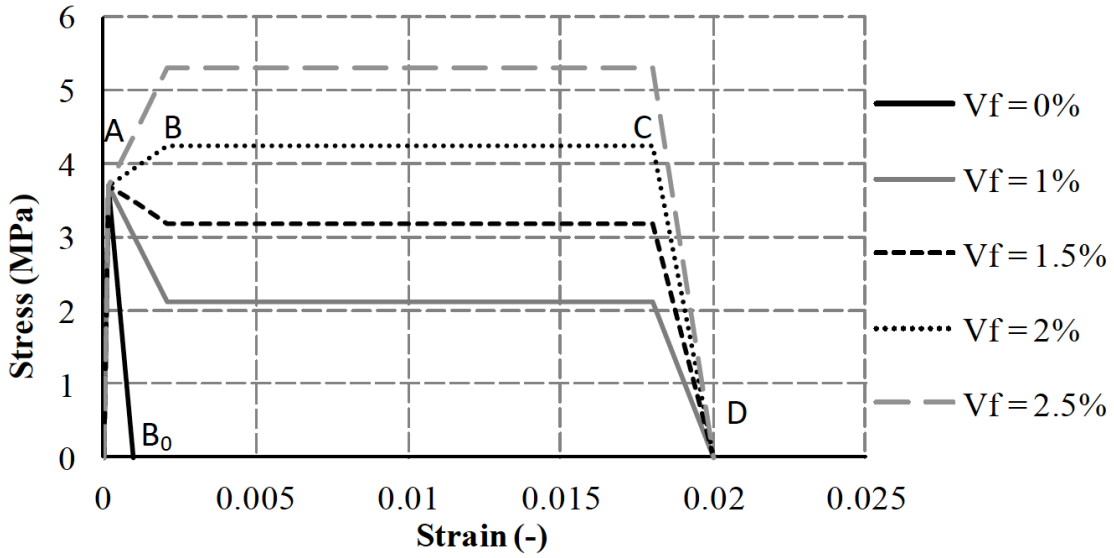

Figure 4.9 *Tensile stress-strain relationships for different fibres volume fractions*

To compare all the beams with different amount of fibres and different stirrups spacing load-deflection curves are obtained. In Figure 4.10 SI=0% so only the fibres volume fraction is modified.

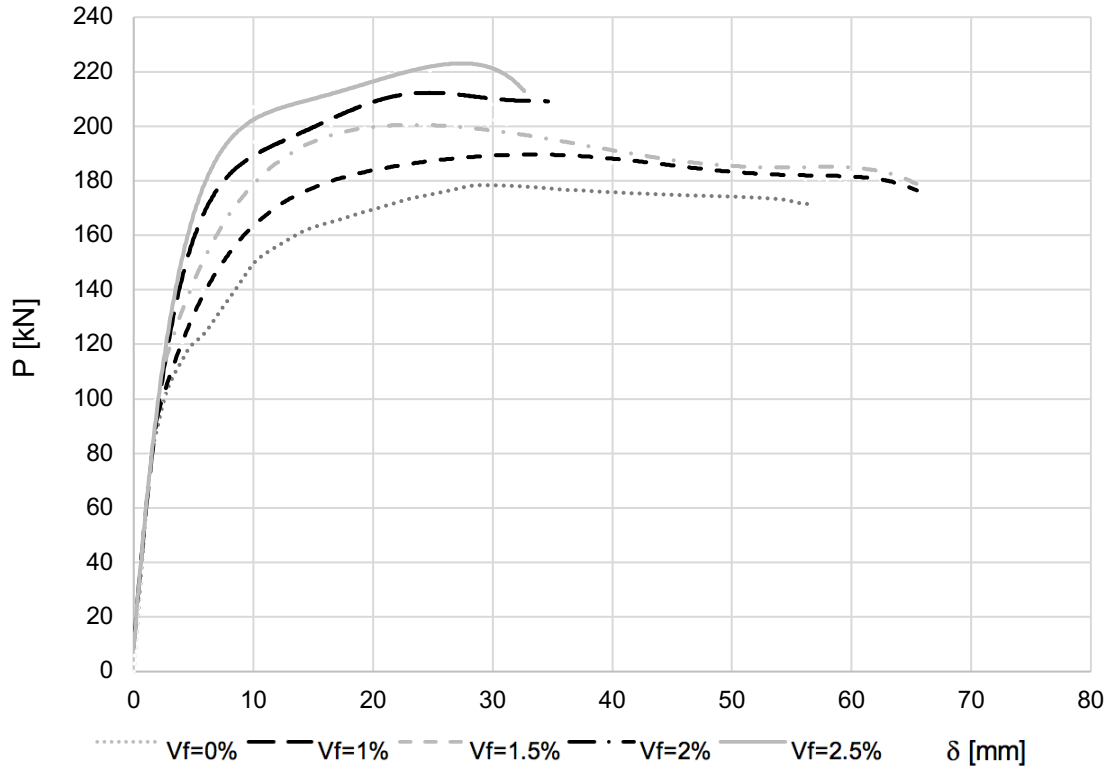

Figure 4.10 *Load-deflection curves for SI=0%*

It is clear from the previous image that there is an improvement in terms of load-carrying capacity due to the increase in the amount of fibres.
In Figure 4.11 the kinetic energies for the different amount of fibres are shown.

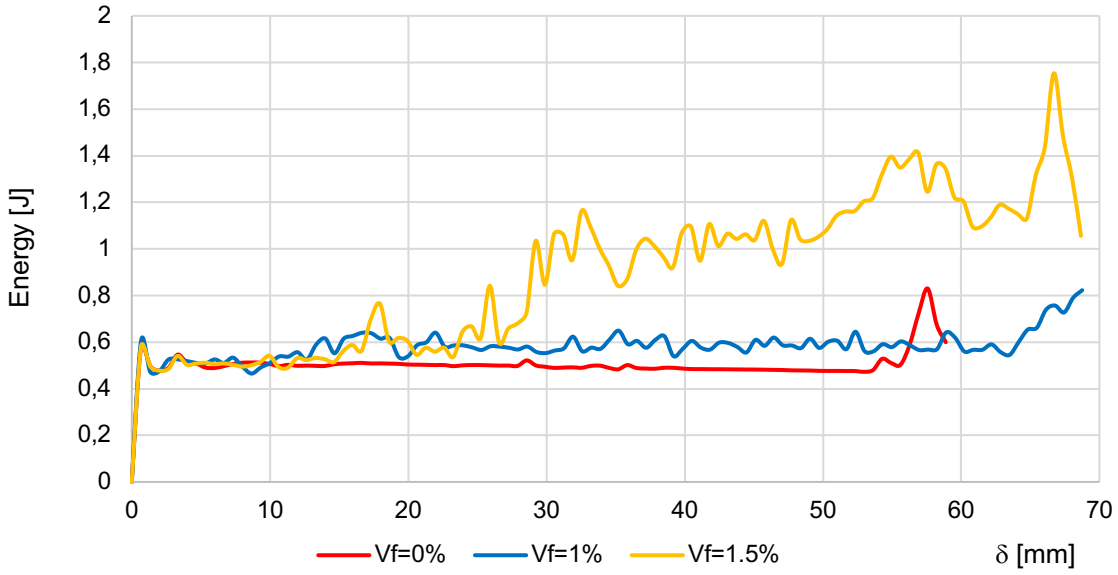

(a)

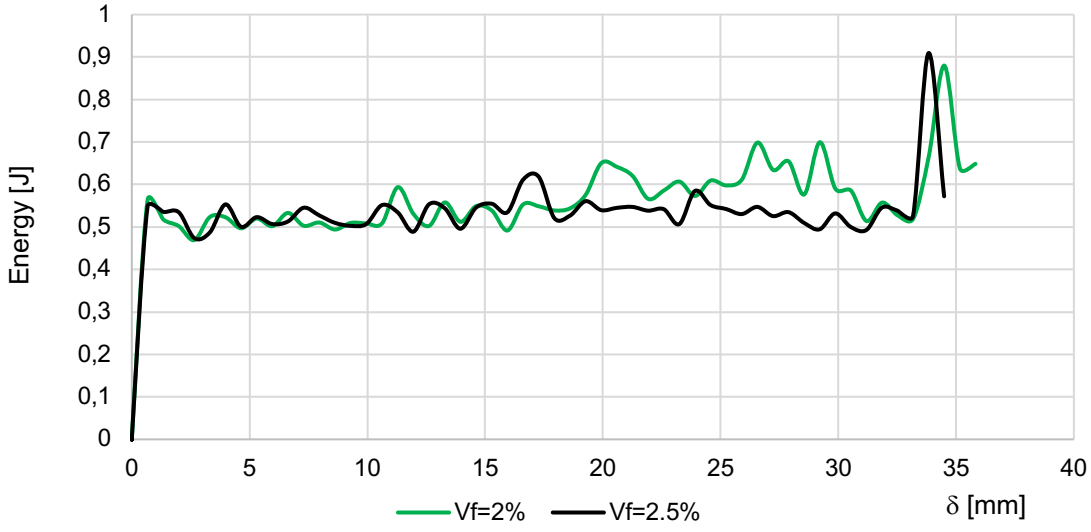

(b)

Figure 4.11 *Kinetic energies with SI=0% for (a) V_f =0%, V_f =1%, V_f =1,5% and (b) V_f =2% and V_f =2,5%*

To carry out a more accurate analysis, in Table 4.4 all the characteristic values of the load-deflection curves are provided.

	P_y [kN]	δ_y [mm]	P_u [kN]	δ_u [mm]	P_{max} [kN]	δ_{Pmax} [mm]	$\mu=\delta_u/\delta_y$	P_{max}/P_y
Vf=0%	145,51	9,3	171,8	53,3	178,3	30,00	5,7	1,225
Vf =1%	160,90	9,3	177,4	64,8	192,45	32,30	6,97	1,196
Vf =1.5%	183,00	10,6	182,1	64,8	203,20	21,99	6,1	1,110
Vf =2%	190,86	9,3	190,86	33,3	214,672	25,32	3,6	1,125
Vf =2.5%	210,64	10,6	218,425	33,3	223,796	23,32	3,1	1,062

Table 4.4 *Load-deflection characteristics for SI=0%*

All the curves are compared against the load-deflection curve obtained using a fibres volume percentage equal to 0%, namely that related to a plain concrete beam. Furthermore, in Figure 4.12 the curves obtained by Abbas et al. (2014) are showed.

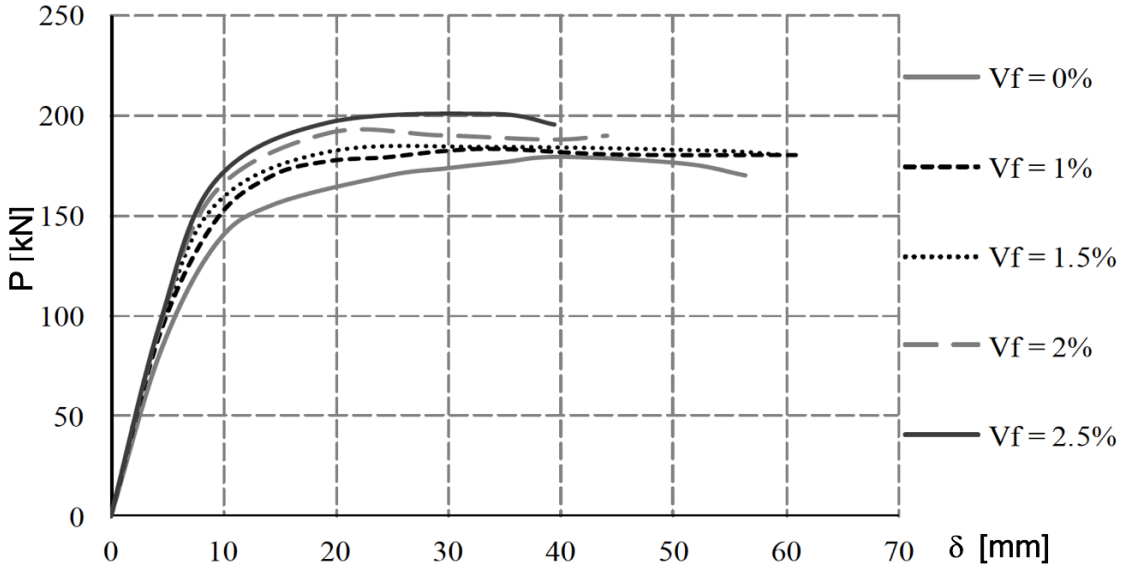

Figure 4.12 *Load-deflection curves for SI=0% with Brittle Cracking Model*

The yield point can be considered constant for a variation in the fibres volume fraction, instead the load at yield increases from 10,5% for V_f = 1% to 44,75% for V_f = 2,5% with an average equal to 28,06%, on the other hand the results obtained using a Brittle Cracking Model showed an increment with an average of 23,5%. Also, the maximum load increases with the V_f, for V_f = 1% the increment is equal to 7,9%, it reaches 25,5% for V_f = 2,5%, for this parameter the average is 16,95%, instead for this case the Brittle Cracking Model obtained an average equal to 13,1%. The outcomes show a good agreement between the two models particularly for the load-carrying capacity.
From these parameters, the expected improving in the load-carrying capacity due to the fibres bridging the crack is confirmed.
The column investigated for a SI=0% and a V_f = 0% will be used as the control column in the following sections.
Now the results obtained by changing the stirrups spacing are provided in Figures 4.13, 4.14, 4.15 and 4.16 with a summary in Tables 4.5 and 4.6 for SI=50% and SI=100% respectively.

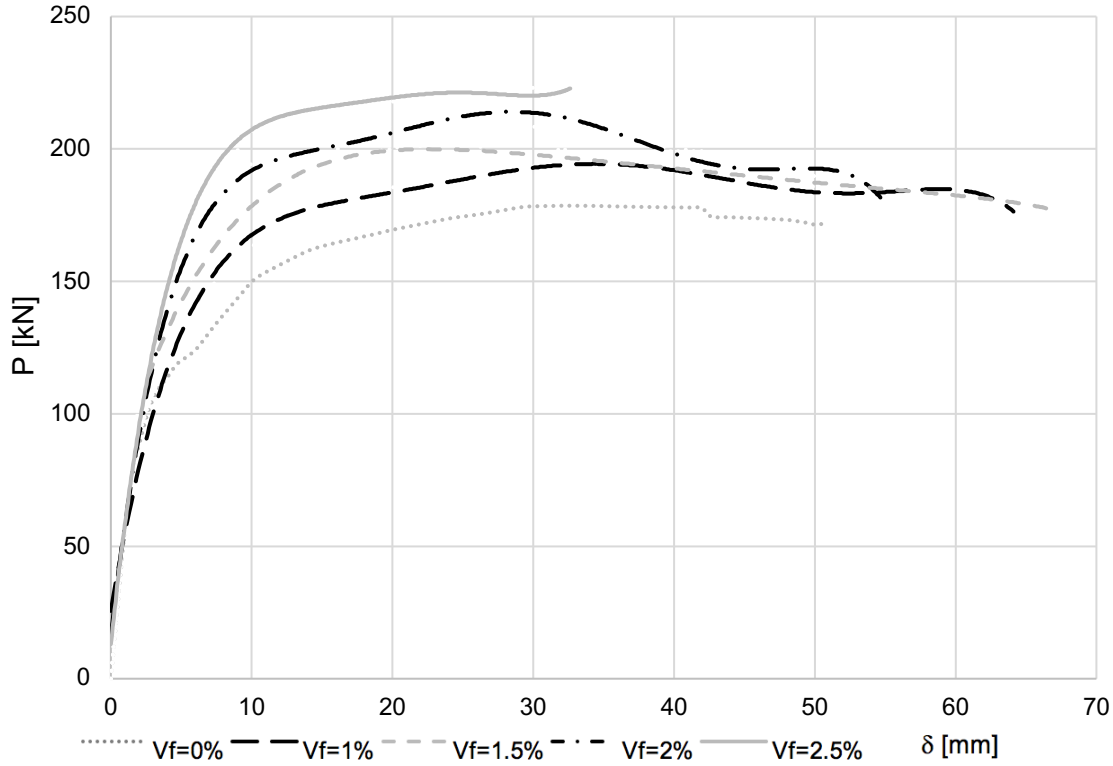

Figure 4.13 *Load-deflection curves for SI=50%*

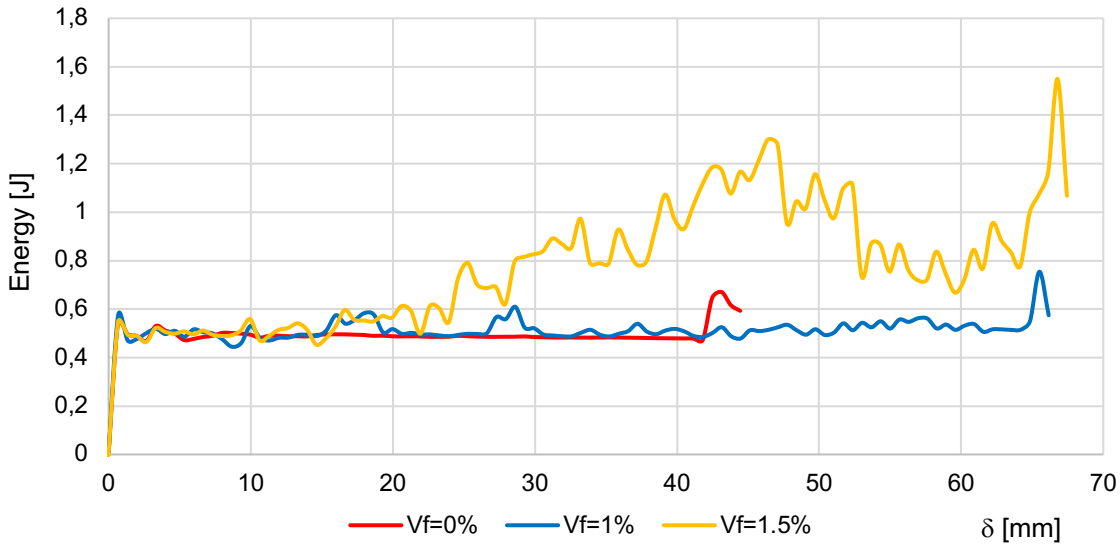

(a)

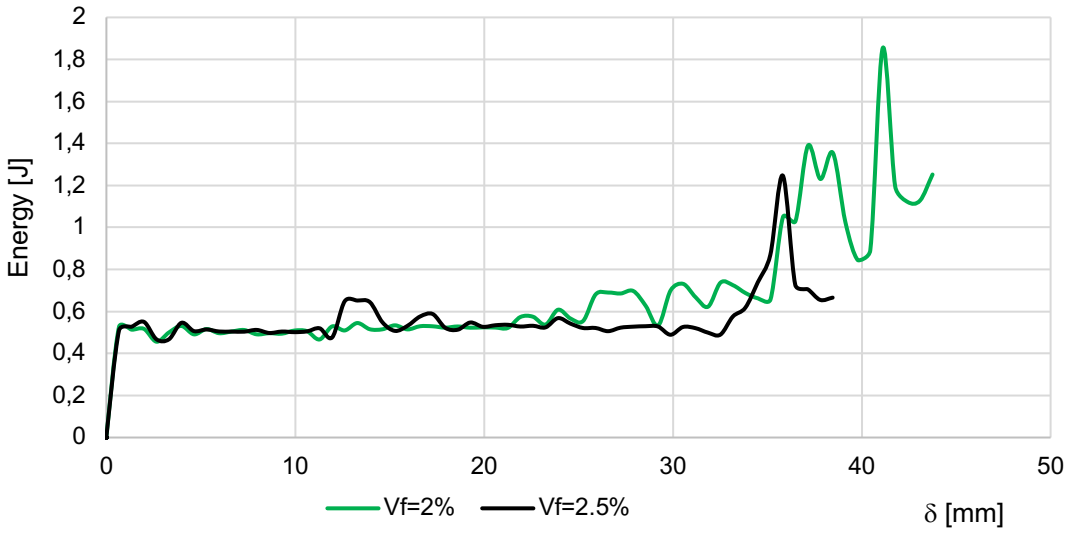

(b)

Figure 4.14 *Kinetic energies with SI=50% for (a) V_f=0%, V_f=1%, V_f=1,5% and (b) V_f =2% and V_f=2,5%*

	P_y [kN]	δ_y [mm]	P_u [kN]	δ_u [mm]	P_{max} [kN]	δ_{Pmax} [mm]	$\mu=\delta_u/\delta_y$	P_{max}/P_y
CC	145,51	9,3	171,8	53,3	178,3	30,00	5,7	1,225
Vf=0%	145,7	9,3	177,7	42,0	178,56	32,02	4,5	1,225
Vf=1%	159,7	9,3	180,2	64,1	193,54	29,36	6,9	1,212
Vf=1.5%	175,48	9,3	177,2	67,5	203,957	24,04	7,2	1,162
Vf=2%	191,3	9,3	199,8	40,7	218	25,37	4,3	1,140
Vf=2.5%	206,7	10	221,2	32,7	223,07	30,03	3,3	1,079

Table 4.5 *Load-deflection characteristics for SI=50%*

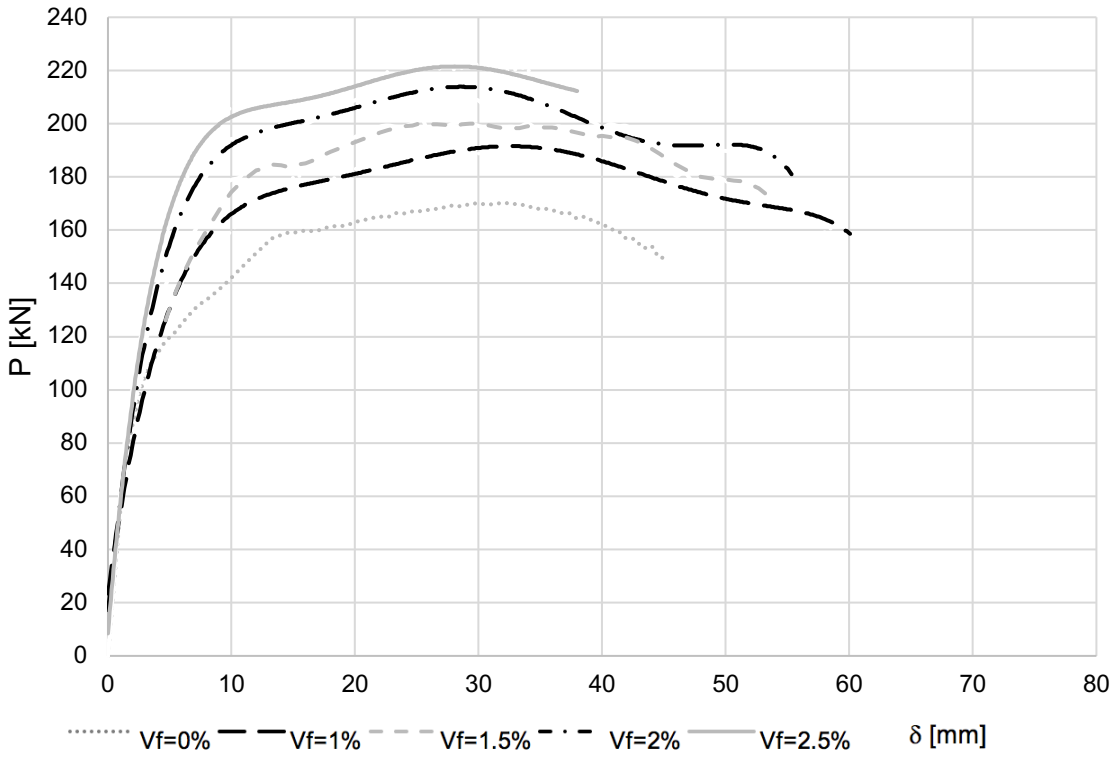

Figure 4.15 *Load-deflection curves for SI=100%*

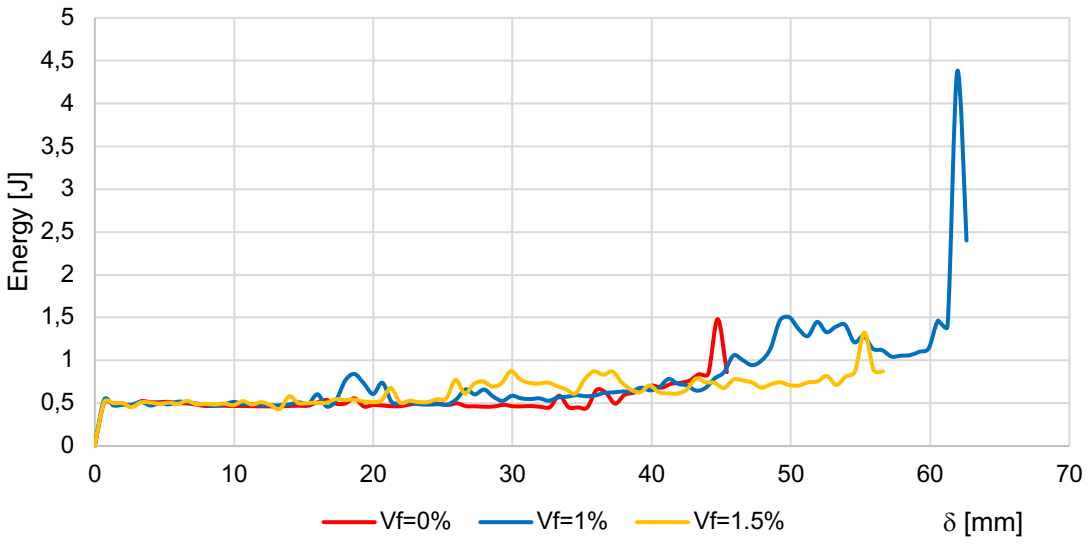

(a)

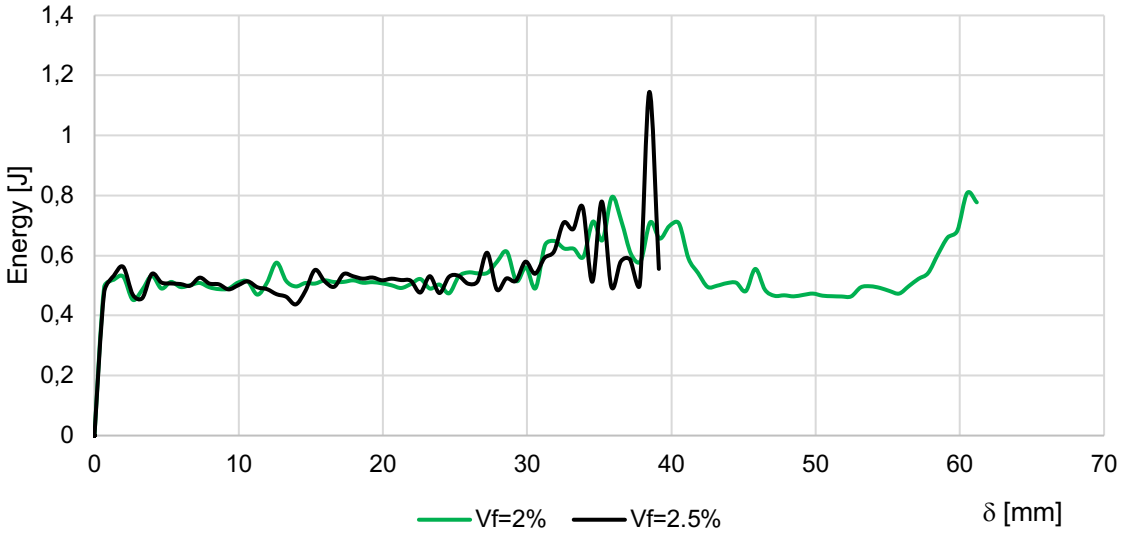

(b)

Figure 4.16 *Kinetic energies with SI=100% for (a) V_f=0%, V_f=1%, V_f=1,5% and (b) V_f =2% and V_f=2,5%*

	P_y [kN]	δ_y [mm]	P_u [kN]	δ_u [mm]	P_{max} [kN]	δ_{Pmax} [mm]	$\mu=\delta_u/\delta_y$	P_{max}/P_y
CC	145,51	9,3	171,8	53,3	178,3	30,00	5,7	1,225
Vf=0%	145,25	10	150,9	45,3	186,4	40,6	4,2	1,283
Vf=1%	159,47	10	161,9	60,1	191	30,7	6,0	1,198
Vf=1.5%	177,17	9,3	166,9	53,3	202,8	25,4	5,7	1,145
Vf=2%	194,29	10	186,5	55,3	217,8	28,7	5,5	1,121
Vf=2.5%	206,69	10	214,1	38,0	222,4	29,4	3,8	1,076

Table 4.6 *Load-deflection characteristics for SI=100%*

In agreement with the outcomes obtained by Abbas et al. (2014), depicted in Figures 4.17 and 4.18, all the beams with different stirrups spacing and different fibres volume percentage show better behaviour in terms of strength properties, namely P_y and P_{max}.

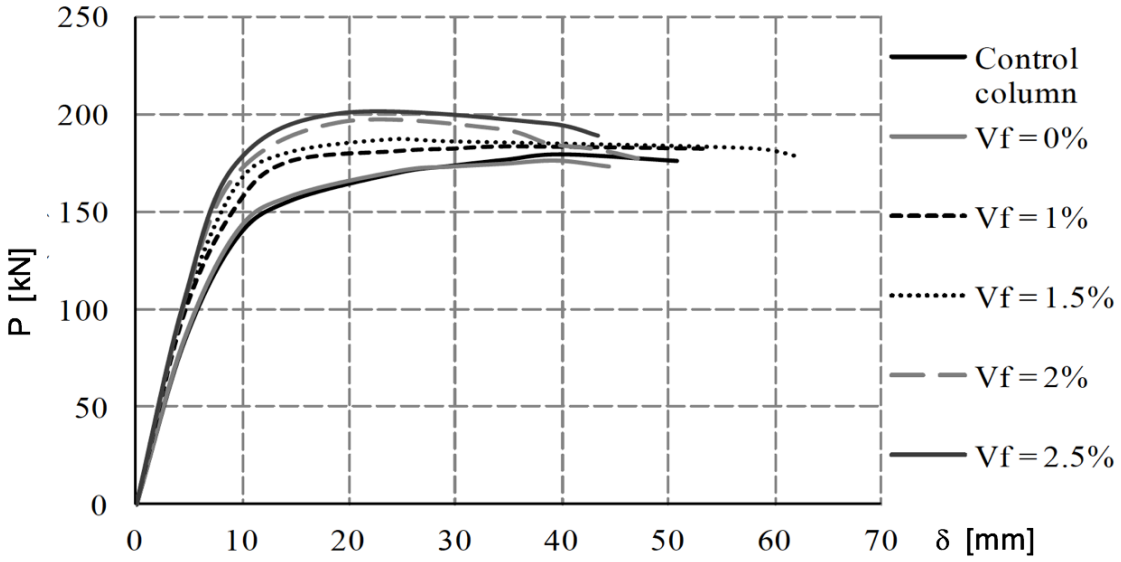

Figure 4.17 *Load-deflection curves for SI=50% with Brittle Cracking Model*

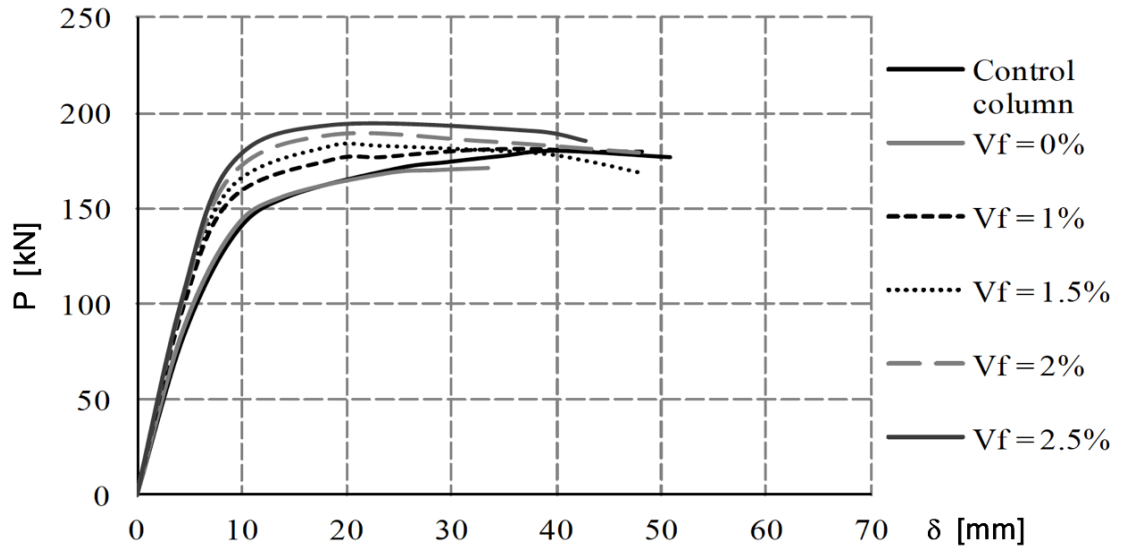

Figure 4.18 *Load-deflection curves for SI=100% with Brittle Cracking Model*

The increment in terms of maximum load is well depicted in Figure 4.19 in which the values of P_{max}, normalized with respect to the respective value of the control column $P_{max,0}$, is drawn in function of the fibres volume fraction.

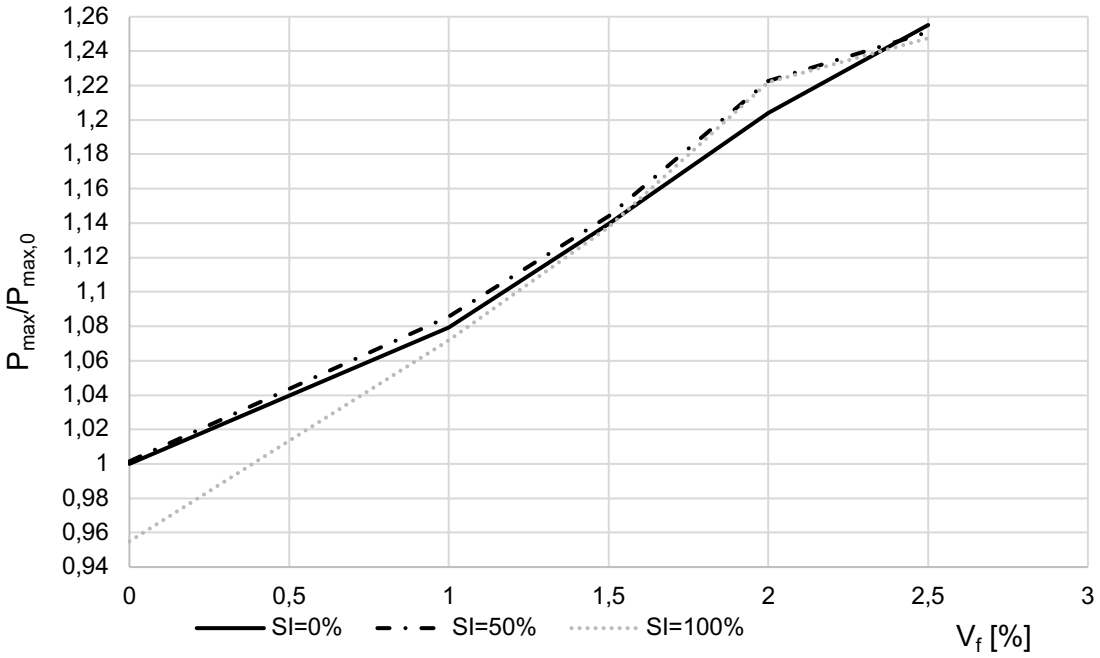

Figure 4.19 *Normalized maximum strength trend in function of V_f*

From the previous figure, it is clear how the increasing in the fibre volume percentage can improve the beam strength. For a SI=50% the trend is similar to that related to SI=0% and it is even higher for a V_f = 2%. The beams with SI=100% show strength values lower than those related to beams with SI=0% from V_f = 0% to V_f = 1,5%, then also for these arrangements the strength increases in correspondence of V_f = 2%. In Table 4.7 all the values are provided and they demonstrate as the fibres can compensate the reduction in reinforcement.

	V_f [%]	P_{max} SI=0%	P_{max} SI=50%	P_{max} SI=100%
$P_{max,0}$ = 178,3kN	0	1	1,001	0,955
	1	1,0793	1,0854	1,0717
	1,5	1,14	1,1439	1,1376
	2	1,2039	1,2226	1,2216
	2,5	1,2551	1,2511	1,2475

Table 4.7 *Normalized maximum strength values for different stirrups spacing*

A comparative analysis with the Brittle Cracking Model was carried out previously for SI=0%, now it is possible to analyse also the differences for SI=50% and SI=100%. For SI=50% the average of the increment of P_{max}, again taking into account the value of $P_{max,0}$, is 11,3%, with the same value for V_f = 0% and a maximum increment of 25,1% for V_f = 2,5%, on the other hand, for the Brittle Cracking Model, the average of increment is 3,9%, with a reduction for V_f = 0% equal to -2,1% and a maximum increment equal to 11,5% for V_f = 2,5%. Considering SI=100%, the results show that the increment has an average equal to 9,6% with a reduction equal to -4,5% for V_f = 0% and an increment equal to 24,75% for V_f = 2,5%, for the Brittle Cracking Model instead, the overall increment average is equal to 2% with a reduction of -5% for V_f =

0% and an increment equal to 7,6% for V_f = 2,5%. In Figure 4.20 the normalized strength derived from the analysis with the Brittle Cracking Model is displayed.

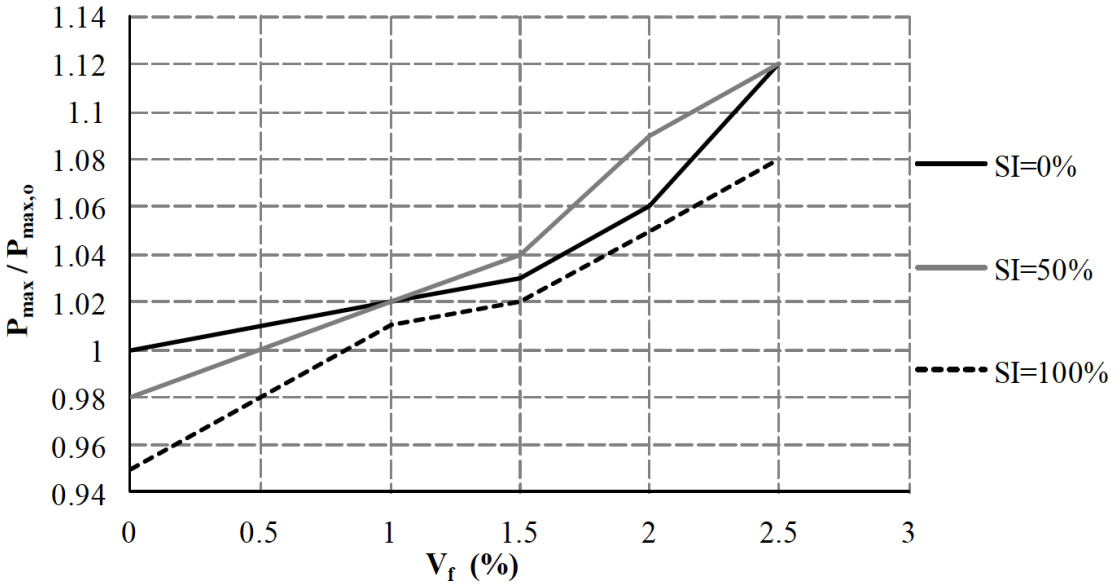

Figure 4.20 *Normalized maximum strength trend in function of V_f with Brittle Cracking Model*

After summarising the results in terms of maximum load, it can be concluded that, using the Damaged Plasticity Model, it is possible to outline the same trend, but there is an overestimation of the maximum load with the increase of the fibre volume fraction. Considering that the response in terms of ultimate deflection and deflection in correspondence of the maximum load are comparable for the two models, the overestimation of the maximum load is not on the safe side and can lead to an overestimation of the beam strength.
All the conclusions deduced from the investigation of the maximum strength are sustained by those made considering the values of the load at yield P_y. In Figure 4.21 these trends are depicted and the values are listed in Table 4.8.

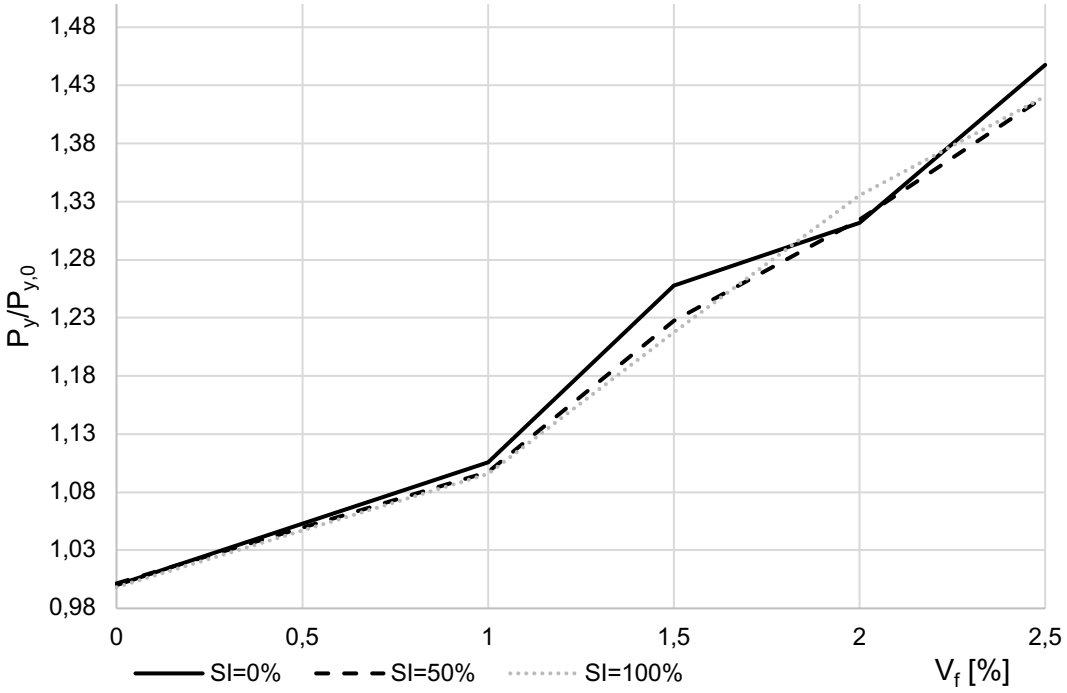

Figure 4.21 *Normalized load at yield trend in function of V_f*

	V_f [%]	P_y SI=0%	P_y SI=50%	P_y SI=100%
	0	1,00	1,0014	1,00
	1	1,11	1,10	1,10
$P_{y,0}$ = 145,51kN	1,5	1,26	1,23	1,22
	2	1,31	1,31	1,34
	2,5	1,45	1,42	1,42

Table 4.8 *Normalized load at yield values for different stirrups spacing*

It is widely admitted that one of the most important parameter for a structure is its ductility, especially for a seismic analysis. In this work to analyse the ductility of a beam two quantities are considered, namely the ultimate deflection and the ductility ratio. The aim of the author, that is sustained from Abbas et al. (2014) as well, is to prove if the use of fibres can lead to good value of ductility even reducing the amount of shear reinforcement. According to this, the ductility ratio for all the different combinations of SI and V_f are evaluated, listed in Table 4.9 and drawn in Figure 4.22.

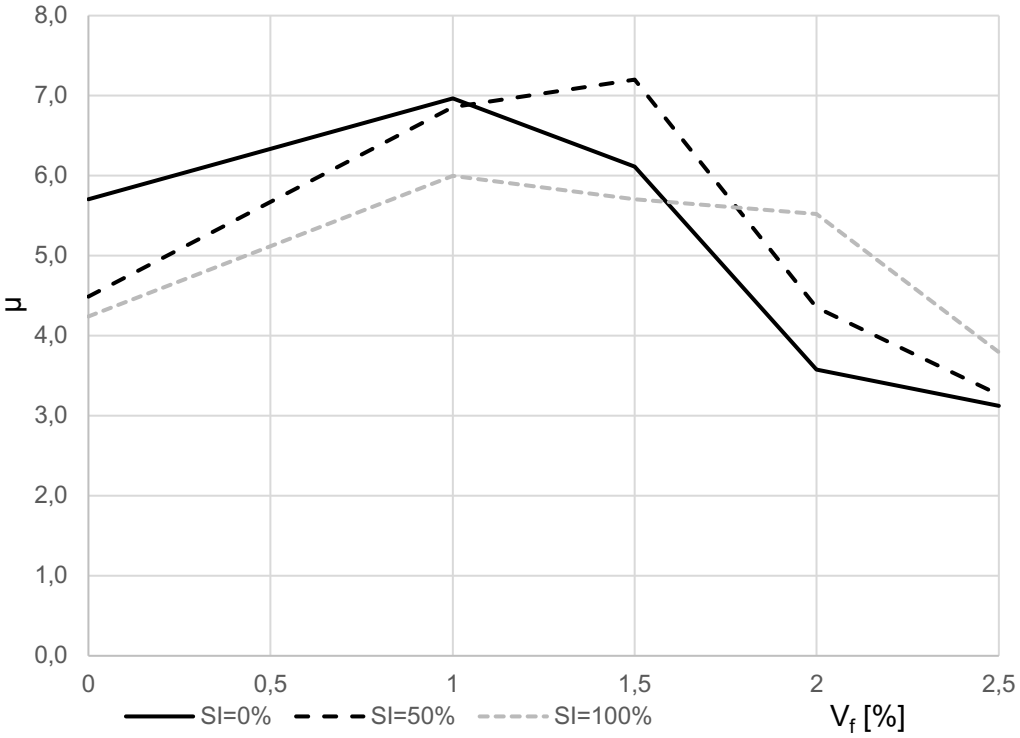

Figure 4.22 *Ductility ratio in function of V_f for different stirrups spacing*

V_f [%]	μ SI=0%	μ SI=50%	μ SI=100%
0	5,7	4,5	4,2
1	6,97	6,9	6,0
1,5	6,1	7,2	5,7
2	3,6	4,3	5,5
2,5	3,1	3,3	3,8

Table 4.9 D*uctility values for different stirrups spacing*

It is clear from the previous figure how the trend is the same for all different SI percentages. The ductility has a growing trend until it reaches a particular V_f percentage, these fibres volume percentage values are called critical values and they grow with the increasing of the stirrups spacing up to SI=50%. In fact, for SI=0% the highest ductility value μ = 6,97 is obtained for a V_f = 1%, for SI=50% the highest value μ = 7,2 is reached for V_f = 1,5%, in the end for SI=100% the maximum ductility is μ = 6,0. Furthermore, it is important to underline how the ductility ratio of the control column is reached in all the beams with stirrups spacing bigger than 0%, this means that fibres, if they are added in the sufficient amount, can restore the ductility of SFRC elements. In addition, SFRC elements undergo the well-known problem of over reinforcing, this phenomenon is a reduction in ductility that affect reinforced concrete elements when the amount of longitudinal reinforcement lead to a stiffer response. This phenomenon is clear if the ductility ratio for each column, normalized with respect the control column ductility ratio, is considered in function of the V_f. These trends are depicted in Figure

4.23, it shows how after the peak point the curves have a decreasing trend with the increasing of the fibres volume fraction, this behaviour starts earlier for the beams with SI=0% in which the amount of reinforcement is clearly bigger. In Table 4.10 the values of each curves are provided.

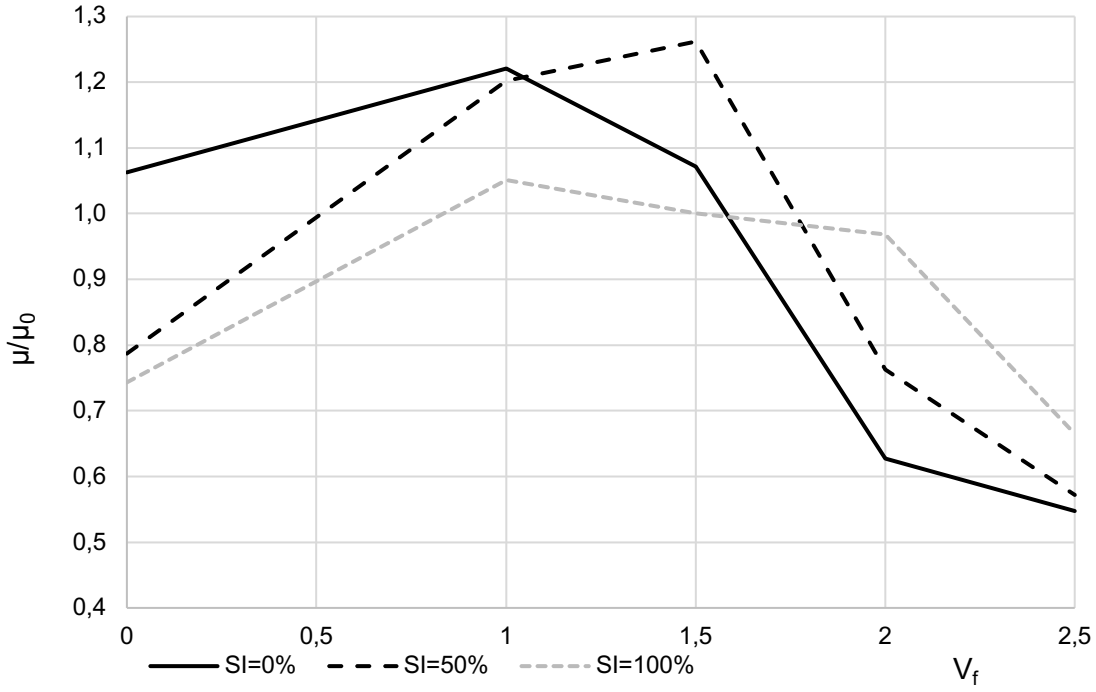

Figure 4.23 *Normalized ductility trend in function of V_f*

	V_f [%]	P_μ SI=0%	P_μSI=50%	P_μ SI=100%
	0	1,1	0,79	0,74
	1	1,22	1,2	1,05
$P_{\mu,0}$ = 6,1	1,5	1,1	1,3	1,00
	2	0,6	0,8	0,97
	2,5	0,5	0,6	0,67

Table 4.10 *Normalized ductility values for different stirrups spacing*

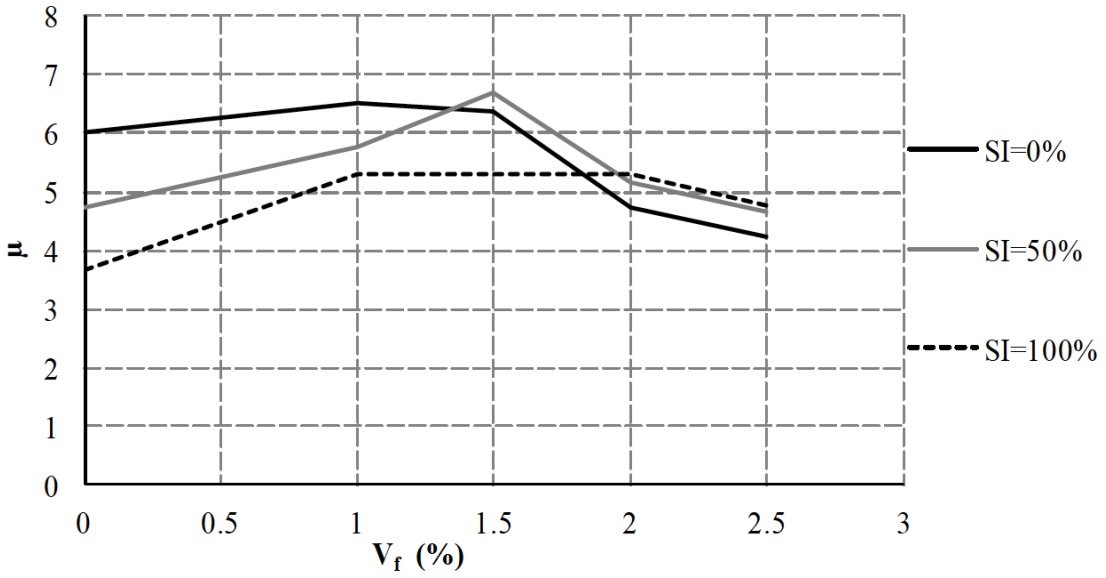

Figure 4.24 *Ductility ratio in function of V_f for different stirrups spacing with Brittle Cracking Model*

In Figure 4.24 the ductility ratio obtained by Abbas et al. (2014) for different SI values are showed. It can be seen how the curves are very similar to those obtained by the author using the CDPM. The maximum value for the ductility ratio is reached for SI=50% for both models, it is equal to 6,71 for the Brittle Cracking Model and equal to 7,2 for the CDPM. In both models, the trends show an increment in the ductility ratio until a critical value that, as explained before, characterise the beginning of an “over reinforced” behaviour. Finally, the ductility ratios evaluated with the CDPM, in its entirety, is comparable with the Brittle Cracking Model, in fact, just the peak value is overestimated.
Using the Concrete Damaged Plasticity Model, it is possible to highlight the formation of cracks thanks to the damage parameters in compression and in tension. Furthermore, analysing the cracks pattern, observations about the different structural behaviours can be done. In Figures from 4.25 to 4.27 the damage parameter patterns in tension for the ultimate deflection are depicted.

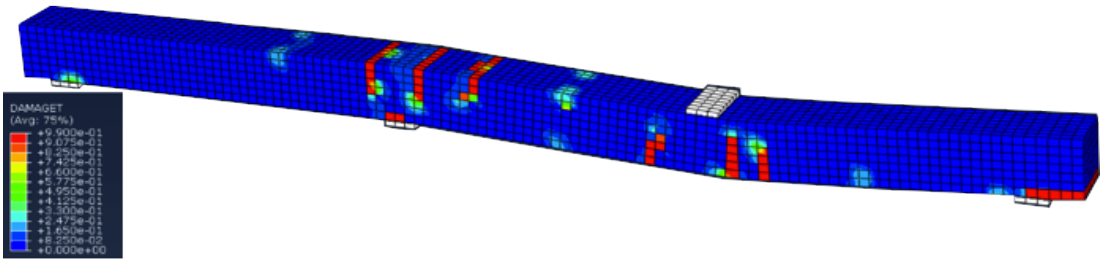

(a) V_f = 0%

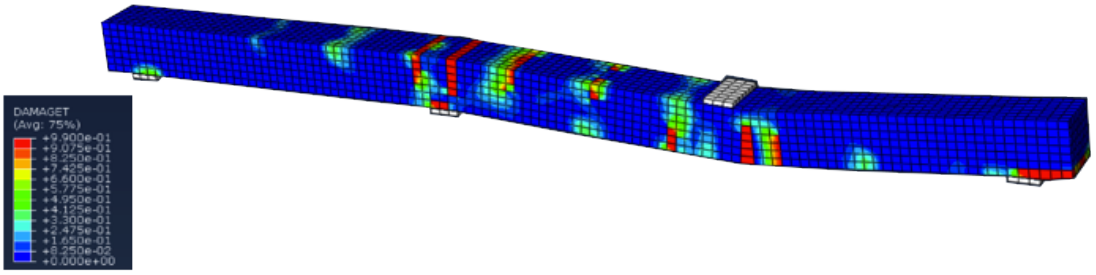

(b) V_f = 1%

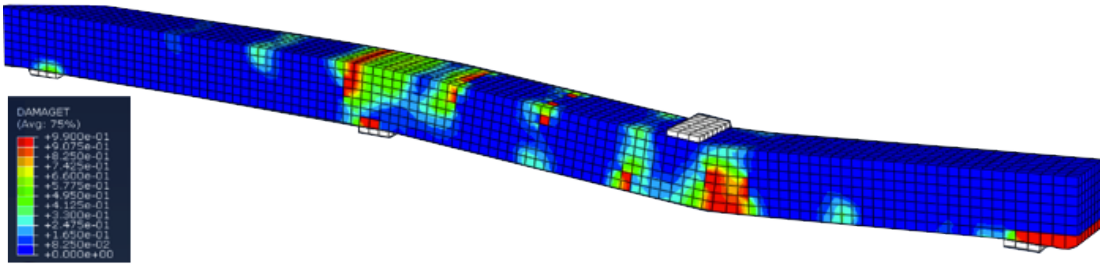

(c) V_f = 1,5%

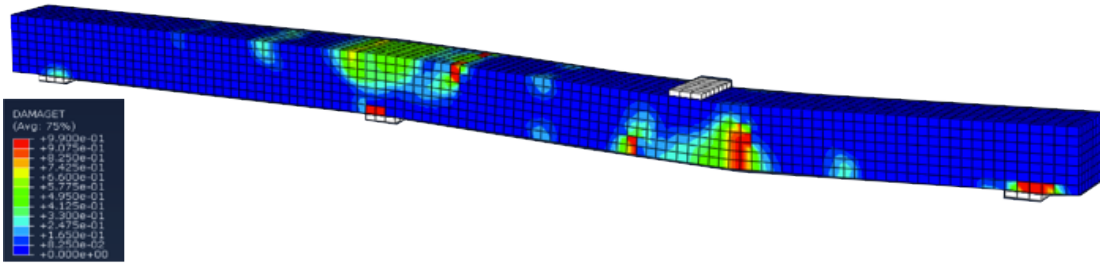

(d) V_f = 2%

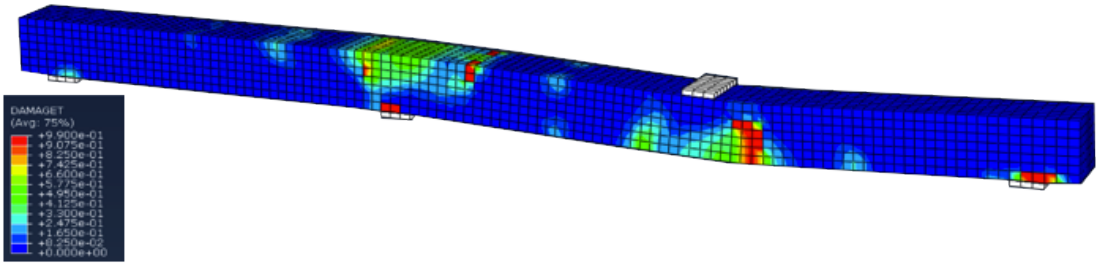

(e) V_f = 2,5%

Figure 4.25 *Damage parameter patterns in tension for SI=0%*

The cracking patterns are similar for all the different fibres volume fractions, cracks develop in correspondence of the point of application of the load, in the bottom side, and around the internal support, on the top side, as for the beam with V_f = 0,4% analysed in section 4.1.1. It is important to notice the differences between the cracking patterns taking into account the different values of the ultimate deflection. For the beams with a low amount of fibres, V_f = 0% and V_f = 1%, the load carrying capacities are the lowest, so, after the cracks developing, the elements fail; this is understandable from Figures 4.22 (a) and (b): the cracks are concentrated and the crack width is bigger compared with the other beams. When the amount of fibres is increased the trend changes. The best structural behaviour is obtained for V_f = 1,5%, in fact for this element the maximum load is higher and the value of the ductility ratio is comparable with the control column one. In Figure 4.22 (c) it can be seen how the number of cracks is grown, this means that after the formation of the first cracks the fibres bridge them allowing the formation of other cracks that are less wide than those examined in the previous beams. The beams with the highest dosage of fibres, V_f = 2% and V_f = 2,5%, represented in Figures 4.22 (d) and (e), show the highest load carrying capacities but, at the same time, the lowest ductility ratio values. This behaviour is caused by the high amount of fibres that bridge a large number of cracks from the beginning of the loading process, allowing the element to better bear the load, but when the maximum load is reached the pull-out failure of fibres occur leading to the sudden propagation of cracks and afterwards to the element failure.

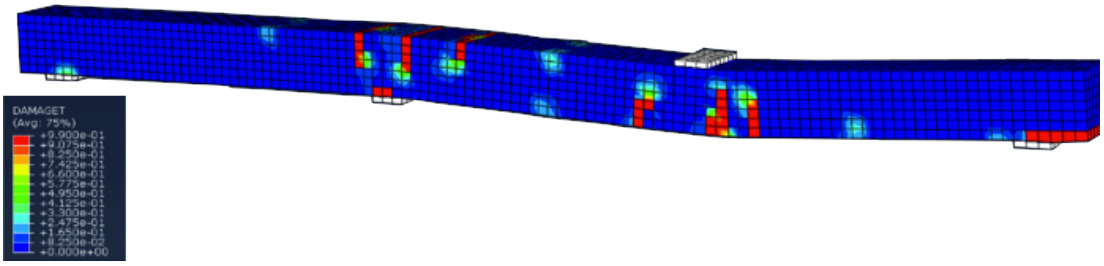

(a) V_f = 0%

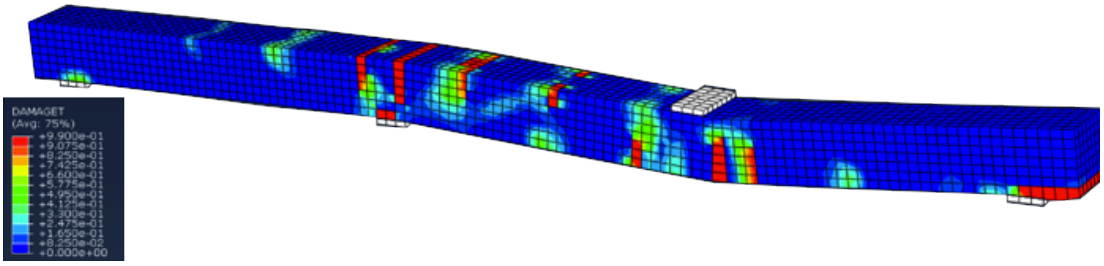

(b) V_f = 1%

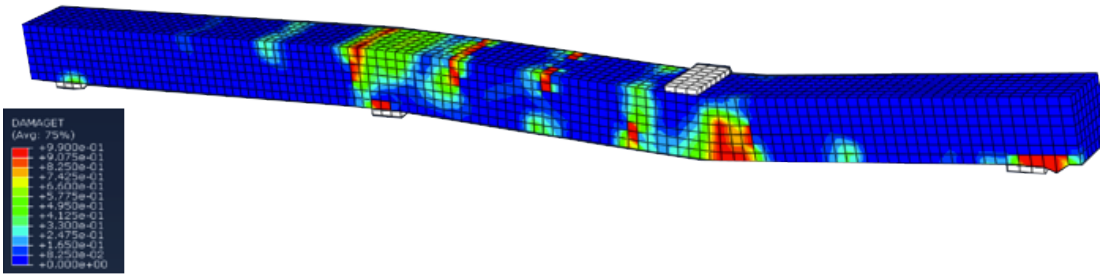

(c) V_f = 1,5%

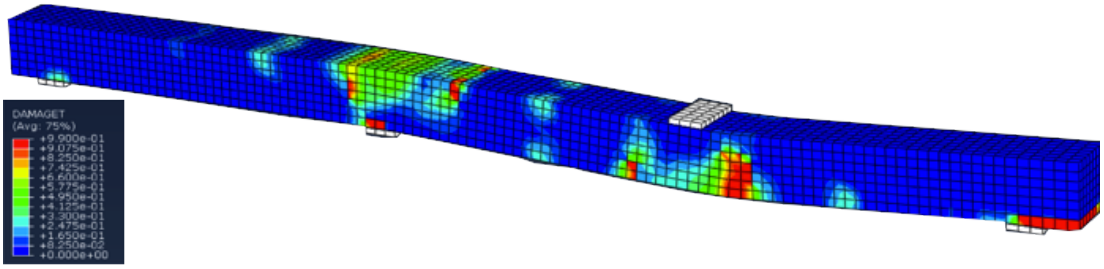

(d) V_f = 2%

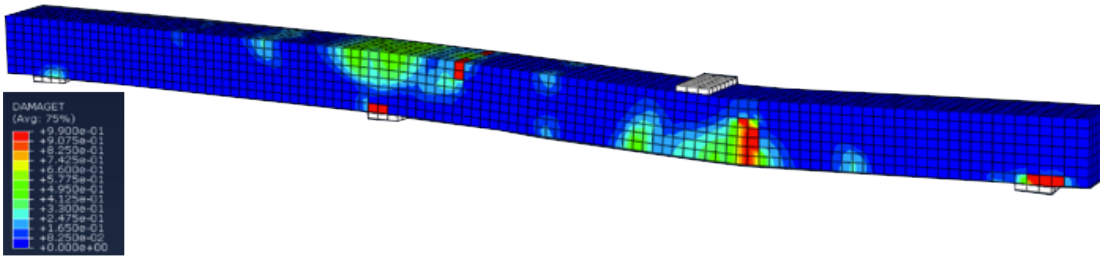

(e) V_f = 2,5%

Figure 4.26 *Damage parameter patterns in tension for SI=50%*

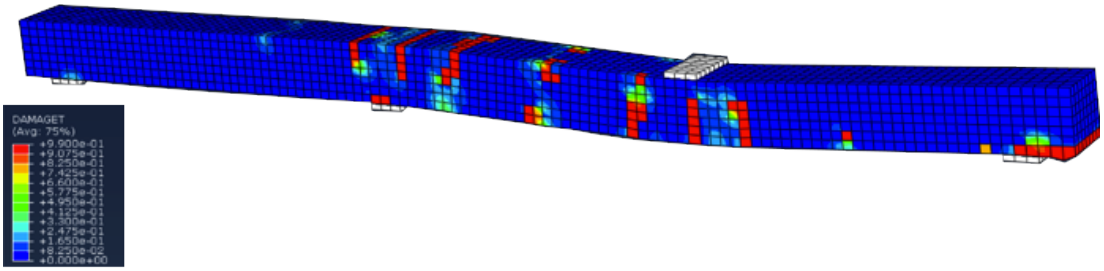

(a) V_f = 0%

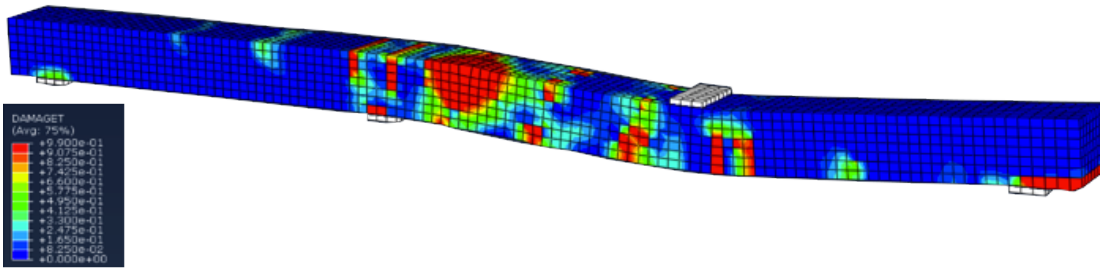

(b) V_f = 1%

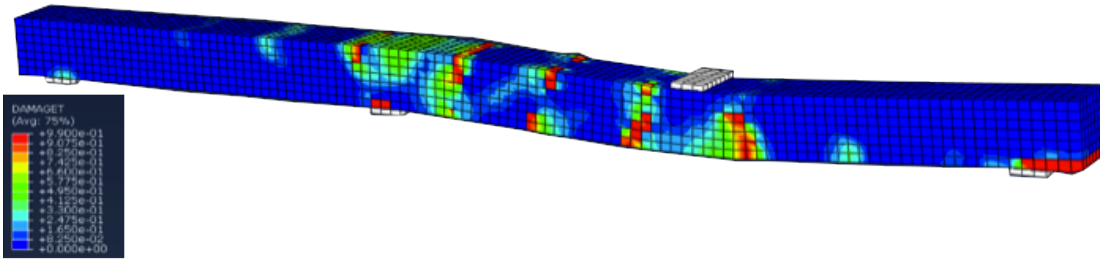

(c) V_f = 1,5%

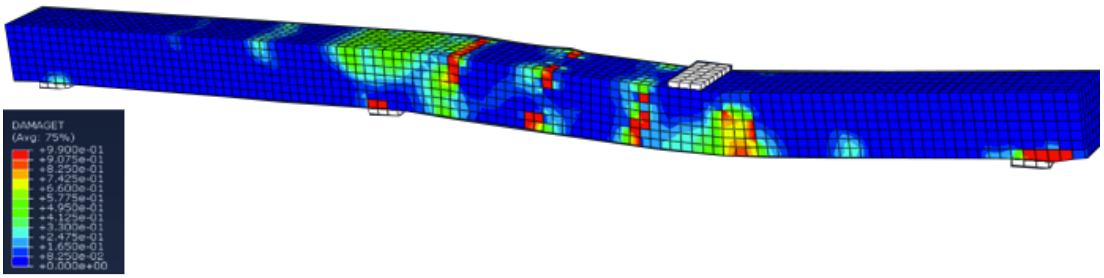

(d) V_f = 2%

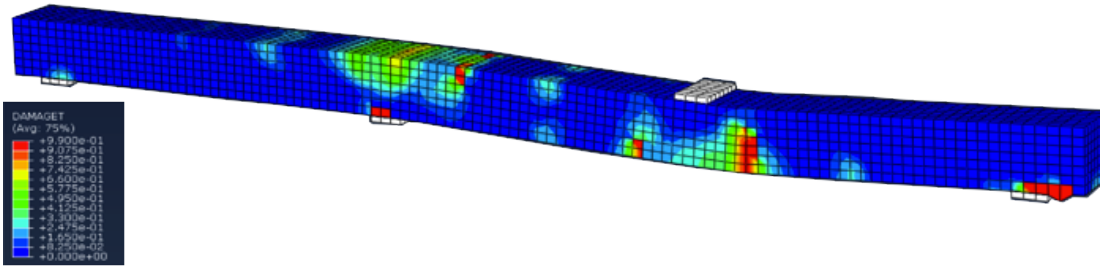

(e) V_f = 2,5%

Figure 4.27 *Damage parameter patterns in tension for SI=100%*

In Figures 4.26 and 4.27 the damage patterns in tension for SI=50% and SI=100% for all the fibres volume percentages are depicted. From the figures, it can be verified how the beams reflect the same behaviour of the beams with SI=0%. It is particularly interesting the element with SI=50% and V_f = 1,5%, it exhibits the highest ductility ratio value, more than the correspondent element with SI=0%. The cracks are scattered and the load carrying capacity reaches a value higher than the correspondent beam for SI=0%. This means that fibres and stirrups are provided with the perfect balance, in fact they do not lead to a high value of stiffness that could cause an over reinforcing behaviour, instead the crack bridging effect allow the element to reach high deflection. On the other hand, the damage patterns in compression are not so indicative of the overall behaviour, in Figures 4.28, 4.29 and 4.30 the damage patterns are displayed for different SI values.

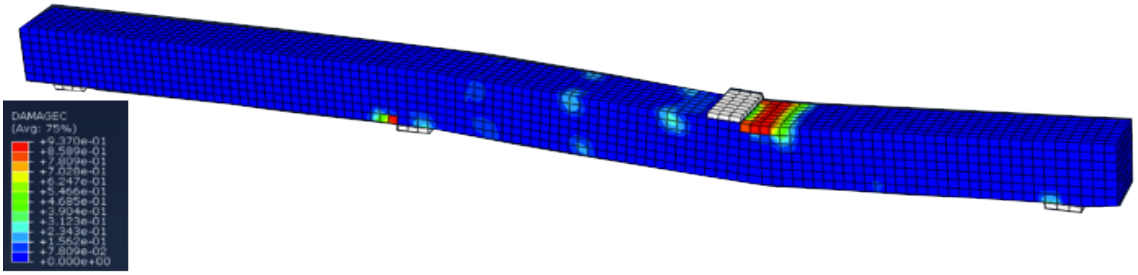

(a) V_f = 0%

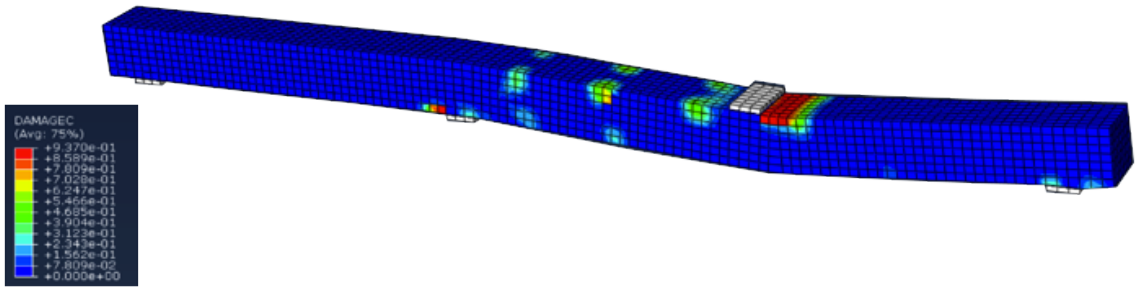

(b) V_f = 1%

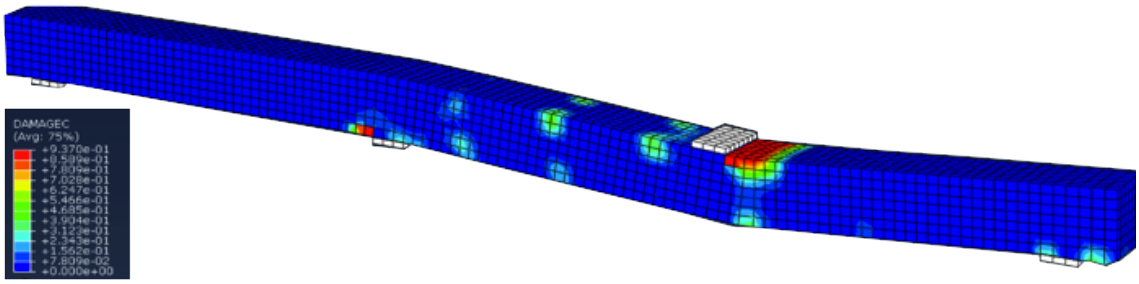

(c) V_f = 1,5%

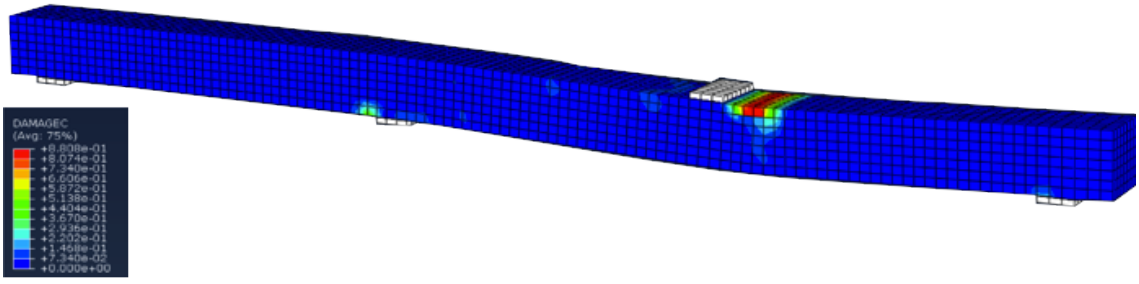

(d) V_f = 2%

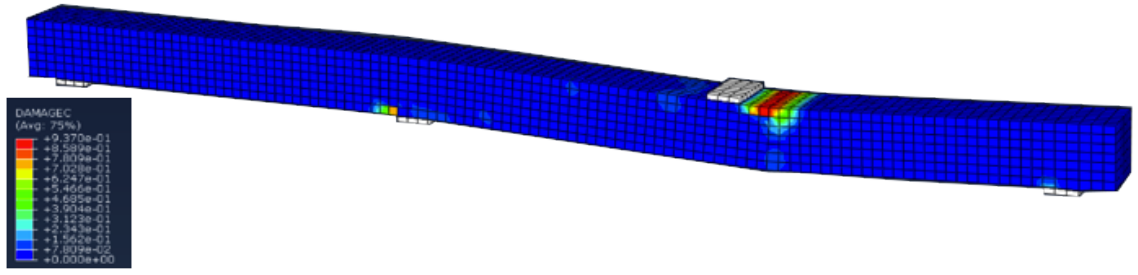

(e) V_f = 2,5%

Figure 4.28 *Damage parameter patterns in compression for SI=0%*

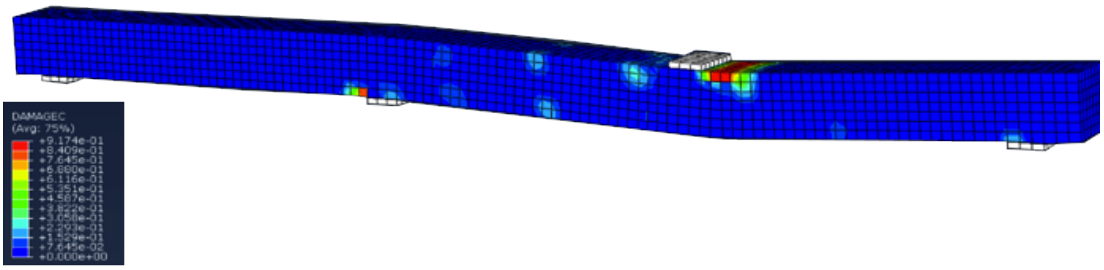

(a) V_f = 0%

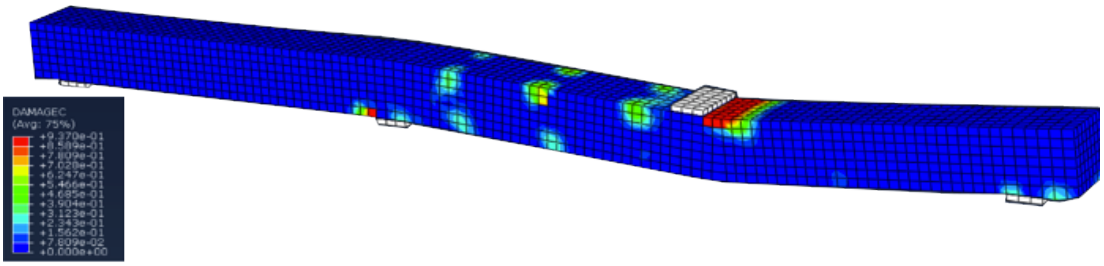

(b) V_f = 1%

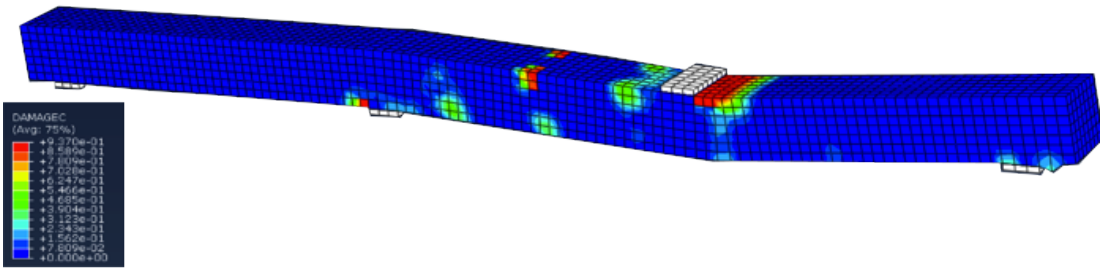

(c) V_f = 1,5%

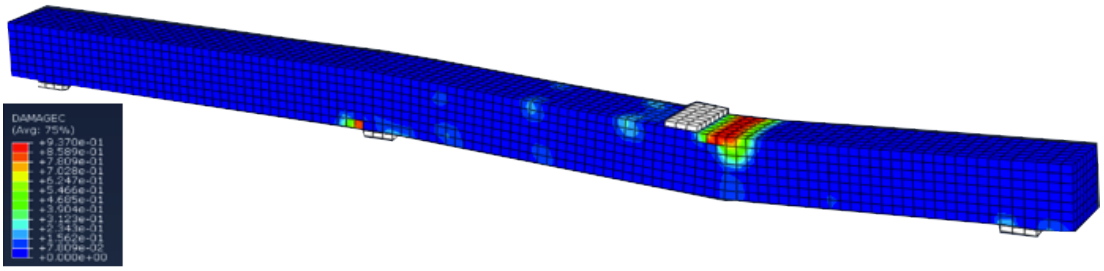

(d) V_f = 2%

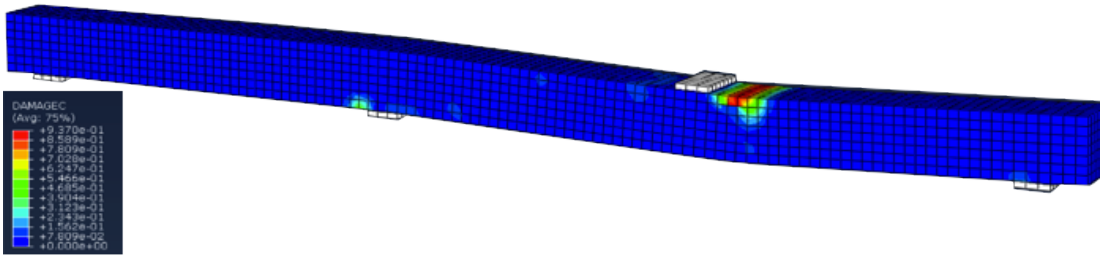

(e) V_f = 2,5%

Figure 4.29 *Damage parameter patterns in compression for SI=50%*

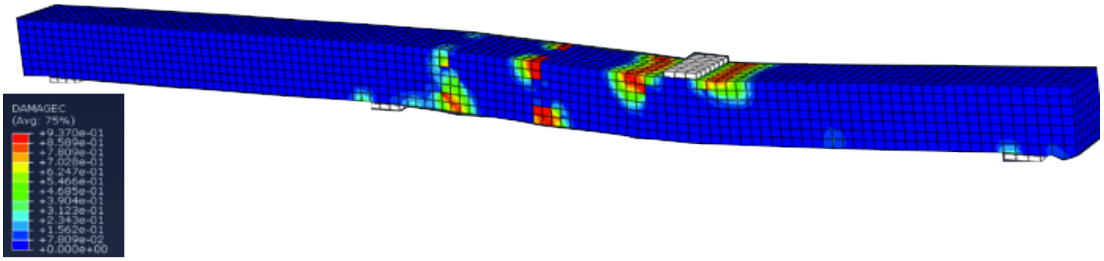

(a) V_f = 0%

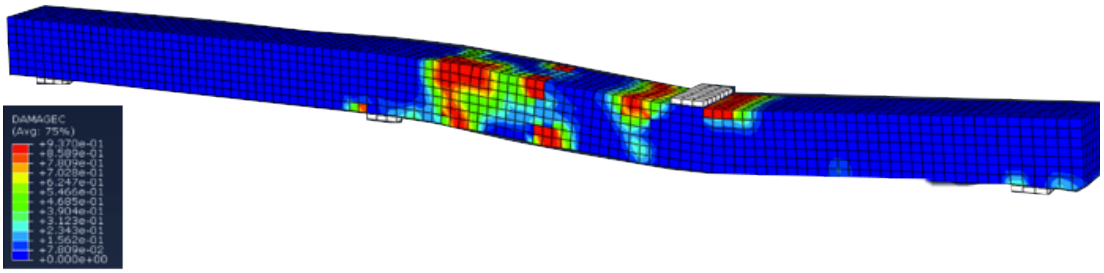

(b) V_f = 1%

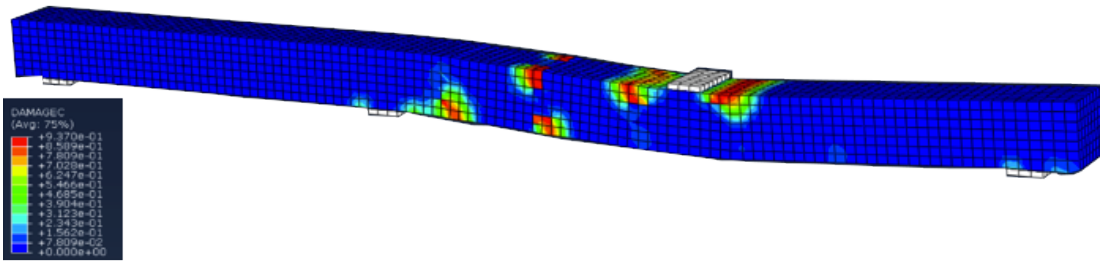

(c) V_f = 1,5%

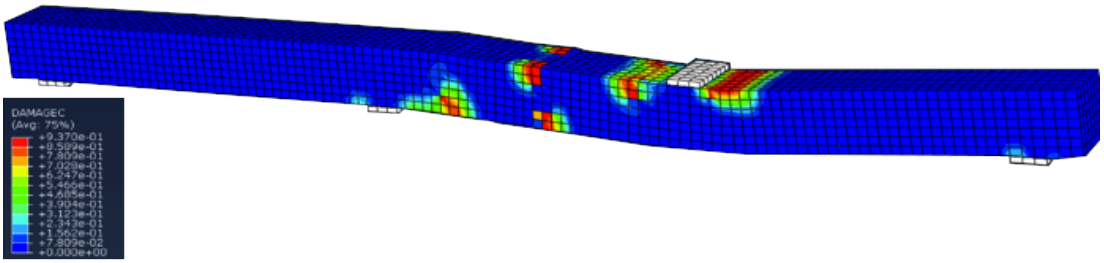

(d) V_f = 2%

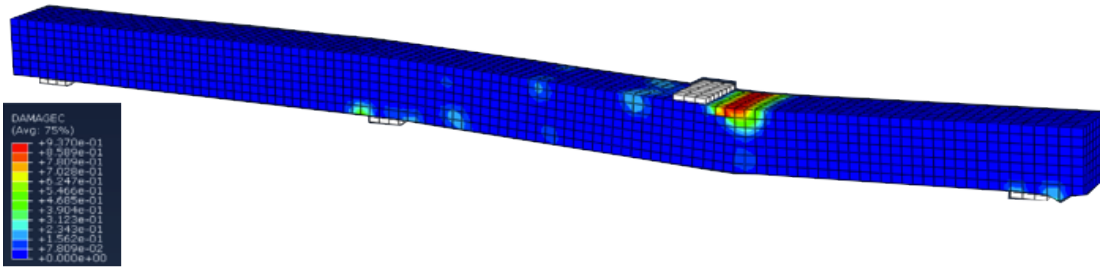

(e) V_f = 2,5%

Figure 4.30 *Damage parameter patterns in compression for SI=100%*

It can be observed how the part that undergoes the crushing is in proximity of the loading plate, in Figures 4.28 and 4.29 it is concentrated just in one side of the plate, in the short span of the beam, afterwards when the SI is increased and so the element becomes weaker it is possible to see the crushing damage in other parts of the beams, as shown in Figure 4.30. It is interesting to notice that the beam with SI=100% and V_f = 2,5% shows the same pattern of the other beams with SI=0% and SI=50%, this means that the amount of fibres is enough to make the element strong as those with more reinforcement.
On the other hand, information about the mode of failure can be obtained from the analysis of the principal strain vector. In Figures 4.31, 4.32 and 4.33, the principal strain vector in correspondence of the failure points are depicted for all the elements analysed. It can be seen that the main mode of failure is the bending-shear one. When the stirrup spacing is low, SI=0% and SI=50%, the failure is clearly in bending, thus as shown in Figures 4.31 and 4.32 the strain vectors show cracks in correspondence of the bottom of the section in which the load is applied and in the top of the section of the intermediate support.

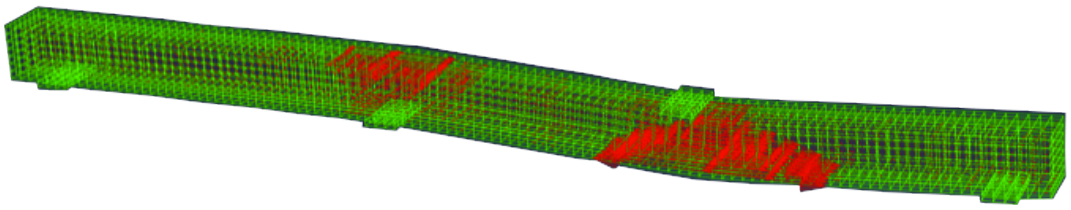

(a) V_f = *0%*

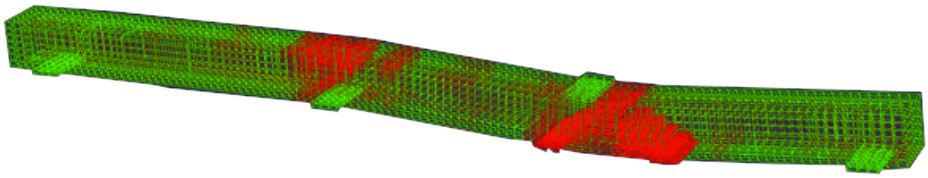

(b) V_f = *1%*

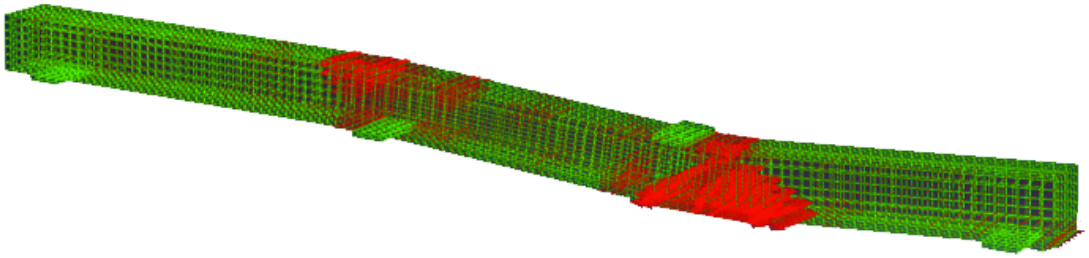

(c) V_f = *1,5%*

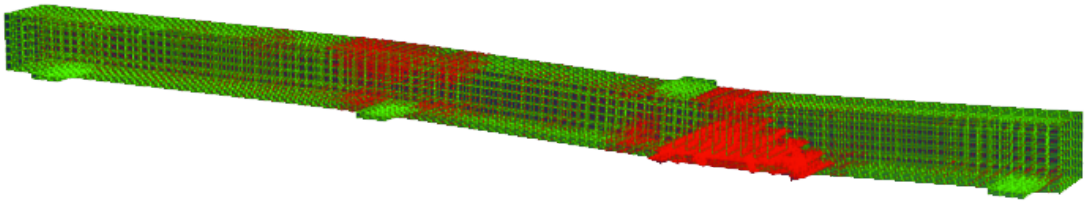

(d) V_f = *2%*

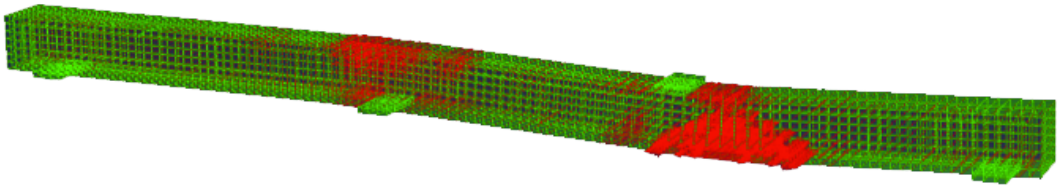

(e) V_f = *2,5%*

Figure 4.31 *Principal strain vector for SI=0%*

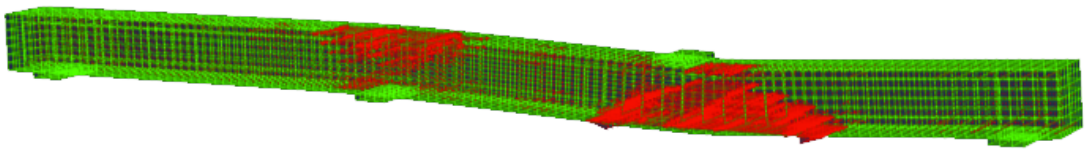

(a) V_f = *0%*

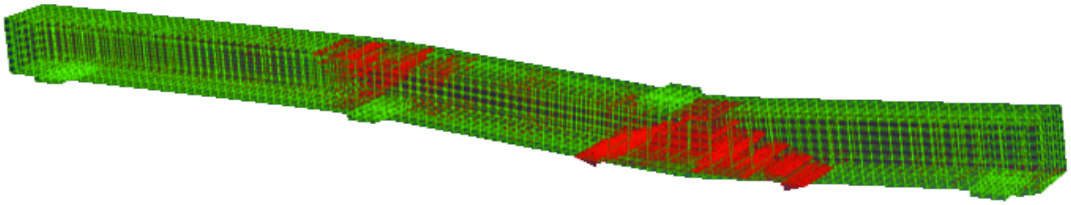

(b) V_f = *1%*

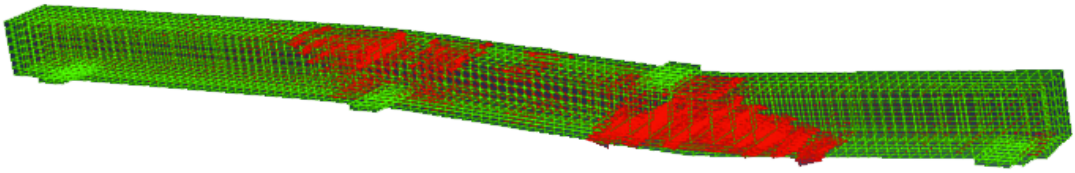

(c) V_f = *1,5%*

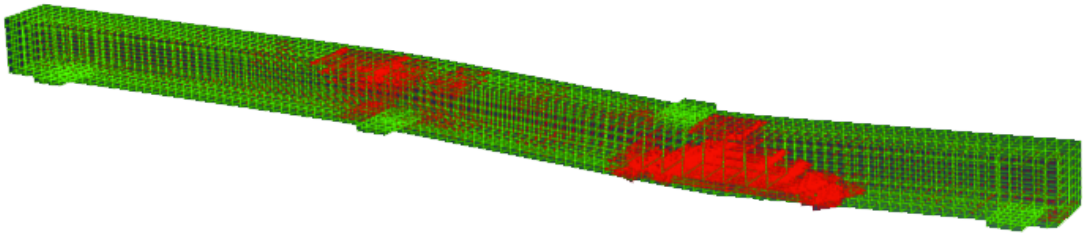

(d) V_f = *2%*

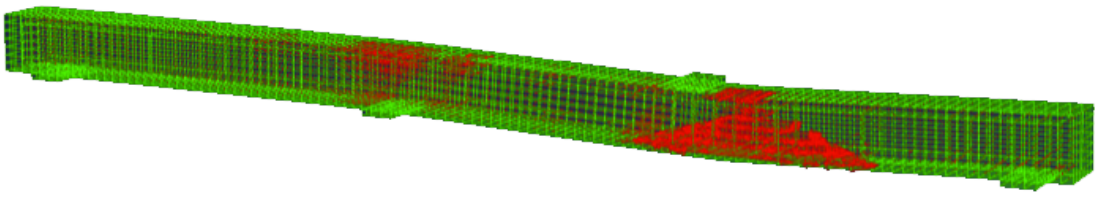

(e) V_f = *2,5%*

Figure 4.32 *Principal strain vector for SI=50%*

When the stirrups spacing increases, as depicted in Figure 4.30, the mode of failure changes from bending to shear. In this case the principal strain vectors show cracks propagated along the span between the load plate and the intermediate support, only the beam with the highest percentage of fibres is characterized by failure in bending, in fact the cracks are concentrated again in correspondence of the support and of the load point. These results are consistent with the analysis of the damage parameter previously carried out (Figures 4.26 and 4.27).

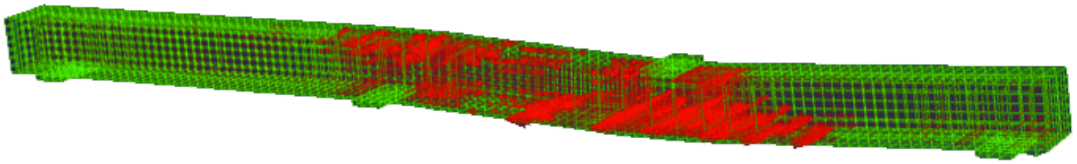

(a) $V_f = 0\%$

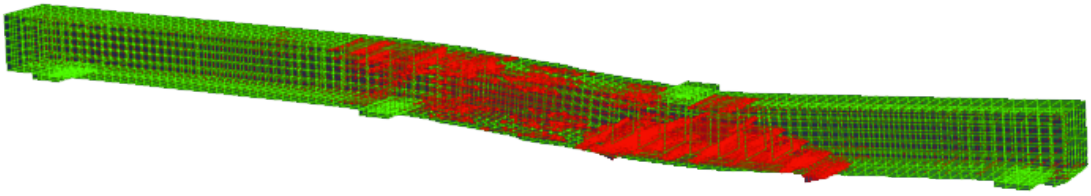

(b) $V_f = 1\%$

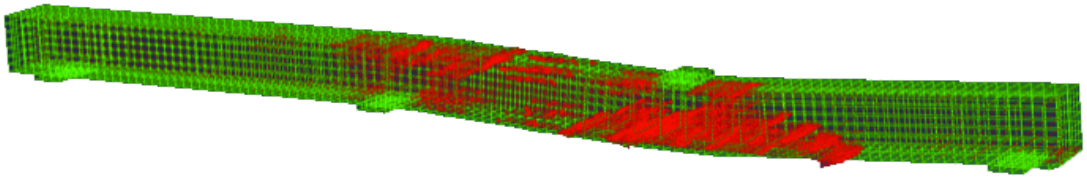

(c) $V_f = 1{,}5\%$

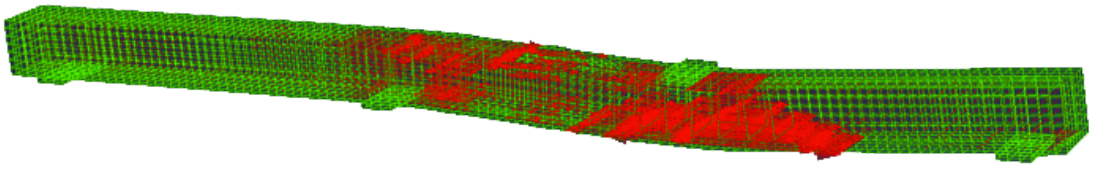

(d) $V_f = 2\%$

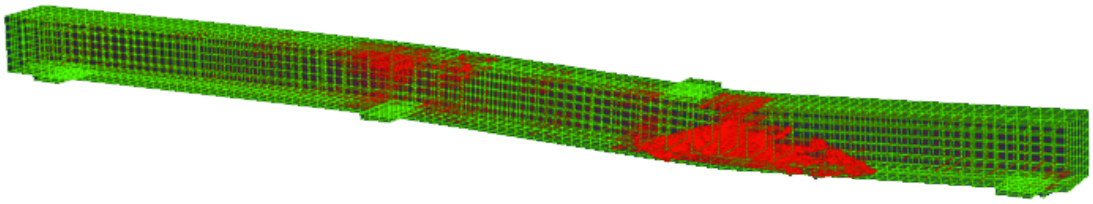

(e) V_f = *2,5%*

Figure 4.33 *Principal strain vector for SI=100%*

4.2 Cyclic Load

After the validation and the parametric studies for the monotonic load, the element was analysed using a cyclic load. The aim to use this loading pattern is to simulate the seismic load that consists in a reverse cyclic load as showed in Figure 3.14. The ABAQUS software, using the Concrete Damaged Plasticity Model, allows to set two stiffness recovery factors, both in tension and in compression, this means that the model can take into account the stiffness recovery for the concrete when the load reverses its direction. The recovery factors range between 0, no recovery, and 1, total recovery. The author used a total recovery, stiffness recovery factor equal to 1, in compression, in this way the crushing damage is totally recovered when the load changes its direction. On the other hand, in tension, the stiffness recovery factor is equal to 0, so when a crack occurs in tension, it does not close when the load direction is inverted in compression. In Figure 4.34 the load deflection curve obtained is showed.

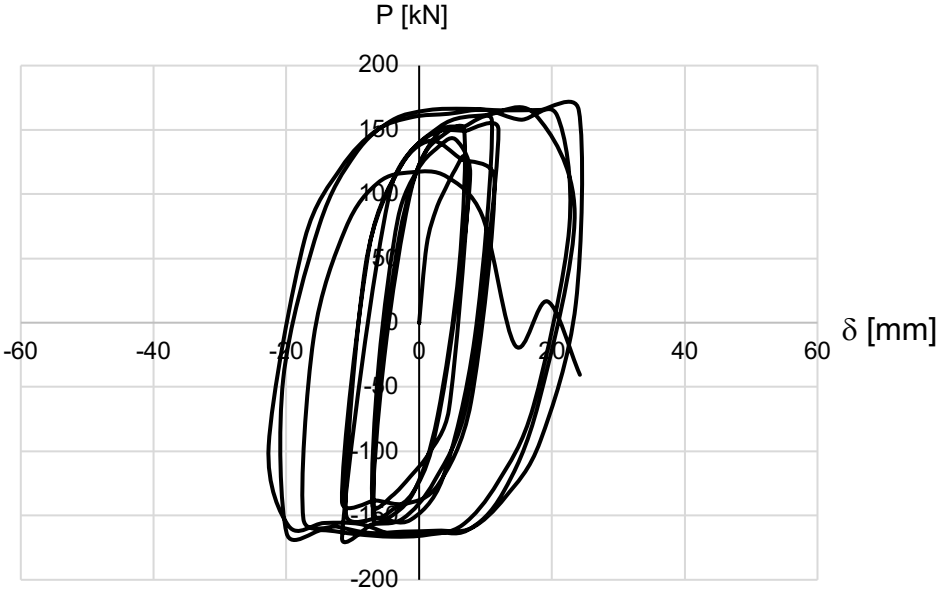

Figure 4.34 *Load deflection curve for cyclic load with CDPM*

With the constitutive model described in Chapter 3 and the plasticity parameters presented in section 4.1, the load deflection curve obtained is comparable with the experimental outcomes and with the Brittle Cracking Model outcomes (both showed in Figure 4.35) in terms of maximum load and point of failure. The maximum load P_{max} for the CDPM is equal to 166,4kN, the maximum experimental load is 183kN and the Brittle Cracking Model maximum load is 181kN. The point of failure obtained by Abbas et al. (2014) and by Kotsovos et al. (2006) occurs respectively at 9,25 cycles and 10,8 cycles. In this work with the CDPM the point of failure is reached for 9,65 cycles, that corresponds with a deflection δ_u equal to 4,15mm.

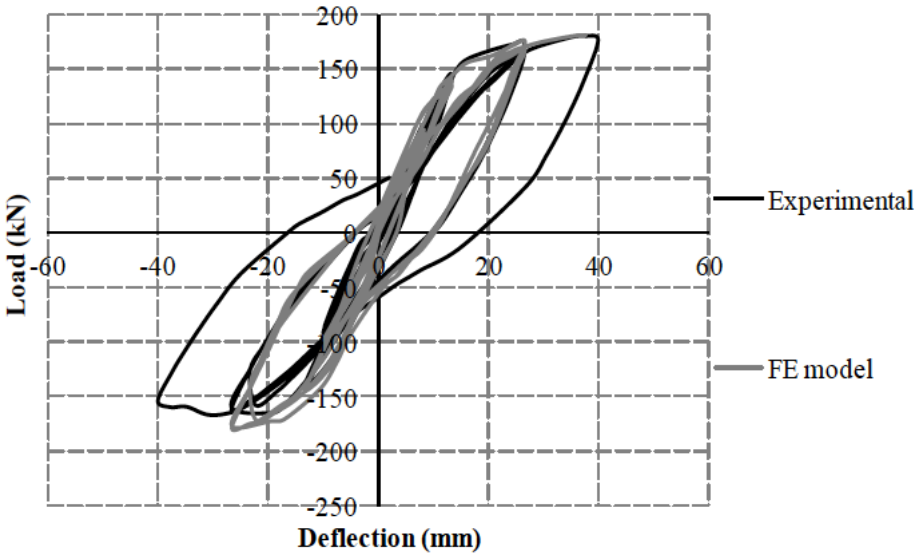

Figure 4.35 *Load deflection curve for cyclic load with Brittle Cracking Model and experimental*

The point of failure is obtained analysing the kinetic energy, in Figure 4.36 the kinetic energy trend is showed. A clear sudden jump occurs at 6,4 seconds indicating the presence of extensive cracks and consequently the element failure.

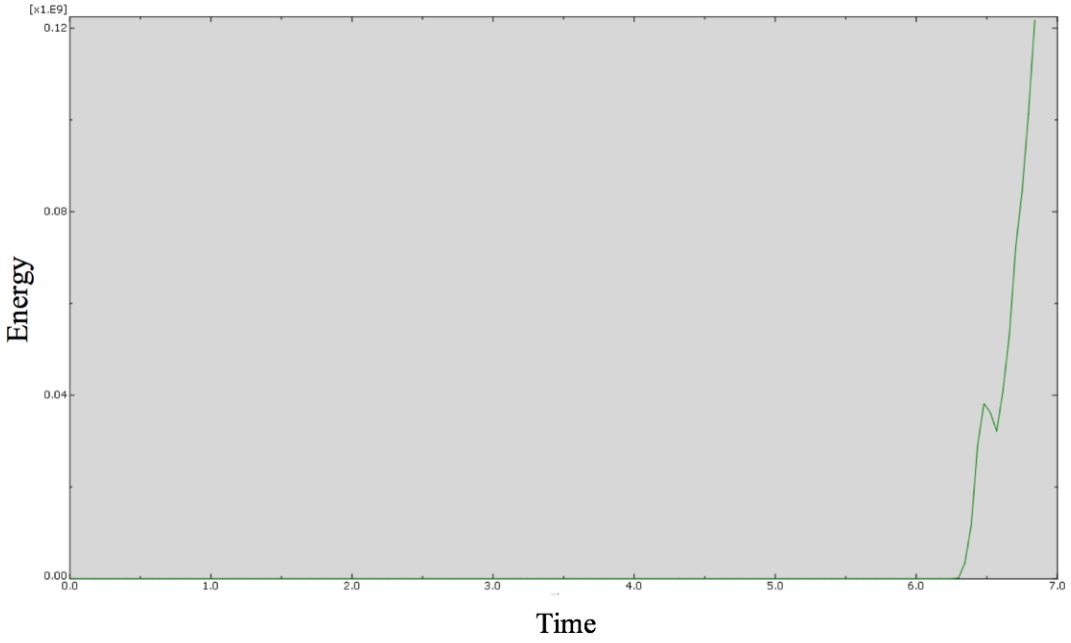

Figure 4.36 *Kinetic energy using CDPM*

Unfortunately, with this configuration, the load deflection trend is not in line with the experimental and the Brittle Cracking Model ones. In Figure 4.35, it is evident as, both for experimental and BCM model, the behaviour is completely elastic for a displacement equal to ±10mm, thus there are not residual strains, afterwards the trend becomes elastic-plastic up to the failure point. Figure 4.34 instead shows a behaviour, for the CDPM, that, since displacements lower than 10mm, is not totally elastic. Thus, at the end of the first cycle, there is already a residual plastic strain. The overall

behaviour is affected by this phenomenon and in conclusion the model validation for the cycle load is not verified.

5. Conclusions and Recommendations

The analysis carried out in this research is focused on an investigation on SFRC elements modelled with a Concrete Damaged Plasticity Model. Taking into account the experimental data obtained by Kotsovos, G., Zeris, C. and Kotsovos, M. (2006), a validation of the model was achieved. Afterwards, following the same procedure carried out by Abbas, A., Mohsin, S. and Cotsovos, D. (2014) using the Concrete Brittle Cracking Model, the author demonstrated the validity of the Concrete Damaged Plasticity Model. The procedure consists in the evaluation of the load-deflection curve, obtained with a displacement-controlled load, varying the fibres volume fraction percentage and the spacing between the stirrups. This procedure was designed with the purpose of highlighting the response in terms of structural behaviour when a substitution of standard reinforcement with steel fibres occurs. Therefore, five different fibres volume fraction percentages were chosen, namely V_f = 0%, V_f = 1%, V_f = 1,5%, V_f = 2% and V_f = 2,5%, and three different increments in the stirrups spacing, SI=0, SI=50% and SI=100% were investigated. From the outcomes, it can be seen how the models are similar, it is possible to recognise the same trends in all the configurations. The main difference in the outcomes lies on the parameters with which the damage can be evaluated: using the Brittle Cracking Model the investigation is carried out analysing the strain vectors and contours, the cracking pattern is linked with maximum strain in the constitutive model. The Concrete Damaged Plasticity model instead contemplates two different parameters for the damage in tension and in compression that represent the damage evolution up to the complete cracking.
Now it is possible to present a summary of all the observations about this research work and its conclusions.

The Concrete Damaged Plasticity Model is able to represent the behaviour of a Steel Fibre Reinforced Concrete beam under monotonic load, using this model it is possible to obtain the correct load-deflection curve and the cracking pattern. Furthermore, the outcomes in terms of load carrying capacity and ductility ratio are close to those obtained with a Brittle Cracking Model. There is a significant overestimation in the load carrying capacity that puts the model not on the safe side.

Regarding the constitutive model, the author chose two different constitutive models: in tension the model designed by Lok, T. and Xiao, J. (1998) was used to take into account the steel fibres contribution; in compression, according to Lok, T. and Xiao, J. (1998) the behaviour of Steel Fibre Reinforced Concrete is the same of plain concrete, but the author used the model developed by Alfarah, B., López-Almansa, F. and Oller, S. (2017) to take into account the explicit equation of the damage parameter. The damage parameters equations both in tension and in compression show cracks pattern consistent with the element configuration.

With the variation in the fibre volume percentage and in the stirrups spacing the fibres contribution in reducing steel bars can be considered. Using the Concrete Damaged Plasticity Model the author could represent correctly the variations in the element behaviour. The analysis was carried out in terms of load-deflection trend, load-carrying capacity and ductility. The outcomes obtained with the CDPM are in line with those obtained with the Concrete Brittle Cracking Model, they show an improvement in the load-carrying capacity when the fibre volume percentage grows up to 2,5%, at the same time the ultimate deflection decreases.

Furthermore, future works could be carried out based on this research to develop and to investigate other aspects of this topic.

In this research, among all the plasticity parameters, only the dilatation angle was changed to obtain better results, it could be interesting to modify other parameters, like the eccentricity, and compare the outcomes to highlight the ability of the Concrete Damaged Plasticity Model to adapt to different configurations.

Regarding the damage parameters, the author used different equations to obtain the damage parameter in tension and in compression because of the different constitutive models used. In tension, the damage parameter grows linearly from 0% to 99%, in this way the damage is related only to the strain. Could be useful to evaluate the damage parameter equation in tension using the model developed by Alfarah et al. (2017) also in tension, and modifying it to take into account the fibres contribution.

Since the cyclic load model is not verified, different techniques can be used to obtain better results. The mesh used by the author is the same for the monotonic and the cyclic load, reducing the mesh size could improve the outcomes, in this way the premature transition from elastic to plastic behaviour could be avoided. Moreover, considering that the plastic behaviour occurs in the first cycle, changing the stiffness recovery factor does not change the overall behaviour.

References

ABAQUS Version 6.7 Documentation, 2007. [Online]. Available at http://www.engine.brown.edu:2080/v6.7/index.html.

Abbas, A., Mohsin, S. and Cotsovos, D. (2014) "Non-linear analysis of statically indeterminate SFRC columns", *Structural Concrete*, 15(1), pp. 94-105. doi: 10.1002/suco.201300004.

Abbas, A., Mohsin, S., Cotsovos, D. and Ruiz-Teran, A. (2014) "Statically-Indeterminate SFRC Columns under Cyclic Loads", *Advances in Structural Engineering*, 17(10), pp. 1403-1417. doi: 10.1260/1369-4332.17.10.1403.

Achilleos, C. et al. (2011) "Proportioning of Steel Fibre Reinforced Concrete Mixes for Pavement Construction and Their Impact on Environment and Cost", *Sustainability*, 3(12), pp. 965-983. doi: 10.3390/su3070965.

Alfarah, B., López-Almansa, F. and Oller, S. (2017) "New methodology for calculating damage variables evolution in Plastic Damage Model for RC structures", *Engineering Structures*, 132, pp. 70-86. doi: 10.1016/j.engstruct.2016.11.022.

Chen, B. and Liu, J. (2005) "Contribution of hybrid fibers on the properties of the high-strength lightweight concrete having good workability", *Cement and Concrete Research*, 35(5), pp. 913-917. doi: 10.1016/j.cemconres.2004.07.035.

Eurocode 8, design of structures for earthquake resistance (2005). London: British Standards Institution.

European Committee for Standardization (2007) " TEST METHODS FOR FIBRES IN CONCRETE - PART 1: REFERENCE CONCRETES"

"Final recommendation of RILEM TC 162-TDF: Test and design methods for steel fibre reinforced concrete sigma-epsilon-design method" (2003), (262), pp. 560-567. doi: 10.1617/14007.

Granju, J. and Ullah Balouch, S. (2005) "Corrosion of steel fibre reinforced concrete from the cracks", *Cement and Concrete Research*, 35(3), pp. 572-577. doi: 10.1016/j.cemconres.2004.06.032.

Grassl, P. (2009) "On a damage–plasticity approach to model concrete failure", *Proceedings of the Institution of Civil Engineers - Engineering and Computational Mechanics*, 162(4), pp. 221-231. doi: 10.1680/eacm.2009.162.4.221.

Guidance for the design of steel-fibre-reinforced concrete (2007). The Concrete Society.

Kmiecik, P. and Kaminski, M. (2011) "Modelling of reinforced concrete structures and composite structures with concrete strength degradation taken into consideration", *Archives of Civil and Mechanical Engineering*, 11(3), pp. 623-636. doi: 10.1016/s1644-9665(12)60105-8.

Kotsovos, G., Zeris, C. and Kotsovos, M. (2006) "The effect of steel fibres on the earthquake-resistant design of reinforced concrete structures", *Materials and Structures*, 40(2), pp. 175-188. doi: 10.1617/s11527-006-9129-5.

Krätzig, W. and Pölling, R. (2004) "An elasto-plastic damage model for reinforced concrete with minimum number of material parameters", *Computers & Structures*, 82(15-16), pp. 1201-1215. doi: 10.1016/j.compstruc.2004.03.002.

Jankowiak, T. and Łodygowski, T. (2005) "Identification of Parameters of Concrete Damage Plasticity Constitutive Model", *Foundations Of Civil and Environmental Engineering*, (6), pp. 53-69.

Lim, T., Paramasivam, P. and Lee, S. (1987) "Analytical Model for Tensile Behavior of Steel-Fiber Concrete", *ACI Materials Journal*, 84(4), pp. 286 – 298. doi: 10.14359/1454.

Lok, T. and Xiao, J. (1998) "Tensile behaviour and moment–curvature relationship of steel fibre reinforced concrete", *Magazine of Concrete Research*, 50(4), pp. 359-368. doi: 10.1680/macr.1998.50.4.359.

Lok, T.S., and Pei, J.S., 1996. Flexural Behavior of Steel Fiber-Reinforced Concrete. *Journal of Materials in Civil Engineering, ASCE,* 10(2); p. 86 – 97.

Lubliner, J., Oliver, J., Oller, S. and Oñate, E. (1989) "A plastic-damage model for concrete", *International Journal of Solids and Structures*, 25(3), pp. 299-326. doi: 10.1016/0020-7683(89)90050-4.

Luccioni, B., Oller, S. and Danesi, R. (1996) "Coupled plastic-damaged model", *Computer Methods in Applied Mechanics and Engineering*, 129(1-2), pp. 81-89. doi: 10.1016/0045-7825(95)00887-x.

Mohsin, S. (2012) *Behaviour of Fibre-Reinforced Concrete Structures under Seismic Loading*. Doctor of Philosophy. Imperial College London.

Nguyen, G. and Korsunsky, A. (2008) "Development of an approach to constitutive modelling of concrete: Isotropic damage coupled with plasticity", *International Journal of Solids and Structures*, 45(20), pp. 5483-5501. doi: 10.1016/j.ijsolstr.2008.05.029.

Pilakoutas, K., Neocleous, K. and Tlemat, H. (2004) "Reuse of tyre steel fibres as concrete reinforcement", *Engineering Sustainability*, 157(3), pp. 131-138. doi: 10.1680/ensu.157.3.131.48644.

Wang, Y., Wu, H. and Li, V. (2000) "Concrete Reinforcement with Recycled Fibers", *Journal of Materials in Civil Engineering*, 12(4), pp. 314-319. doi: 10.1061/(asce)0899-1561(2000)12:4(314).

Zollo, R. (1997) "Fiber-reinforced concrete: an overview after 30 years of development", *Cement and Concrete Composites*, 19(2), pp. 107-122. doi: 10.1016/s0958-9465(96)00046-7.